The Preprophase Band of Microtubules for Division Plane Specification in Land Plants

By

MARIA XIMENA ANLEU GIL

DISSERTATION

Submitted in partial satisfaction of the requirements for the degree of

DOCTOR OF PHILOSOPHY

in

Plant Biology

in the

OFFICE OF GRADUATE STUDIES

of the

UNIVERSITY OF CALIFORNIA

DAVIS

Approved:

_____

Bo Liu, Chair

_____

Lesilee S. Rose

_____

Savithramma Dinesh-Kumar

Committee in Charge

2024

Table of contents

Abstract

The precise spatial control of the division plane is crucial for tissue and organ patterning in plants, and the preprophase band (PPB) is a cytoskeletal structure that regulates division plane orientation in somatic cells. The PPB is primarily composed of bundled cortical microtubules (MTs) with actin and protein components and functions to organize a cortex region that becomes the future division site. The PPB-dependent cue is a positional landmark that guides centrifugal phragmoplast expansion during cytokinesis.

Chapter 1 of this thesis offers a comprehensive literature review on the PPB, delving into our current understanding of the molecular mechanisms controlling its formation and function and tracing its evolutionary origins.

In Chapter 2, we identify and characterize the IQ Domain (IQD) containing proteins 6/7/8 as microtubule-binding proteins associated with PPB MTs. Triple mutant plants of these *IQD* genes exhibit oblique cell division planes caused by disorganized PPBs that led to the misspecification of the division plane. Our studies show that robust and solid PPBs are crucial for precise division plane control and that *IQD6/7/8* are necessary for properly organizing PPB MTs. Another discovery highlights the cooperation between the MT-polymerase CLIP Associated Protein (CLASP) and IQD6/7/8 in maintaining PPB MT organization and stability. Considering the conserved IQ67 domain in IQD proteins is known to bind calmodulin (CaM) in the presence of calcium (Ca^{2+}), it raises intriguing questions about the role of Ca^{2+}/CaM in division plane regulation.

Chapter 3 focuses on the regulation of PPB formation by cyclin and cyclin-dependent kinase (CDK). We confirm that the cyclin A1;1 (CYCA1;1) and CDKA;1 localize at the PPB when expressed under native promoters, revealing an interdependence between CDKA;1 and CYCA1;1 for their PPB localization. However, the specific functions of CDKA;1 and CYCA1;1 at the PPB still need to be clarified. Our findings introduce a connection between cell cycle regulators and the mitotic cytoskeleton machinery potentially influencing PPB emergence or disassembly.

In summary, these studies contribute to our understanding of molecular modules that control plant development by studying how plants control their division plane placement. Such knowledge is crucial for understanding how plants build their tissues and organs, which constitute the basis of human food systems.

Dedication

Dedicado a mi familia y a mi hogar Guatemala.
Que la ternura de las plantas sea nuestra guía a un futuro más justo y amoroso.

Dedicated to my family and my home Guatemala.
May the tenderness of plants be our guide to a more just and loving world.

Acknowledgments

Thank you to everyone who helped me get here.

Thanks to everyone in the Liu lab. Particularly my advisors, Dr. Bo Liu and Dr. Yuh-Ru (Julie) Lee. Your knowledge about cell biology and the plant cytoskeleton is inspiring, and I'm so thankful for all your support. Thank you to fellow Liu lab graduate students Calvin Huang, Man Kei (Constance) Tse, and Huan (Howard) Huo for their motivation, conversations, and help with research and graduate school. Thank you to the undergrads in the lab, particularly Yibo Shi, for helping isolate the quadruple *clasp iqd6/7/8* mutant. Thank you to visiting students (particularly Dr. Xiaojiang Guo) and professors who have worked in the Liu lab for help with experiments and interesting discussions.

Thanks to my thesis committee - Dr. Lesilee Rose, Dr. Savithramma Dinesh-Kumar, and Dr. Bo Liu for their insightful comments, time, patience, and suggestions on my research and thesis.

Thanks to my cohort, fellow PBGG grad students, Plant Biology department faculty, and staff. Thanks to my students.

Thank you to all the scientific mentors I've had– Dr. Nick Kaplinsky, Dr. Dominique Bergmann, Dr. Michael Raissig, Dr. Heike Lindner, Dr. Annika Weimer, Dr. Diego Wengier, Dr. Nidhi Sharma, Dr. Anne Vaten, Dr. Martin Bringmann, Dr. Kimmy Ho, Dr. Julien Alassimone, Dr. Laura Lee, Dr. Camila López-Anido, and Dr. Lior Tal. Also, thanks to Carmen Isais for her constant motivation and insightful advice.

Thanks to all UAW2865 and UAW5810 fellow union members for their solidarity. Thanks to all the workers who keep the UC running.

Thanks to my family: Mami, Papi, Ine, Javi, Mabel, tios, y primos. I am here thanks to their love, sacrifice, patience, and support. Thanks to my old and new friends for their support and camaraderie during this process. Thanks to my pets Puppy, Brownie, Spice, Frodo, Kira, Puki for their cross-species love and wisdom.

Thanks to Dr. Peter Lynagh for being my rock and favorite plant biologist.

Thanks also to all the art, books, and music that kept me whole and my dreams alive throughout graduate school. Thanks to my Arabidopsis plants, I wouldn't have been able to do this without them.

Chapter 1

The preprophase band of microtubules for division plane placement in land plants

Authors: M. Ximena Anleu Gil and Bo Liu*

Affiliations: Department of Plant Biology, University of California, Davis

*Corresponding author: Bo Liu (bliu@ucdavis.edu)

Author Contributions: The manuscript was written by MXAG and BL. All figures were designed and prepared by MXAG.

Abstract

This review explores the molecular intricacies of preprophase band (PPB) formation, a critical process in determining the division plane during plant cell mitosis. The TON1-TRM-PP2A (TTP) complex, including regulators like IQD6/7/8 and MAP65-4, plays a central role in stabilizing PPB microtubule structures. The connection between cell cycle regulators, specifically cyclin-dependent kinases, and PPB dynamics is discussed. Key proteins, such as TAN and POK1/2, contribute to the cortical division site (CDS) function after PPB disassembly. Evolutionary aspects highlight the unique emergence of the PPB in land plants and its collaboration with the phragmoplast. Understanding PPB regulation has implications for crop improvement, as precise division plane placement influences plant tissue organization and morphology. This review provides a concise overview of the molecular mechanisms governing PPB formation and its significance in plant development and evolution.

Introduction

Specific cell division patterns and subsequent cell expansion form the complex 3D geometry of plants. Unlike non-plant eukaryotes, plant cells divide by depositing new cell wall material between the two daughter cells instead of dividing their cytoplasm through centripetal cleavage. Since plant cells are immobile, the division plane influences tissue geometry, mechanics, and growth. Errors in cell plate placement have developmental consequences; thus, plants must tightly control division plane placement during morphogenesis.

Like all eukaryotic cells, plant cells rely on the cytoskeleton for cell division. This process involves dramatic reorganization of the cytoskeleton (Figure 1.1), as shown by the formation of dynamic microtubule (MT) structures like the spindle, which separates the duplicated genetic material, and the phragmoplast, which completes cytokinesis. In vegetative tissues, the division plane is determined earlier in prophase by the preprophase band (PPB), a transient ring of bundled cortical MTs, actin, and cytoskeleton-associated proteins that forms at the cortex of cells preparing to enter mitosis. Since its discovery in 1966 (Pickett-Heaps & Northcote, 1966), the PPB has been linked to the process of division plane establishment in dividing cells because it precisely predicts the position of the future cell plate. Genetic and pharmacological studies have shown that the division plane is compromised without a robust PPB structure (Bouchez et al., 2014; Duroc et al., 2011; Mineyuki, Murata, et al., 1991). Molecular studies have found that the PPB leaves behind a “memory” or spatial cue of its position at the cortex- after its disappearance – the cortical division site (CDS) (Smertenko et al., 2017). The CDS houses proteins that guide the centrifugally expanding phragmoplast to meet this PPB-determined position in the parental cell wall. Thus, the PPB is an essential component of cell division in plant vegetative tissues.

Formation of the PPB

When a vegetative plant cell enters the cell division cycle, the PPB replaces the cortical MT (CMT) array. During interphase, the CMT array is composed of MTs evenly organized transversely underneath the plasma membrane and guides the deposition of cellulose microfibrils at the cell wall. Consequently, CMTs influence the rate and

direction of growth during plant cell expansion. In late G2 phase, after a cell enters the mitotic division cycle, the CMT array gradually reorganizes into a wide bundled array at a position equatorial to the nucleus and generally 90.º to the parental wall in the cell division axis. By prophase, PPBs MTs are highly bundled. This process is presumably driven by localized MT stabilization, de-novo polymerization, and MT depolymerization.

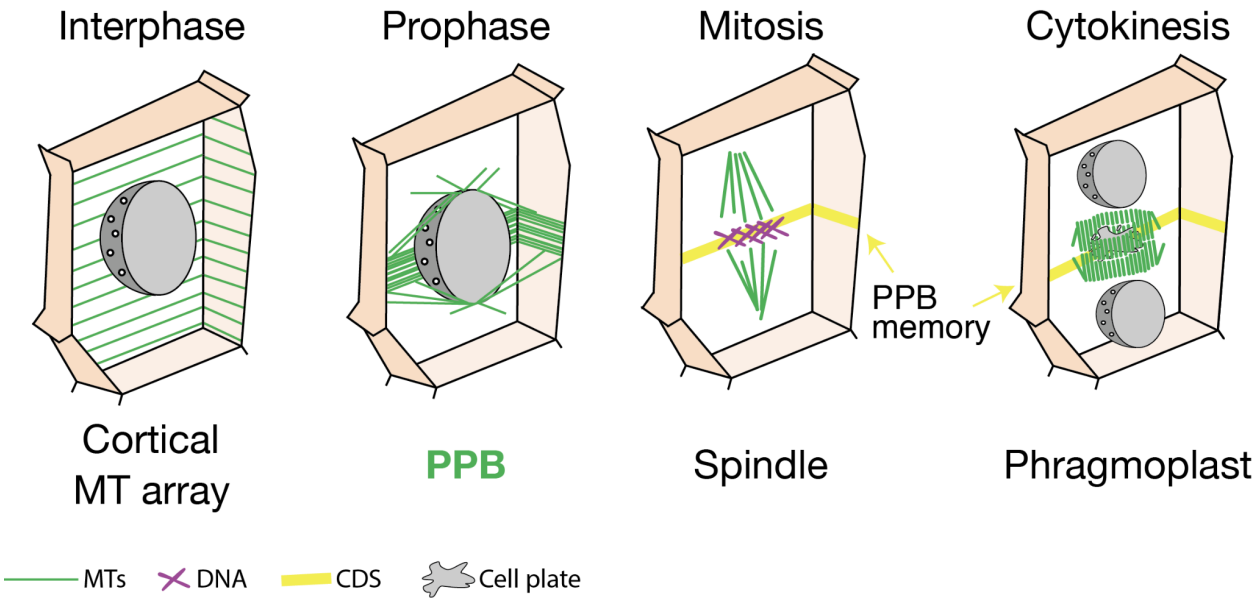

Figure 1.1. – Organization of the cytoskeleton during the plant cell cycle
Diagrammatic representation of microtubule (MT) organization changes during the plant cell cycle. The preprophase band (PPB) sets up the division plane as the cortical division site (CDS in yellow) and records the position previously occupied by the PPB.

The first known MT regulators involved in PPB formation are upstream regulators, which also affect CMT dynamics during interphase. These include protein phosphatase type 2A (PP2A, TONNEAU2(TON2)/FASS), centrin-like proteins (TON1), and MT-binding proteins like TON1 RECRUITING MOTIF proteins (TRMs), altogether acting as the TON1-TRM-PP2A (TTP) complex. Plants mutant for key components of the TTP complex are often dwarfed, misshaped, and display aberrant cell division and

elongation patterns caused by impaired PPBs and CMTs (Azimzadeh et al., 2008; Camilleri et al., 2002; Spinner et al., 2010, 2013; Traas et al., 1995). Enzymatic activity of the TTP network at the cortex may be necessary to regulate CMT stabilization and organization, including the PPB (Kirik et al., 2012; Spinner et al., 2013). Therefore, the TTP complex serves as a master regulator for PPB formation.

Mutants that affect the PPB specifically but not CMTs are essential to further our understanding of the molecular mechanisms that regulate PPB formation, such as the *trm6/7/8* triple mutant (Schaefer et al., 2017). TRM6/7/8s are functionally redundant MT-associated proteins that decorate PPB MTs specifically, and in their absence, mutant cells cannot make proper PPBs. Within the TTP complex, TRMs are thought to aid with assembling the protein complex and targeting it to CMTs (Spinner et al., 2013). In root tissues of plants mutant for TRM6/7/8, the division plane departs dramatically from WT in cells with impaired PPBs. Therefore, correct division plane specification requires proper PPBs. A different study found MT-binding IQ-Domain proteins IQD6/7/8, mitotic isoforms of a plant-specific family of MT and Ca^{2+}/CaM binding proteins associated exclusively with PPB MTs (Kumari et al., 2021). The proteins' accumulation at the PPB and impaired division plane specification in *iqd6/7/8* mutant plants support the notion that IQD6/7/8 function in PPB formation and division plane positioning. Based on this evidence, while the TTP complex is necessary for controlling CMT dynamics to begin PPB formation, TRM6/7/8, and IQD6/7/8 are needed to organize PPB MTs to allow consolidation of the CDS precisely.

The functions of several other MT regulators are associated with PPB formation and maintenance. Mutants of conserved MT regulators like MOR1 (MT Organization 1)

Arabidopsis homolog of Xenopus MT associated protein 215 kDa (XMAP215), a TOG (Tumor Overexpressed Gene) domain-containing MT polymerase, CLASP (another TOG domain MT polymerase), and FRA2 (Fragile fiber 2, the catalytic subunit of the MT severing protein katanin) display defective PPBs. Temperature-sensitive mutant *mor1* under restrictive temperature lacks PPBs or has very sparse or poorly developed ones (Kawamura et al., 2006), *clasp* has widened PPBs of ununiform width and density (Ambrose et al., 2007), and in *fra2/lue1* PPBs were loosely organized or incomplete (Panteris et al., 2011). In addition, the mutants show division plane defects. These phenotypes point to the possible functions of MOR1, CLASP, and KATANIN1 in PPB MT organization.

MT bundler of the evolutionarily conserved MAP65/Ase1/PRC1 family, MAP65-4, is also highly enriched in the PPB and remains at the CDS. However, no apparent roles in division orientation have been assigned, while it plays a semi-redundant role with MAP65-3 crosslinking anti-parallel MTs in the phragmoplast (Li et al., 2017). It is plausible that MAP65-4 activity bridging neighboring MTs contributes to PPB stability. An open question for future study is how all these molecular players work together to modulate MT dynamics and input into the selection and definition of the division plane.

The emerging picture is that the PPB MT structure requires the concerted action of MT binding proteins to provide stabilization and that narrowing down the PPB array is crucial for precisely selecting the division plane. In addition to MT-associated players such as IQD6/7/8 and MAP65-4, actin is also involved in PPB MT consolidation. Actin accumulates in early PPBs but is absent in late PPBs and the CDS (Liu & Palevitz, 1992). Electron tomography studies in onion epidermal cells revealed that short actin

microfilaments mediate initial PPB MT bundling (Takeuchi et al., 2016). Pharmacological studies showed that actin depolymerization in prophase cells induces PPB widening and division plane placement errors (Eleftheriou & Palevitz, 1992; Mineyuki & Palevitz, 1990). MT-actin interactions at the PPB stage may be mediated by actin motors, particularly of the Myosin XI family, for cells to specify the cell plate fusion site (Huang et al., 2022).

PPB development is cell cycle-dependent and coincides spatiotemporally with specific events such as pre-division nuclear migration. Further, the PPB disappears coincidently with nuclear envelope breakdown and entry into prometaphase. Therefore, communication between the cell cycle machinery and the cytoskeleton is critical for PPB formation and function. Several critical cell cycle regulators associate with the PPB in different plant species. Cyclin-dependent kinases (CDKs) were the first cell cycle core proteins identified at the PPB. Since then, a specific CDK (CDKA;1) and cyclin (CYCA1;1) have been consistently detected at the PPB by immunolabeling (Colasanti et al., 1993; Mineyuki, Yamashita, et al., 1991) and overexpression of fluorescently-tagged proteins (Boruc et al., 2010). Other regulators, such as a CDK activator (CKS2) and an inhibitor (ICK4), also accumulate at the PPB when overexpressed in tobacco BY2 cells (Boruc et al., 2010). The accumulation of cell-cycle regulators at the PPB is intriguing and suggests that these proteins act as potential regulators of PPB development. CDKs require cyclin for their kinase activity and substrate recognition. The CDKA;1/CYCA1;1 complex may regulate the activity of MT-associated PPB determinants like the TTP complex, TRM, IQD, TON1, and MAP65-4 proteins through phosphorylation. These proteins all have predicted CDK phosphorylation sites. In addition, CDKA;1 co-purifies

with TON1 (Van Leene et al., 2007). More clues come from studies in cultured BY-2 cells where PPBs do not disassemble (Katsuta & Shibaoka, 1992) or broaden and loosen (Nogami & Mineyuki, 1999) with the application of kinase inhibitors. Conversely, applying phosphatase inhibitors abolishes PPB formation (Hasezawa & Nagata, 1992). Additionally, microinjection of an active CDK/Cyclin complex in *Tradescantia* stamen hair cells induces rapid disassembly of the PPB (Hush et al., 1996). These observations point to a role for CDK in PPB formation and disassembly. Further studies are needed to delineate the precise functions of cell cycle regulators at the PPB and the mechanism of action.

In addition to the CMT changes of the PPB, a set of MTs emerges from the nuclear envelope in cells preparing to undergo mitosis forming the prophase spindle (or prospindle). Ample evidence links the PPB to the definition of the prophase spindle poles (Ambrose & Cyr, 2008; Chan et al., 2005), which mark the location of the mitotic spindle poles after nuclear envelope breakdown (NEB). Indeed, mutants with abnormal PPBs like *trm6/7/8, ton1,* and *iqd6/7/8* have enriched perinuclear MTs that fail to coalesce into two well-formed poles. Cells with defective PPBs can establish bipolar mitotic spindles after NEB, but spindle orientation is more variable (Chan et al., 2005; Schaefer et al., 2017). Therefore, the PPB likely facilitates the formation of a bipolar prophase spindle, which aids in forming a robust mitotic spindle.

PPB-directed establishment of the division plane

The PPB defines the CDS after its disassembly by leaving a positional memory. The first characterized CDS resident was the basic protein TANGLED, which

accumulates at the PPB and persists at the division site (Walker et al., 2007). The *tan* mutation in maize causes abnormal cell divisions in the leaf epidermis (Smith et al., 1996) that arise from incorrect phragmoplast guidance to the former PPB site (Cleary & Smith, 1998). POK1 and POK2 are two kinesin-12 discovered as TAN interactors that redundantly maintain the division site by guiding the rapidly expanding phragmoplast (Müller et al., 2006), with POK2 playing a role in phragmoplast dynamics (Herrmann et al., 2018). *pok1pok2* mutant plants have stunted growth and aberrant cell division orientations. Since they are both MT-associated factors, TAN1 and POKs may be functionally interdependent for retaining CDS resident proteins at the division site (Lipka et al., 2014; Mills et al., 2022). In addition to MT-associated factors like TAN and POK1/2, Ran GTPase Activating Protein (RanGAP1), although a regulator of nucleocytoplasmic transport, begins accumulating at the PPB stage and is also a continuous marker of the CDS (Xu et al., 2008). Therefore, the PPB is necessary for the assembly of CDS protein complexes. However, we still have much to learn about how the expanding phragmoplast communicates with the CDS during cytokinesis.

The PPB in plant evolution

The cytokinesis mechanism has changed during the evolution of plants from algae to flowering plants. Early diverging groups of green plants like Chlorophytes divide by centripetal cleavage instead of forming the PPB or phragmoplast (Brown & Lemmon, 1990). The phragmoplast is an evolutionary landmark that emerged before the occurrence of the ZCC (Zygnematophyceae, Coloechaetophyceae, and Charophyceae) grade of Streptophyte algae (Buschmann & Zachgo, 2016; Doty et al.,

2014; Schreiber et al., 2022) and may have permitted branching and three-dimensional growth (Buschmann, 2020). The PPB is an autapomorphy (derived character specific to a monophyly) of land plants. However, some ZCC Streptophyte algae species make PPB-like structures (Domozych & Bagdan, 2022), so some primitive PPB forms may have appeared in these algae. Further examination is needed to determine whether these structures function as PPBs. Since the phragmoplast evolved first, it is interesting how these early phragmoplasts orient without a PPB mechanism. Further comparative studies could uncover how the phragmoplast-PPB cooperation emerged.

As the oldest land plants, bryophytes may provide some clues about the evolutionary role of PPBs, given the diverse arrays different bryophyte species show (Brown & Lemmon, 1990, 2011). Mosses, for instance, make PPBs in leafy gametophores, which are three-dimensional structures, but not in filamentous protonema, which are two-dimensional. On the other hand, liverwort PPBs collaborate with centrosome-like structures called polar organizers, which are involved in division plane alignment and PPB formation (Buschmann et al., 2016). Centrosomes are central for spindle organization in most animal mitosis and are present in algae but not in most cells of land plants. These observations suggest that the PPB evolved stepwise during evolution and could have been an adaptation to sustain parenchymatous growth that entails switching division planes during cell division.

With a couple of exceptions, all somatic divisions in vascular plants use PPBs to set up the division plane. Generally, the PPB occurs in somatic cells where nuclear division (karyokinesis) precedes cytokinesis. In contrast, cell types such as endosperm and gametophytes, where the nucleus may undergo divisions before cytokinesis, do not

make PPBs but instead use an alternative method relying on a “radial MT system” to set up the position of the new walls (Brown et al., 2018; Olsen, 2001; Otegui & Staehelin, 2000). Furthermore, suspension-cultured cells and those of callus also produce the PPB, suggesting that PPB formation is autonomous to the isolated mitotic cells.

Conclusion and significance of dissertation research

The PPB is a cytoskeletal structure that directs division plane selection in somatic divisions in land plants. PPB formation and division plane selection require the activity of MTs, actin, cytoskeletal-associated proteins, and the cell cycle machinery (Figure 1.2). We have learned much about the dynamics of PPB formation from the detailed analysis of mutants and complementation lines. Building on decades of earlier work on cytokinesis, advances in microscopy, and molecular biology techniques have helped uncover the dynamics of relevant players in division plane placement. Mapping more PPB- and division-plane proteins in mutants with impaired division-plane placement may reveal how their functions act in concert to specify the PPB and CDS location. There are also numerous reports of proteins at the PPB without known function. With the advance of cell biology techniques in plants, we can alter their localization or activity to elucidate their function.

The cytokinesis mechanism of plants has changed throughout their evolution. The phragmoplast evolved first in Streptophyte algae, but the PPB appears conspicuously only in land plants. The emergence of both structures had repercussions on the cytokinetic mechanisms and evolutionary history of plants. However, the function of PPB-like structures and division plane positioning in Streptophyte algae remains

unclear. With the development of more tools for non-model systems, like the release of more algae genomes and gene-editing technologies, we can learn more about these structures and the ancestral functions of PPB proteins, as some of them are already encoded in Streptophyte algae genomes. Evo-devo research concerning cell division can provide insight into the body shape modifications accompanying the evolutionary history of plants, including their terrestrialization.

Control of division plane placement is relevant for plants because their cells are encased in a cellulosic matrix, making them immobile. When and where plant cells divide impacts the overall organization of plant tissues and organs. Plants are our primary food source; therefore, knowledge about the molecular control of cell division, organ shape, and size can help develop new crop varieties with agronomically desired traits (Lazzaro et al., 2018; Wu et al., 2018).

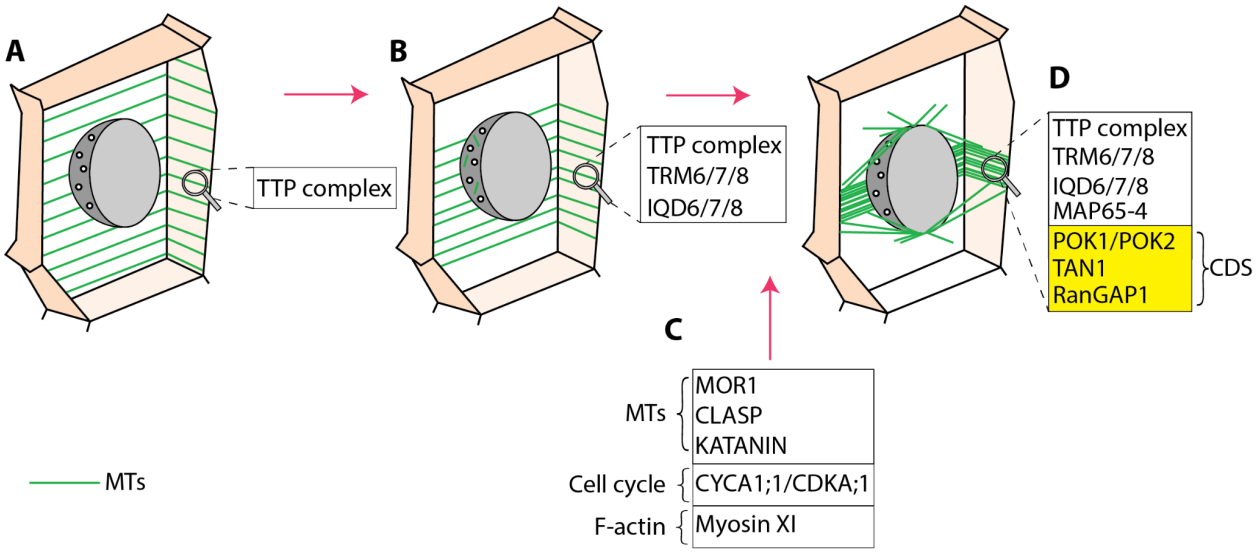

Figure 1.2. – Proteins involved in PPB development
Diagrammatic representation of the different stages of PPB development and the proteins involved.
(A). TTP complex controls MT dynamics throughout interphase and prophase.

(B). Early PPB is broad and specifically decorated by TRM6/7/8 and IQD6/7/8. Formation of PPB requires TTP complex as well as IQDs.
(C). Division plane selection requires the contributions of MT regulators–MOR1, CLASP, KATANIN, MAP65-4, cell cycle regulators–CYCA1;1/CDKA;1; F-actin and actin motor Myosin XI.
(D). Proteins that set up the CDS or PPB memory assemble as a complex at the PPB stage (yellow).

References

1. Ambrose, J. C., & Cyr, R. (2008). Mitotic spindle organization by the preprophase band. *Molecular Plant*, *1*(6), 950–960.

2. Ambrose, J. C., Shoji, T., Kotzer, A. M., Pighin, J. A., & Wasteneys, G. O. (2007). The Arabidopsis CLASP gene encodes a microtubule-associated protein involved in cell expansion and division. *The Plant Cell*, *19*(9), 2763–2775.

3. Azimzadeh, J., Nacry, P., Christodoulidou, A., Drevensek, S., Camilleri, C., Amiour, N., Parcy, F., Pastuglia, M., & Bouchez, D. (2008). Arabidopsis TONNEAU1 proteins are essential for preprophase band formation and interact with centrin. *The Plant Cell*, *20*(8), 2146–2159.

4. Boruc, J., Mylle, E., Duda, M., De Clercq, R., Rombauts, S., Geelen, D., Hilson, P., Inzé, D., Van Damme, D., & Russinova, E. (2010). Systematic localization of the Arabidopsis core cell cycle proteins reveals novel cell division complexes. *Plant Physiology*, *152*(2), 553–565.

5. Bouchez, D. D., Van Damme, D., Boruc, J., Schaefer, E., & Pastuglia, M. (2014). *Cell division plane determination in plant development*. Springer Verlag, Heidelberg. https://doi.org/10.1007/978-1-4614-7881-2_15-1

6. Brown, R. C., & Lemmon, B. E. (1990). MONOPLASTIDIC CELL DIVISION IN LOWER LAND PLANTS. *American Journal of Botany*, *77*(4), 559–571.

7. Brown, R. C., & Lemmon, B. E. (2011). Dividing without centrioles: innovative plant microtubule organizing centres organize mitotic spindles in bryophytes, the earliest extant lineages of land plants. *AoB Plants*, *2011*, lr028.

8. Brown, R. C., Lemmon, B. E., & Nguyen, H. (2018). Endosperm Development. In *Annual Plant Reviews online* (pp. 205–233). John Wiley & Sons, Ltd. https://doi.org/10.1002/9781119312994.apr0052

9. Buschmann, H. (2020). Into another dimension: how streptophyte algae gained morphological complexity. *Journal of Experimental Botany*, *71*(11), 3279–3286.

10. Buschmann, H., Holtmannspötter, M., Borchers, A., O'Donoghue, M.-T., & Zachgo, S. (2016). Microtubule dynamics of the centrosome-like polar organizers from the basal land plant Marchantia polymorpha. *The New Phytologist*, *209*(3), 999–1013.

11. Buschmann, H., & Zachgo, S. (2016). The Evolution of Cell Division: From Streptophyte Algae to Land Plants. *Trends in Plant Science*, *21*(10), 872–883.

12. Camilleri, C., Azimzadeh, J., Pastuglia, M., Bellini, C., Grandjean, O., & Bouchez, D. (2002). The Arabidopsis TONNEAU2 gene encodes a putative novel protein phosphatase 2A regulatory subunit essential for the control of the cortical cytoskeleton. *The Plant Cell*, *14*(4), 833–845.

13. Chan, J., Calder, G., Fox, S., & Lloyd, C. (2005). Localization of the microtubule end binding protein EB1 reveals alternative pathways of spindle development in

Arabidopsis suspension cells. *The Plant Cell*, *17*(6), 1737–1748.

14. Cleary, A. L., & Smith, L. G. (1998). The Tangled1 gene is required for spatial control of cytoskeletal arrays associated with cell division during maize leaf development. *The Plant Cell*, *10*(11), 1875–1888.

15. Colasanti, J., Cho, S. O., Wick, S., & Sundaresan, V. (1993). Localization of the Functional p34cdc2 Homolog of Maize in Root Tip and Stomatal Complex Cells: Association with Predicted Division Sites. *The Plant Cell*, *5*(9), 1101–1111.

16. Domozych, D. S., & Bagdan, K. (2022). The cell biology of charophytes: Exploring the past and models for the future. *Plant Physiology*, *190*(3), 1588–1608.

17. Doty, K. F., Betzelberger, A. M., Kocot, K. M., & Cook, M. E. (2014). Immunofluorescence localization of the tubulin cytoskeleton during cell division and cell growth in members of the Coleochaetales (Streptophyta). *Journal of Phycology*, *50*(4), 624–639.

18. Duroc, Y., Bouchez, D., & Pastuglia, M. (2011). The Preprophase Band and Division Site Determination in Land Plants. In B. Liu (Ed.), *The Plant Cytoskeleton* (pp. 145–185). Springer New York.

19. Eleftheriou, E. P., & Palevitz, B. A. (1992). The effect of cytochalasin D on preprophase band organization in root tip cells of Allium. *Journal of Cell Science*, *103*(4), 989–998.

20. Hasezawa, S., & Nagata, T. (1992). Okadaic acid as a probe to Analyse the cell cycle progression in plant cells. *Botanica Acta: Berichte Der Deutschen Botanischen Gesellschaft = Journal of the German Botanical Society*, *105*(1), 63–69.

21. Herrmann, A., Livanos, P., Lipka, E., Gadeyne, A., Hauser, M.-T., Van Damme, D., & Müller, S. (2018). Dual localized kinesin-12 POK2 plays multiple roles during cell division and interacts with MAP65-3. *EMBO Reports*, *19*(9). https://doi.org/10.15252/embr.201846085

22. Huang, C. H., Peng, F. L., Lee, Y.-R. J., & Liu, B. (2022). The microtubular preprophase band recruits Myosin XI to the division site for plant cytokinesis. In *bioRxiv* (p. 2022.11.08.515512). https://doi.org/10.1101/2022.11.08.515512

23. Hush, J., Wu, L., John, P. C., Hepler, L. H., & Hepler, P. K. (1996). Plant mitosis promoting factor disassembles the microtubule preprophase band and accelerates prophase progression in Tradescantia. *Cell Biology International*, *20*(4), 275–287.

24. Katsuta, J., & Shibaoka, H. (1992). Inhibition by kinase inhibitors of the development and the disappearance of the preprophase band of microtubules in tobacco BY-2 cells. *Journal of Cell Science*, *103*, 397–405.

25. Kawamura, E., Himmelspach, R., Rashbrooke, M. C., Whittington, A. T., Gale, K. R., Collings, D. A., & Wasteneys, G. O. (2006). MICROTUBULE ORGANIZATION 1 regulates structure and function of microtubule arrays during mitosis and cytokinesis in the Arabidopsis root. *Plant Physiology*, *140*(1), 102–114.

26. Kirik, A., Ehrhardt, D. W., & Kirik, V. (2012). TONNEAU2/FASS regulates the geometry of microtubule nucleation and cortical array organization in interphase Arabidopsis cells. *The Plant Cell*, *24*(3), 1158–1170.

27. Kumari, P., Dahiya, P., Livanos, P., Zergiebel, L., Kölling, M., Poeschl, Y., Stamm, G., Hermann, A., Abel, S., Müller, S., & Bürstenbinder, K. (2021). IQ67 DOMAIN proteins facilitate preprophase band formation and division-plane orientation. *Nature Plants*, *7*(6), 739–747.

28. Lazzaro, M. D., Wu, S., Snouffer, A., Wang, Y., & van der Knaap, E. (2018). Plant organ shapes are regulated by protein interactions and associations with microtubules. *Frontiers in Plant Science*, *9*, 1766.

29. Li, H., Sun, B., Sasabe, M., Deng, X., Machida, Y., Lin, H., Julie Lee, Y.-R., & Liu, B. (2017). Arabidopsis MAP65-4 plays a role in phragmoplast microtubule organization and marks the cortical cell division site. *The New Phytologist*, *215*(1), 187–201.

30. Lipka, E., Gadeyne, A., Stöckle, D., Zimmermann, S., De Jaeger, G., Ehrhardt, D. W., Kirik, V., Van Damme, D., & Müller, S. (2014). The Phragmoplast-Orienting Kinesin-12 Class Proteins Translate the Positional Information of the Preprophase Band to Establish the Cortical Division Zone in Arabidopsis thaliana. *The Plant Cell*, *26*(6), 2617–2632.

31. Liu, B., & Palevitz, B. A. (1992). Organization of cortical microfilaments in dividing root cells. *Cell Motility and the Cytoskeleton*, *23*(4), 252–264.

32. Mills, A. M., Morris, V. H., & Rasmussen, C. G. (2022). The localization of PHRAGMOPLAST ORIENTING KINESIN1 at the division site depends on the microtubule-binding proteins TANGLED1 and AUXIN-INDUCED IN ROOT CULTURES9 in Arabidopsis. *The Plant Cell*, *34*(11), 4583–4599.

33. Mineyuki, Y., Murata, T., & Wada, M. (1991). Experimental obliteration of the preprophase band alters the site of cell division, cell plate orientation and phragmoplast expansion in *Adiantum* protonemata. *Journal of Cell Science*, *100*(3), 551–557.

34. Mineyuki, Y., & Palevitz, B. A. (1990). Relationship between preprophase band organization, F-actin and the division site in *Allium*. *Journal of Cell Science*, *97*(2), 283–295.

35. Mineyuki, Y., Yamashita, M., & Nagahama, Y. (1991). p 34cdc2 kinase homologue in the preprophase band. *Protoplasma*, *162*(2), 182–186.

36. Müller, S., Han, S., & Smith, L. G. (2006). Two kinesins are involved in the spatial control of cytokinesis in Arabidopsis thaliana. *Current Biology: CB*, *16*(9), 888–894.

37. Nogami, A., & Mineyuki, Y. (1999). Loosening of a preprophase band of microtubules in onion (Allium cepa L.) root tip cells by kinase inhibitors. *Cell Structure and Function*, *24*(5), 419–424.

38. Olsen, O.-A. (2001). ENDOSPERM DEVELOPMENT: Cellularization and Cell Fate

Specification. *Annual Review of Plant Physiology and Plant Molecular Biology*, *52*, 233–267.

39. Otegui, M., & Staehelin, L. A. (2000). Cytokinesis in flowering plants: more than one way to divide a cell. *Current Opinion in Plant Biology*, *3*(6), 493–502.

40. Panteris, E., Adamakis, I.-D. S., Voulgari, G., & Papadopoulou, G. (2011). A role for katanin in plant cell division: microtubule organization in dividing root cells of fra2 and lue1Arabidopsis thaliana mutants. *Cytoskeleton* , *68*(7), 401–413.

41. Pickett-Heaps, J. D., & Northcote, D. H. (1966). Organization of microtubules and endoplasmic reticulum during mitosis and cytokinesis in wheat meristems. *Journal of Cell Science*, *1*(1), 109–120.

42. Schaefer, E., Belcram, K., Uyttewaal, M., Duroc, Y., Goussot, M., Legland, D., Laruelle, E., de Tauzia-Moreau, M.-L., Pastuglia, M., & Bouchez, D. (2017). The preprophase band of microtubules controls the robustness of division orientation in plants. *Science*, *356*(6334), 186–189.

43. Schreiber, M., Rensing, S. A., & Gould, S. B. (2022). The greening ashore. *Trends in Plant Science*, *27*(9), 847–857.

44. Smertenko, A., Assaad, F., Baluška, F., Bezanilla, M., Buschmann, H., Drakakaki, G., Hauser, M.-T., Janson, M., Mineyuki, Y., Moore, I., Müller, S., Murata, T., Otegui, M. S., Panteris, E., Rasmussen, C., Schmit, A.-C., Šamaj, J., Samuels, L., Staehelin, L. A., … Žárský, V. (2017). Plant Cytokinesis: Terminology for Structures and Processes. *Trends in Cell Biology*, *27*(12), 885–894.

45. Smith, L. G., Hake, S., & Sylvester, A. W. (1996). The tangled-1 mutation alters cell division orientations throughout maize leaf development without altering leaf shape. *Development* , *122*(2), 481–489.

46. Spinner, L., Gadeyne, A., Belcram, K., Goussot, M., Moison, M., Duroc, Y., Eeckhout, D., De Winne, N., Schaefer, E., Van De Slijke, E., Persiau, G., Witters, E., Gevaert, K., De Jaeger, G., Bouchez, D., Van Damme, D., & Pastuglia, M. (2013). A protein phosphatase 2A complex spatially controls plant cell division. *Nature Communications*, *4*(1), 1863.

47. Spinner, L., Pastuglia, M., Belcram, K., Pegoraro, M., Goussot, M., Bouchez, D., & Schaefer, D. G. (2010). The function of TONNEAU1 in moss reveals ancient mechanisms of division plane specification and cell elongation in land plants. *Development* , *137*(16), 2733–2742.

48. Takeuchi, M., Karahara, I., Kajimura, N., Takaoka, A., Murata, K., Misaki, K., Yonemura, S., Staehelin, L. A., & Mineyuki, Y. (2016). Single microfilaments mediate the early steps of microtubule bundling during preprophase band formation in onion cotyledon epidermal cells. *Molecular Biology of the Cell*, *27*(11), 1809–1820.

49. Traas, J., Bellini, C., Nacry, P., Kronenberger, J., Bouchez, D., & Caboche, M. (1995). Normal differentiation patterns in plants lacking microtubular preprophase bands. *Nature*, *375*(6533), 676–677.

50. Van Leene, J., Stals, H., Eeckhout, D., Persiau, G., Van De Slijke, E., Van Isterdael, G., De Clercq, A., Bonnet, E., Laukens, K., Remmerie, N., Henderickx, K., De Vijlder, T., Abdelkrim, A., Pharazyn, A., Van Onckelen, H., Inzé, D., Witters, E., & De Jaeger, G. (2007). A Tandem Affinity Purification-based Technology Platform to Study the Cell Cycle Interactome in Arabidopsis thaliana*. *Molecular & Cellular Proteomics: MCP*, *6*(7), 1226–1238.

51. Walker, K. L., Müller, S., Moss, D., Ehrhardt, D. W., & Smith, L. G. (2007). Arabidopsis TANGLED identifies the division plane throughout mitosis and cytokinesis. *Current Biology: CB*, *17*(21), 1827–1836.

52. Wu, S., Zhang, B., Keyhaninejad, N., Rodríguez, G. R., Kim, H. J., Chakrabarti, M., Illa-Berenguer, E., Taitano, N. K., Gonzalo, M. J., Díaz, A., Pan, Y., Leisner, C. P., Halterman, D., Buell, C. R., Weng, Y., Jansky, S. H., van Eck, H., Willemsen, J., Monforte, A. J., … van der Knaap, E. (2018). A common genetic mechanism underlies morphological diversity in fruits and other plant organs. *Nature Communications*, *9*(1), 4734.

53. Xu, X. M., Zhao, Q., Rodrigo-Peiris, T., Brkljacic, J., He, C. S., Müller, S., & Meier, I. (2008). RanGAP1 is a continuous marker of the Arabidopsis cell division plane. *Proceedings of the National Academy of Sciences of the United States of America*, *105*(47), 18637–18642.

Chapter 2

The role of IQD6/7/8 proteins in preprophase band formation for accurate division plane specification in plants

Authors: M. Ximena Anleu Gil, Yibo Shi, Huiyin Miao, Xueer Jiang, Yuh-Ru Julie Lee, and Bo Liu*

Affiliations: Department of Plant Biology, University of California, Davis

*Corresponding author: Bo Liu (bliu@ucdavis.edu)

Author Contributions: MXAG and BL conceived the project and designed the experiments. YS, HM, and XJ isolated mutants and produced the rescue plasmids. YJL provided technical support. All figures were designed and prepared by MXAG. Plants were cared for by MXAG, YS, and BL. The manuscript was written by MXAG and BL.

Abstract

Cell division and differentiation give rise to the different tissues and organs that make up the plant body. Since plant cells are immobile, they must control their division plane precisely to regulate tissue shape and size. Division plane is determined early in the cell division cycle by the preprophase band (PPB), a transient ring of highly bundled cortical microtubules (MTs), actin filaments, and cytoskeleton-associated proteins that assembles at the cortex of somatic plant cells preparing to enter mitosis. The PPB sets up the division plane by leaving a molecular memory that directs phragmoplast and cell plate expansion during cytokinesis. To elucidate cell-cycle mechanisms that control PPB formation, we analyzed a triple mutant missing three mitotic isoforms of the IQ67-Domain family of proteins, namely *iqd6/7/8*. IQD6/7/8 MT-binding proteins with high homology that specifically localize to the PPB. Unlike wild-type (WT) plants, roots of the *iqd6/7/8* mutant plants frequently display oblique cell division planes instead of transverse ones. Microscopic analysis revealed that PPB MT arrays in mutant cells were often disorganized and uneven. Live-cell imaging demonstrated that defective PPB arrays preceded phragmoplast misalignment, coincident with the uneven cortical accumulation of PPB-associated proteins, including MAP65-4 and TAN1. This aberrant pattern led to discontinuity in the cortical division site in *iqd6/7/8* cells, suggesting that the phragmoplast received only partial guidance during cytokinesis. Lastly, we uncover the synergistic roles of IQD6/7/8 and CLASP in maintaining PPB robustness. Our results indicate that IQD6/7/8 play a critical role in the PPB MT array's stabilization and maturation. A robust and solid PPB array is essential to delimit the division plane

around the cell's circumference, which is necessary for organizing divisions in 3D space.

Introduction

Cell division is tightly controlled spatially and temporally for proper patterning of multicellular organisms. In plants, spatial control of the division plane is of particular significance since plant cells are encased in a carbohydrate-enriched cell wall that provides structural support but constrains cellular movement and the cell division mechanism. Plant cells use the phragmoplast, a cytoskeletal apparatus that builds a new cell wall (the cell plate) *de novo* centrifugally to divide. In all somatic cells of land plants, the location where the phragmoplast inserts the cell plate at the parental plasma membrane (PM) is determined earlier in the division cycle by a cortical array of primarily tightly bundled microtubules (MTs) named the pre-prophase band (PPB). The PPB appears uniform and usually forms at the cell's equator surrounding the nucleus. The PPB disassembles when the nuclear envelope breaks down. Remarkably, the site previously occupied by PPB retains a molecular memory of its position throughout mitosis and cytokinesis as the cortical division site (CDS) to orient the phragmoplast as it builds the cell plate.

The PPB is primarily made up of MTs, with actin and other protein components. MTs are evenly organized underneath the PM during most of the plant cell cycle, forming the cortical MT (CMT) array. By the end of the G2 phase, MTs at the cortex increasingly bundle until they form a discrete band. MT-binding proteins (MAPs) and other regulatory proteins control MT dynamics and organization during this process. For

instance, the TON1-TRM-PP2A (TTP) complex composed of TONNEAU1 (TON1), TON1 RECRUITING MOTIF proteins (TRMs), and protein phosphatase type 2A (PP2A, TONNEAU2 (TON2)/FASS) are necessary for forming the PPB (Azimzadeh et al., 2008; Camilleri et al., 2002; Spinner et al., 2013; Traas et al., 1995). However, MT dynamics during interphase are also affected in null mutant plants of *TON1* and *TON2* as they lack typical transverse CMTs. PPB-specific mutants were unknown until the *trm6/7/8* mutant was described, in which PPB formation was specifically compromised (Schaefer et al., 2017). The absence of PPBs in these mutants led to abnormal division plane positioning. Therefore, the enzymatic activity of the TTP complex at the cortex is necessary to stabilize and organize CMTs (Kirik et al., 2012; Spinner et al., 2013).

More recently, IQ67 DOMAIN (IQD) 6/7/8 proteins were implicated in regulating division plane specification (Kumari et al., 2021). However, it is still unclear how these proteins affect PPB formation. The IQD family includes plant-specific proteins characterized by having a conserved 67 amino acid domain (IQ67 domain) with three copies of the IQ motif, which can bind calmodulin (CaM) in the presence of calcium (Ca^{+2}) (Abel et al., 2005). The founding member of the IQD family, IQD1, has been shown to bind CaM and CaM-like (CML) proteins in a calcium-dependent manner *in vitro* (Bürstenbinder et al., 2013; Levy et al., 2005). Additionally, many IQDs localize to MTs and the PM when overexpressed in *N. benthamiana* (Bürstenbinder et al., 2017). IQDs may be integrators of Ca^{+2}/CaM signaling and cytoskeletal reorganization at the cortex that impact various processes of plant growth and development (Lazzaro et al., 2018; Sugiyama et al., 2017) with potential involvement in division plane determination.

To investigate the mechanism through which plant cells build PPBs, the proteins involved, and the regulation of PPB MT dynamics, we characterized the *A. thaliana iqd6/7/8* mutant by analyzing its microtubule arrays throughout cell division. Specifically, we analyzed the contributions of IQD6/7/8 in PPB organization and division plane specification by immunostaining and time-lapse imaging. While the *iqd6/7/8* mutations did not abolish PPB formation, they compromised PPB integrity, leading to division plane misspecification. We examined PPB- and CDS-localized proteins, namely MAP65-4 and TAN1, to determine how disorganized PPBs affect other proteins that accumulate at the PPB and the establishment of the division plane. Lastly, our results indicate synergistic functions of IQD6/7/8 and CLASP in making robust PPBs. This study reveals mechanistic details about PPB formation and MT regulation and enhances our understanding of plant division plane specification.

Results

IQD6/7/8 associate with PPB and play a role in division plane orientation

To determine the function of the IQD6, IQD7, and IQD8, we isolated *A. thaliana* mutants carrying T-DNA insertions at the three corresponding loci to analyze cell division phenotypes. Because the proteins are close phylogenetically, have similar domain structures (SF2.1) and expression patterns, and their single mutants do not have noticeable phenotypes, we generated the triple mutant *iqd6/7/8* to overcome redundancy. We first examined the orientation of cell divisions in wild-type Col-0 (WT) and the *iqd6 iqd7 iqd8 (iqd6/7/8)* triple homozygous mutants by staining six days post-

germination (dpg) roots with propidium iodide and imaging them under a confocal microscope (Figure 2.1A). WT root cells divide in regular patterns with the plane of division usually positioned at a region that minimizes the division interface area to yield two daughter cells of equal size, generally perpendicular to the root's growth axis (Figure 2.1B; WT mean 3.704, SD=3.471, n=285 measurements from 8 plants). When observed with the same methods, roots of *iqd6/7/8* mutant exhibited a higher degree of tilted walls (Figure 2.1B; *iqd6/7/8* mean 5.927, SD=7.346, n=343 measurements from 7 plants; WT vs. *iqd6/7/8* adjusted P value <0.0001), primarily affecting lateral root cap and epidermal cell layers (Figure 2.1A, magenta arrows).

We generated complementation constructs containing ~1 kB upstream 5' sequence and genomic regions for *IQD6, IQD7*, and *IQD8* fused to a C-terminus GFP introduced individually into the *iqd6/7/8* mutant. IQD8, IQD6, and IQD7 complementation constructs were able to rescue the division plane defects of *iqd6/7/8* as exemplified here with IQD8-GFP (Figure 2.1B; rescue mean 4.198, SD=3.043, n=177 measurements from 5 plants; rescue vs *iqd6/7/8* adjusted P value <0.001). Extensive phenotypic analysis by a previous study (Kumari et al., 2021) showed that IQD6 and IQD8 can complement the *iqd6/7/8* oblique division plane phenotype and IQD7 alone to a lesser extent.

To determine the subcellular localization of IQD6, IQD7, and IQD8, we analyzed the complementation lines with immunostaining and live imaging (Figure 2.2, SF2.2, and SF2.3). Immunostaining of cells derived from T2 plants showed that IQD8-GFP associates with the PPB (n=50), phragmoplast midline, the CDS, and the cell plate (n=28 phragmoplasts). We observed similar patterns with live-cell imaging (SF2.4).

IQD6-GFP and IQD7-GFP were also observed at the PPB, phragmoplast midline, and cell plate with immunostaining (SF2.2 and SF2.3). However, accumulation at the CDS was inconsistent. We focused our protein manipulations on IQD8 since it showed a higher expression level in the root than the other two paralogs.

Characterization of IQD8 domains

To parse out the contributions of the different domains of AtIQD8, we divided the protein into an N-terminal domain (Met1-Ala88), a central IQ67 domain (Phe87-Ala153), and a C-terminal domain (Gly247-Gly414). We generated constructs carrying the individual N- and C-terminal domains of the IQD8 protein (referred to as IQD8N and IQD8C, respectively) and having the IQ67 domain eliminated (referred to as IQD8ΔIQ) (SF2.5). We inserted these truncated proteins individually into a plasmid with a C-terminal GFP under the Cauliflower mosaic virus (CaMV) 35S promoter. We expressed these constructs transiently in *N. benthamiana* epidermal cells induced into mitosis via over-expression of the G1/S cyclin AtCYCA3;1 (Xu et al., 2020) and imaged them under a confocal microscope. We also transformed these constructs into *A. thaliana* and analyzed T2 plants via immunofluorescent microscopy. A similar over-expression construct for the full-length IQD8 was used as a control in this experiment.

Transient and stable over-expression of the full-length IQD8 led to its accumulation at the PPB, mitotic spindle, and phragmoplast. With immunostaining in *A. thaliana* (SF2.6), we observed IQD8-GFP at the PPB, prophase spindle (n=12 prophase cells), and metaphase spindle (n=2) but less prominently at phragmoplast and absent from the cell plate (n=6). When mitotic tobacco cells were examined by confocal

microscopy (SF2.7), IQD8-GFP was detected at the PPB (n=3), phragmoplast (n=3), cell plate (n=3), and interphase CMTs (n=2). On the other hand, the truncated IQD8ΔIQ-GFP did not localize at the PPB or CDS in both *N. benthamiana* and *A. thaliana* (SF2.8). In *A. thaliana*, we could observe the truncated protein in the cytoplasm during prophase and metaphase (n=13) and at the phragmoplast midline (n=7) during cytokinesis (SF2.8A). In *N. benthamiana* (SF2.8B), IQD8ΔIQ-GFP associated with interphase CMTs (n=15) and inconsistently with phragmoplast MTs (n=3) and the cell plate (n=2). These findings suggest that IQD8's association with the PPB requires an intact IQ domain.

Next, we analyzed the localization of IQD8 N- (IQD8N-GFP) and C-terminal (IQD8C-GFP) domains. With confocal in *N. benthamiana,* we observed that IQD8N-GFP associated with cortical regions of the cell during prophase (n=5), potentially with the PM, and was then observed in the phragmoplast midline and cell plate later in cytokinesis (n=5) (SF2.9A). With immunostaining against GFP of T2 *A. thaliana* lines, we could detect only the phragmoplast midline and cell plate signals (n=4) (SF2.9B). Lastly, we observed IQD8C-GFP along CMTs during interphase (n=6), suggesting that the C-terminal fragment contained a microtubule-binding site (SF2.10). These findings suggest IQD8 may be associated with the PM via the N-terminal and CMTs via the C-terminal domain.

IQD6/7/8 are necessary for proper PPB morphology

The division plane defects of the *iqd6/7/8* mutants prompted us to examine their mitotic and cytokinetic cytoskeletal structures in detail. With anti-tubulin immunostaining

of meristematic root cells of *A. thaliana* undergoing division, we found that PPBs in WT were dense and even-width across the cellular perimeter. At a medial optical section (or nuclear plane) of WT cells, the PPB appeared in two cortical patches of MTs, usually of the same thickness, on either side of the nucleus (n=96; Figure 2.3A and D). As prophase progressed, more MTs accumulated on the nuclear envelope to form the prophase spindle around the nuclear envelope. The PPB is at its densest when the prophase spindle is noticeable.

In comparison, immunostaining of *iqd6/7/8* mutant root cells revealed a variety of PPB morphologies in the mutant (n=128). In about 23% of the cells analyzed in a medial plane, PPB MT density was discernible on only one side of the cell, instead of forming two MT patches at both sides of the nucleus like in WT (Figure 2.3A, B, E - light grey box). About 32% of the cells observed had a more-or-less complete PPB, but the PPB appeared disorganized and of uneven width (Figure 2.3E - dark grey box). 44% of the PPBs were even and showed dense MT accumulation (Figure 2.3E - black box). Unlike previous reports (Kumari et al., 2021), all mutant cells analyzed showed some MTs at the PPB site, albeit disorganized or uneven (Figure 2.3F). To further our analysis and ascertain the unevenness of PPBs in the *iqd6/7/8* mutant, we measured the ratio of the PPB widths at the two sides of the cell in *iqd6/7/8* and WT. The smaller side was always in the numerator to accurately reflect the comparisons. A decrease in mean ratio was observed for *iqd6/7/8* compared to WT (WT mean ratio=0.841, SD=0.135, n=117 cells; *iqd6/7/8* mean ratio=0.581, SD=0.288, n=108 cells; $P<0.001$; Figure 2.3C), suggesting that IQD6/7/8 are crucial for making even PPBs across the perimeter of the cell.

Defective PPBs lead to oblique division planes

To determine how division plane mistakes arose in the *iqd6/7/8* mutant, we imaged the MT reporter *TUB6p:VisGreen-TUB6* in WT and the *iqd6/7/8* mutant (Figure 2.4 and SF2.11). In WT, the PPB is evident from the accumulation of the VisGreen-TUB6 signal at the two edges of the dividing cell in an orientation perpendicular to the growth axis of the root (green arrows in 4A, 0'; n=4). The PPB disappears with the formation of the spindle, and the phragmoplast expands to reach the position previously occupied by the PPB (54'). However, in the *iqd6/7/8* mutant cells, the PPB appeared uneven, with only one side showing some enrichment of MTs (green arrow in 4B, 0; n=18). The phragmoplast expanded directly towards the side that contained a PPB mark (45') but randomly towards the side with no previous PPB landmark. Superposing the images corresponding to the PPB site (Figure 2.4C, green channel) with images at the phragmoplast stage (Figure 2.4C, magenta and yellow channels) allows us to compare the PPB position and the final orientation of the completed division, highlighting the misoriented orientation in *iqd6/7/8.*

MAP65-4 and TANGLED accumulate unevenly at the PPB in *iqd6/7/8*

To determine how *iqd6/7/8* mutations affected the organization of other MAPs at the PPB, we tested the activities of important proteins for cytokinesis like MT ASSOCIATED PROTEIN 65-4 (MAP65-4) and TANGLED (TAN1). MAP65-4 belongs to the conserved MAP65/Ase1/PRC1 family of proteins that contribute to cell cycle-dependent MT bundling. AtMAP65-4 accumulates at the PPB and CDS, but specific functions during cytokinesis are unknown (Li et al., 2017). TAN1 accumulates at the

PPB and CDS, contributing to CDS maintenance after PPB disassembly and during cytokinesis (Mills et al., 2022). When expressed under the control of their native promoters in their respective mutants, MAP65-4-GFP and TAN1-GFP decorated PPB MTs evenly (Figure 2.5A, E). In WT, most of the observed cells (97%) showed an even accumulation of MAP65-4 at the two lateral faces of the cell in medial sections (total n=59; SF2.12A), which colocalized with PPB MTs. All TAN1-GFP cells counted showed an even accumulation of GFP at the cortex, matching the localization of PPB MTs (n=30; SF2.12B). In addition to observing cells laterally, we could observe that the MAP65-4 and TAN1 signals decorated PPB MTs and formed complete rings at the cell cortex when viewed from the top (n=8 for MAP65-4 and 6 for TAN1; Figure 2.5C and 2.5G).

In the *iqd6/7/8* mutant, the MAP65-4-GFP signal at the PPB often appeared incomplete and disorganized. While 57% of cells showed MAP65-4 in two even patches resembling WT localization, 23% of cells counted showed signal on one face of the cell only corresponding to one-sided PPBs, and 30% of cells had very wide MAP65-4 patches (total n=73; Figure 2.5B and SF2.12A). These differences were also noticeable when the cell was observed in the top view (n=12; Figure 2.5D), highlighting the uneven accumulation of MAP65-4-GFP across the cell's perimeter.

The TAN1 localization patterns at the PPB in the *iqd6/7/8* mutant cells were similar to MAP65-4's, with 20% of cells showing TAN1-GFP on one side of the cell only, 30% with expanded patches of fluorescence, and 50% with even accumulation of fluorescence on both sides of the cell (total n=62; Figure 2.5F and SF2.12B). From the top view, in cells with incomplete PPBs, the TAN1-GFP ring also appeared incomplete

(n=12; Figure 2.5H). Together, MAP65-4's and TAN1's uneven localization patterns at the PPB site pointed to the critical role of IQD6/7/8 in setting up these factors by organizing PPB MTs.

The defective distribution of CDS proteins is associated with discontinuous cortical division sites in the *iqd6/7/8* mutant

In WT, MAP65-4 and TAN1 remained at the CDS after PPB disassembly and when cells formed spindles and phragmoplasts (Figure 2.6A and 2.6B), with TAN1 playing a crucial role in CDS maintenance during cytokinesis. We focused on cells at the spindle and phragmoplast stages when the CDS had been specified previously by the PPB to explore how the lack of IQD6/7/8 affected CDS specification.

In WT, most cells (87%) show even MAP65-4 patches on both edges of the cortex in medial sections (total n=52; Figure 2.6A; SF2.13A). In contrast, at the same plane, only 13% of *iqd6/7/8* cells expressing MAP65-4-GFP showed even signals on the two sides of the cell (total n=60; SF2.13A). Most cells (56%) exhibited uneven accumulation at only one side of the cell (Figure 2.6B*)*. The signal patches were expanded and uneven in 27% of cells, and no cortical signal was detected in 8% of cells (SF2.13A). In WT, MAP65-4 also accumulated on phragmoplast MTs and became more conspicuous in the phragmoplast midline (Figure 2.6A, arrowhead). This localization did not change in *iqd6/7/8* (Figure 2.6B and SF2.13A, arrowheads). From the top view, MAP65-4 accumulated in a distinct dot-like pattern around the entire cell's circumference (n=8; Figure 2.6C); however, the signal was sporadic and incompletely circumvented the cell perimeter in *iqd6/7/8* (n=19; Figure 2.6D).

From a lateral view of WT cells, we observed that during mitosis and cytokinesis, TAN1 accumulated in clear foci at the cell cortex in a midplane position (n=40; Figure 2.6E). The top view showed that TAN1-GFP decorated the entire cell circumference in WT (n=13; Figure 2.6G). In *iqd6/7/8*, however, about 20% of the observed mutant cells showed TAN1-GFP at only one face of the cell (total n=82; Figure 2.6F), and 34% showed expanded patches of TAN1-GFP at the CDS (SF2.13B). About 48% of cells showed even patterns of TAN1 accumulation at the two sides of the CDS (SF2.13B). From the top view, the TAN1 signal appeared as an incomplete ring around the cell's circumference (n=41; Figure 2.6H).

To discern how defects in PPB might have impaired the CDS pattern, we performed time-lapse imaging to observe the dynamics of MAP65-4-GFP and TAN1-GFP in WT and the i*qd6/7/8* mutant live cells. In WT by confocal imaging, MAP65-4-GFP was noticeable at the PPB (Figure 2.7A, yellow arrows in 0', n=3) and the spindle and phragmoplast midline (12'+). Its localization at the CDS was challenging to capture consistently due to the sensitivity of the confocal microscope. However, in *iqd6/7/8,* the MAP65-4-GPF signal was observed in disorganized patterns around the cell during the PPB stage (Figure 2.7B, yellow arrows in 0', SF2.14, n=3), with the PPB signal appearing one-sided and dim when compared to WT, and sometimes appearing aggregated and disorganized. Consequently, the phragmoplast expands with a slant in *iqd6/7/8*, unlike in WT, where it could begin at a slant but corrects to reach the location marked by the PPB.

We observed TAN1-GFP under the same conditions under confocal microscopy. At the PPB stage in WT, TAN1-GFP appeared as two foci at either side of the nucleus,

which also showed prominent TAN-1-GFP signal (Figure 2.8A, magenta arrows 0'; n=3). Although we lacked a MT-marker in these lines, it is evident that TAN-1 remained at the CDS throughout mitosis and cytokinesis. TAN1 became visible again in the nucleoplasm during cytokinesis as the two daughter cell nuclei reformed (42'). In the *iqd6/7/8* mutant, only one focus of TAN1 was observed on one side of the cell and remained visible throughout the completion of mitosis and cytokinesis, while the side unmarked during prophase did not recover TAN1-GFP signal at later stages (Figure 2.8B and SF2.15; n=5). The nuclear TAN-1 signal remained unchanged in the *iqd6/7/8* mutant.

These results indicate that IQD6/7/8 are necessary for accurately depositing PPB proteins that demarcate the CDS, such as MAP65-4 and TAN1. Time-lapse imaging confirmed our immunostaining results that with the loss of proper PPB patterning and CDS specification, signals that orient the phragmoplast during cytokinesis became disorganized.

Simultaneous loss of CLASP and IQD6/7/8 leads to PPB absence

Elimination of IQD6/7/8 proteins was not sufficient to entirely prevent PPB formation. Other cytoskeletal regulators might play synergistic roles in MT organization for PPB formation. We turned to the CLASP (CLIP170-associated protein), a plus-end tracking MT-polymerase protein with structural similarity with XMAP215/chTOG proteins thought to promote MT stability at cell geometric edges (Ambrose et al., 2011). CLASP associates with the PPB (Kirik et al., 2007) and was suggested to contribute to the formation of robust PPB as its mutant showed widened PPBs (Ambrose et al., 2007).

We generated *clasp iqd6/7/8* quadruple mutants by a standard genetic cross between the *clasp* and *iqd6/7/8 A. thaliana* mutants. While *iqd6/7/8* mutant plants grow similarly to the WT control grown under the same conditions, the *clasp* mutant appears dwarfed. The *clasp iqd6/7/8* quadruple mutant plants looked like the *clasp* mutant in overall stature but not leaf morphology. Leaves in the quadruple *clasp iqd6/7/8* mutant appeared smoother and more elongated than the *clasp* mutant alone (Figure 2.9A and 2.9B).

We analyzed the division plane orientation in *clasp iqd6/7/8* mutants and found a higher degree of tilted walls than the individual *iqd6/7/8* and *clasp* mutants compared to the WT roots (Figure 2.9C and 2.9D; WT and *iqd6/7/8* values are the same as Figure 2.1 B; *clasp* mean=4.281, n=201 measurements from 7 plants, SD= 3.460; *clasp iqd6/7/8* mean=7.819, n=279 measurements from 6 plants, SD=10.128). This observation prompted us to analyze cytokinetic structures in detail in *clasp iqd6/7/8* mutants. With immunostaining, we found that most cells of the *clasp* mutant possessed even, two-sided PPBs (88%; total n=96, Figure 2.9E and 2.9F). However, in the *clasp iqd6/7/8* quadruple mutant, only 25% showed complete PPBs resembling those seen in WT cells (compared to 44% in *iqd6/7/8* alone; total n=128, Figure 2.9E and 2.9F). A new, PPB-less class of cells was evident in this population, with 20% of cells counted showing no PPB MTs. 54% of cells had abnormal PPBs, 16% had one-sided PPBs, and 38% had disorganized PPBs with uneven width. Cells that completely lacked PPBs also showed hyperaccumulation of MTs at the nuclear envelope (Figure 2.9E), as observed in previous PPB-less mutants (Schaefer et al., 2017). This data suggests that CLASP

and IQD6/7/8 play synergistic roles in PPB MT stability to form a stable and complete PPB ring.

Discussion

This study investigated the PPB of MTs in *A. thaliana* by analyzing proteins involved in its formation and the mechanism of division plane determination. Our results showed that IQD6/7/8 are necessary to form robust PPBs that specify the division plane. Defective PPBs formed in the *iqd6/7/8* mutant failed to define a precise and narrow CDS, which led to slanted divisions. IQD6/7/8-dependent organization of the PPB MTs directs the accumulation patterns of PPB- and CDS-proteins, like MAP65-4 and TAN1. Therefore, the mis-patterning of PPBs resulted in altered localization of CDS proteins. Lastly, our study reveals the synergistic contributions of plant-specific IQD6/7/8 proteins and the evolutionarily conserved CLASP protein in PPB formation and integrity.

While PPBs were not entirely absent in *iqd6/7/8,* these mutations compromised PPB organization and stability. This observation leads to questions about how protein networks at the PPB coordinate their functions to organize the PPB MT array. Interestingly, we demonstrate that the PPB often was abolished entirely in *clasp iqd6/7/8* quadruple mutants. While previous studies suggested *clasp* mutants showed PPBs of uneven thickness, we found that only a small fraction of cells in *clasp* showed altered PPBs. Indeed, division plane patterns in *clasp* roots are similar to those in WT. Since the *iqd6/7/8* mutant PPBs are already weakened, removing CLASP enhanced the

phenotype of defective or lacking PPBs. These results revealed an unexpected cooperative function of IQD6/7/8 and CLASP in stabilizing PPB MTs.

Future experiments are needed to determine how the phragmoplast is oriented in PPB-less cells of the *clasp iqd6/7/8* quadruple mutant. Time-lapse imaging of mitotic and cytokinetic cytoskeletal structures in the quadruple mutant and analysis of division plane placement examining CDS protein localization could begin to answer this question. It would also be interesting to explore the expression of CLASP in the *iqd6/7/8* mutant to determine whether CLASP localization at the PPB depends on IQD6/7/8. More experimentation is needed to ascertain whether these proteins interact physically.

IQD proteins are known to be associated with the PM through basic residues in their N terminal domains (Sugiyama et al., 2017; Feng et al., 2022). A study found that IQD13 stabilizes CMT patterns during xylem vessel development to restrict Rho GTPase domains in secondary cell wall pit formation (Sugiyama et al., 2017). We hypothesize that IQD6/7/8 may interact with the PM and PPB MTs to confine the PPB-designated areas and CDS factors to determine the division plane. We have evidence that the IQD8 N-terminal segment localized to the PM, phragmoplast midline, and cell plate when overexpressed in *N. benthamiana*, while the C-terminal segment may interact with MTs. Therefore, IQD6/7/8 may be acting by anchoring MTs to the PM and directing PPB orientation.

What determines IQD6/7/8 localization? We demonstrated that removing the IQ domain from IQD8 eliminated its cell cycle-dependent PPB localization, suggesting Ca^{2+}/CaM binding possibly regulates IQD6/7/8 localization at the PPB for PPB MT stability. A recent study showed that Ca^{2+} spikes at the division site accompany

cleavage furrow ingression and cell separation in the fission yeast *Schizosaccharomyces pombe* (Poddar et al., 2021). While confidently detecting changes of free Ca^{2+} during plant cell division has remained a challenge with classical Ca^{2+} probes, this does not exclude the possibility that undetected local changes in Ca^{2+} concentration occur and may be significant for localization of IQD6/7/8 during PPB formation and CDS establishment.

In conclusion, this study provides evidence for the cell cycle-dependent role of IQD6/7/8 in organizing PPB MTs. More interestingly, these IQD proteins function synergistically with the MT polymerase CLASP. CLASP is one of the key regulators of MT dynamics, and its loss causes aberrant MT bundling and organization of both interphase and mitotic arrays, e.g., PPBs with nonuniform width and MT density (Ambrose et al., 2007; Kirik et al., 2007). In contrast, IQD6/7/8 associate specifically with PPB MTs and the phragmoplast midzone, and the triple mutant shows PPBs with sparse MTs (Kumari et al., 2021 and this study). So, the frequent disappearance of the PPB array shown here indicated that multiple MT stabilizing factors contributed to PPB MT organization in both cell cycle-dependent and independent manners that act on PPB MTs specifically or on all dynamic MTs, respectively. The synergistic functions of CLASP and IQD proteins are important for division plane determination during cell division simply because of their contributions to MT organization in *A. thaliana*. CLASP exhibits an MT plus end-tracking activity, but IQD proteins localize along microtubules. It would be interesting to analyze whether their localizations were reciprocally dependent on each other and whether there is a direct interaction between IQD and CLASP in vivo. Collectively, our data supports the model of PPB function, where this structure

determines the localization of the division plane by assembling multiple protein players at an appropriate CDS position that guides centrifugal expansion of the phragmoplast during cytokinesis. Without the PPB due to the simultaneous loss of CLASP and IQD6/7/8, plant cells lose control of division plane specification, which impacts overall plant growth and development.

Materials and Methods

Plant Materials and Growth Conditions

The *Arabidopsis thaliana* plants used in this study include control WT (Col-0) plants, *iqd6/7/8, clasp, map65-4,* and *clasp iqd6/7/8*. The homozygous *iqd6, iqd7,* and *iqd8* mutant plants were isolated from the seed stocks SALK_137365 (*iqd6),* SALK_025224 *(iqd7),* and SALK_107689C *(iqd8)* from the *Arabidopsis* Biological Research Center (ABRC) at Ohio State University in Columbus, Ohio, USA. Standard genetic crosses were carried out to give rise to the homozygous *iqd6/7/8* triple mutant. The *clasp* mutant was isolated from the seed stock of CS1001270 (SK5266) at ABRC. The *clasp iqd6/7/8* quadruple mutant was created by crossing *clasp* and *iqd6/7/8* mutant. The primers used for genotyping are listed in Table S2.1. The LP and RP primer pairs were used for detecting the WT allele of the corresponding genes, while the LBb1.3 and SKTAIL1 were used for detecting the insertional mutations of the SALK and SK lines, respectively, when paired with the RP primers. WT Col-0 plants were used as the negative control. The *map65-4* mutant was previously described (Li et al., 2017).

All plants were grown in growth chambers at 21°C with 16-h light and 8-h dark cycles. When grown on plates, sterilized seeds were placed on solid media containing 1/2 Murashige & Skoog salt mixture.

Plasmid construction

The genomic fragments of *AtIQD6 (*AT2G26180.1*), AtIQD7* (AT1G17480)*, and AtIQD8* (AT1G72670), including ~1kb of 5' non-coding regions, were amplified using primer pairs of IQDx_FWD and IQDx_FWD (Table S2.1, x meaning 6, 7, or 8) with Phusion DNA polymerase (Thermo Fisher). The PCR products were cloned into pDONR207 by BP clonase reaction to give rise to the *pENTR-IQDx* plasmids. These plasmids were used for recombination by LR reaction with the destination vector pGWB4 to generate the binary vectors for expression in plants.

The *pJL414_MAP65-GFP* vector uses the reporter *MAP65-4p:MAP65-4-GFP (Li et al., 2017)* and the MT marker *TUB6p:mCherry-TUB6 (Liu et al., 2019)* combined on the same vector.

The TAN1 expression vector was made by first amplifying the genomic fragment of *AtTAN1* (AT3G05330) using vectors TAN1_FWD and TAN1_REV for cloning into pENTR/D-TOPO to make *pENTR_TAN1*. This plasmid was used for recombination by LR reaction with the destination vector pGWB650 to give rise to the expression vector.

All other plasmids containing IQD8 and modifications were prepared using IQD8 coding region sequences. The coding region of IQD8 was amplified from *A. thaliana* cDNA using vectors IQD8_CDS_FWD and IQD8_CDS_REV for cloning into pENTR/DTOPO. The resulting *pENTR_IQD8_CDS* plasmid was used for recombination

by LR reaction with the pGWB605 vector as the destination to make *pGWB605_35S:IQD8-GFP. pGWB605_35S:IQD8ΔIQ-GFP* vector was created by amplifying the coding sequence of IQD8 without the IQ domain from the *pENTR_IQD8_CDS* plasmid using primers IQD867D_FWD and IQD867D_REV with complementary sequences for Gibson reaction and the Phusion DNA polymerase. The purified amplicon was re-circularized by the Gibson reaction. This resulting plasmid was recombined with the destination vector pGWB605 by LR reaction to give rise to the final expression vector.

pGWB605_35S:IQD8N-GFP and *pGWB605_35S:IQD8N-GFP* were prepared similarly, first by amplification with primers IQD8N_FWD and IQD8N-REV and IQD8C_FWD and D-prom-R1_REV, respectively, with the Phusion enzyme. Then, the purified amplicons were re-circularized using Gibson reaction.

Plant transformation

Constructs for the expression of all fusion proteins were delivered into *A. thaliana* with corresponding genotypes via *Agrobacterium*-mediated transformation using the standard floral dipping method (Clough & Bent, 1998). Transgenic plants were selected according to antibiotic markers carried by respective vectors. The legend of each figure indicates what transformant generation was analyzed for each experiment. At least 2-3 different T2 lines were analyzed for each line.

Constructs for the transient expression of fusion proteins were delivered into WT *N. benthamiana* via *Agrobacterium*-mediated transformation concomitant with the overexpression of CYCD3;1 and a MT reporter (*TUB6p:mCherry-TUB6*) to study their

expression in mitotic cells like previously described (Xu et al., 2020). All counts presented for *N. benthamiana* images correspond to cell counts from >2 infiltrated plants.

Production of cells for immunostaining

To obtain and visualize meristematic root cells, ~10mg of *A. thaliana* seeds were plated and grown for 5-6 days. Seedlings were fixed on-plate for 45 minutes (first 5 minutes in a vacuum) in freshly prepared 4% paraformaldehyde in PME buffer (0.05 M PIPES buffer, pH 6.9, 1 mM $MgSO_4$, and 5 mM EGTA), rinsed several times in PME, and partially digested for 25 min in 1% cellulase solution in the PME buffer. After rinsing with PME several times, root tips were cut off individually to isolate meristematic cells and placed on glass slides coated with 0.2% chromium potassium sulfate and gelatin. Individual cells were released into solution by gently squashing the excised root tips onto slides. After air-drying and rehydrating with PME, cells were treated with 0.5% Triton X-100 in PME for 15-30min and washed. Cells were treated with methanol at -20ºC for 15-30min, then rehydrated in phosphate buffer saline (PBS).

Cells were stained first with the primary and second with the secondary antibody combinations described in Table S2.2 diluted 100-fold in 1XPBS and 3% BSA. Cells were mounted in SlowFade containing DAPI (4’6-diamidino-2-phenylindole) for visualizing DNA.

All counts presented for immunostaining images correspond to cell counts from >50 T2 plants.

Immunostaining of WT Arabidopsis cells expressing *35S:GFP* was used as control for immunostaining all experiments (SF2.16).

Microscopy

An Axio Observer inverted microscope equipped with the LSM710 laser scanning confocal module with standard settings for eGFP and mCherry (Carl Zeiss) and a 40x C-Plan (water) objective were used for live-cell imaging. For division plane counting, the roots of 5dpg (days post germination) seedlings were stained with propidium iodide (PI, 0.2 µg/mL stock) and mounted in water. For timelapses, plants were grown in Petri dishes with coverslip bottoms and observed directly on the microscope. For *N. benthamiana* observations, a leaf disc from the infiltrated leaf area was mounted in water. Images were acquired using the ZEN software (Carl Zeiss) and processed in ImageJ/Fiji (www.imagej.nih.gov/ij).

Fixed and stained root cells were observed by using an Eclipse 600 epifluorescence microscope with a Plan-Fluor 100x objective (Nikon). Images were acquired with an OptiMOS sCMOS camera (Photometrics) controlled by µManager software package (Edelstein et al., 2014).

Quantifications

Division plane quantification was performed in FIJI with images of PI-stained roots. Then, line ROIs were used to calculate the angle. The absolute values were plotted.

Fluorescence intensity profiles of PPB MTs (Figure 2.1) were made by drawing a 3-pixel wide line in FIJI that traced the cell periphery (SF2.17). Immunofluorescence

signal was normalized by measuring five separate regions at the cortex, using cytoplasmic and regions without cells as the background. Mean intensity was measured with FIJI and averaged to get a single value for background per cell. The fluorescence signal at each position along the line scan was divided by the background value before being plotted.

PPB phenotypes in WT, *iqd6/7/8,* and *clasp iqd6/7/8* were determined from immunofluorescence images from 5dpg plants. PPB presence/absence was scored based on fluorescence accumulation at the cortex.

Statistics

All statistics were performed using GraphPad Prism version 10.0.0 for Mac (GraphPad Software, Boston, Massachusetts USA, www.graphpad.com).

Figures

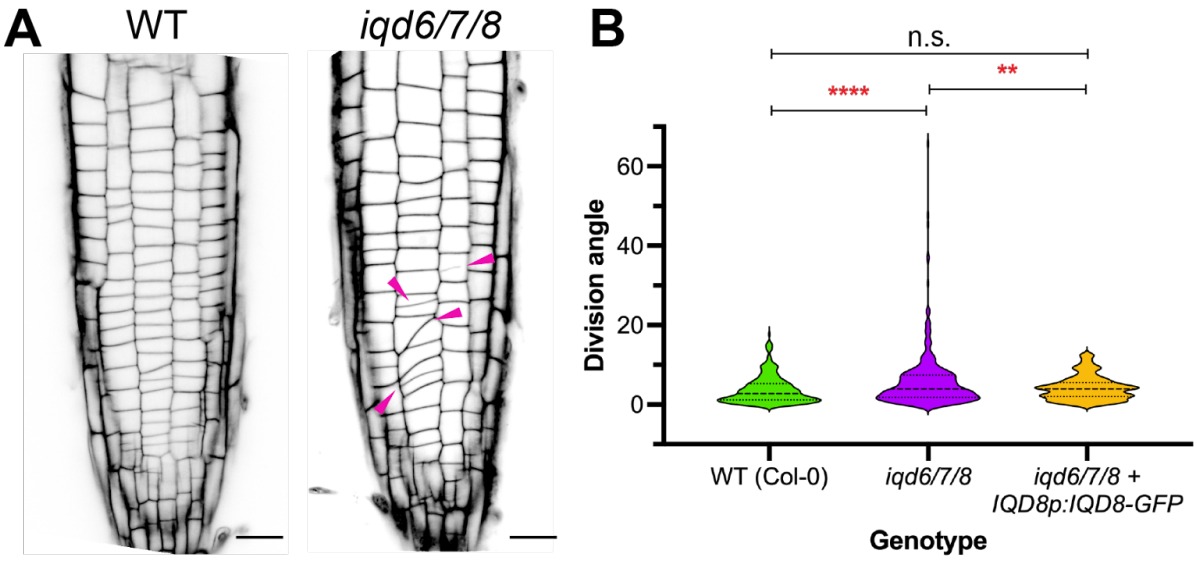

Figure 2.1. – IQD6/7/8 are required for division plane orientation
(A). Propidium iodide staining of wild type (WT) and *iqd6/7/8* roots at 6dpg observed under a confocal microscope. Magenta arrows mark oblique division planes. Scale bars = 20µm.
(B). Quantification of division plane angles in WT (Col-0), *iqd6/7/8,* and rescue (*iqd6/7/8 + IQD8p:IQD8-GFP*). The values for division angle indicate angles measured from a line perpendicular to the root growth axis. WT (green) mean=3.704 and SD=3.471 (n=285 measurements from 8 plants). *iqd6/7/8* (purple) mean=5.927 and SD=7.346 (n=343 measurements from 7 plants). Rescue (yellow) mean=4.198 and SD=3.043 (n=177 measurements from 5 plants). In the violin plot, the dashed line indicates the median; dotted lines represent the upper and lower quartiles. n.s.=not significant; **=p<0.001; ****=p<0.0001 (based on One-way ANOVA followed by Šídák's multiple comparisons test).

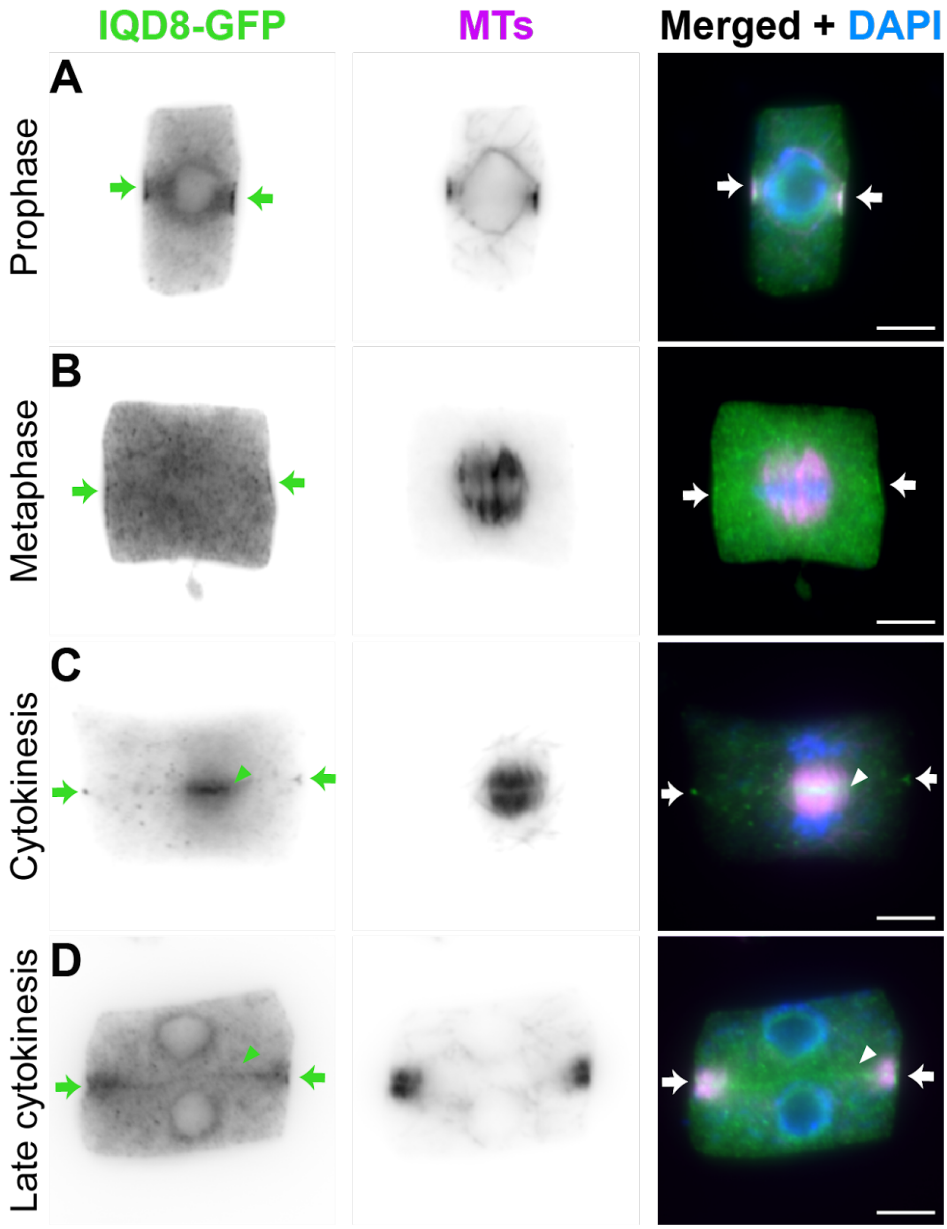

Figure 2.2. – IQD8's localization during mitosis and cytokinesis
Immunolocalization of IQD8-GFP with MTs as reference during mitosis and cytokinesis in T2 plants of *iqd6/7/8* expressing *IQD8p:IQD8-GFP*. The merged images show IQD8-GFP in green, MTs in magenta, and DNA in blue.
(A). IQD8 labeled the PPB during late G2 and prophase (n=50).
(B). In metaphase, some signal was detected at the CDS (arrows). Accumulation with DNA was inconsistent (n=13).
(C). During early cytokinesis. IQD8-GFP remained at the CDS (arrows) and was also apparent at the phragmoplast midline (arrowhead).
(D). IQD8-GFP was observed in the cell plate in late cytokinesis (arrowheads; n=28 for early and late phragmoplasts). Scale bars = 5μm.

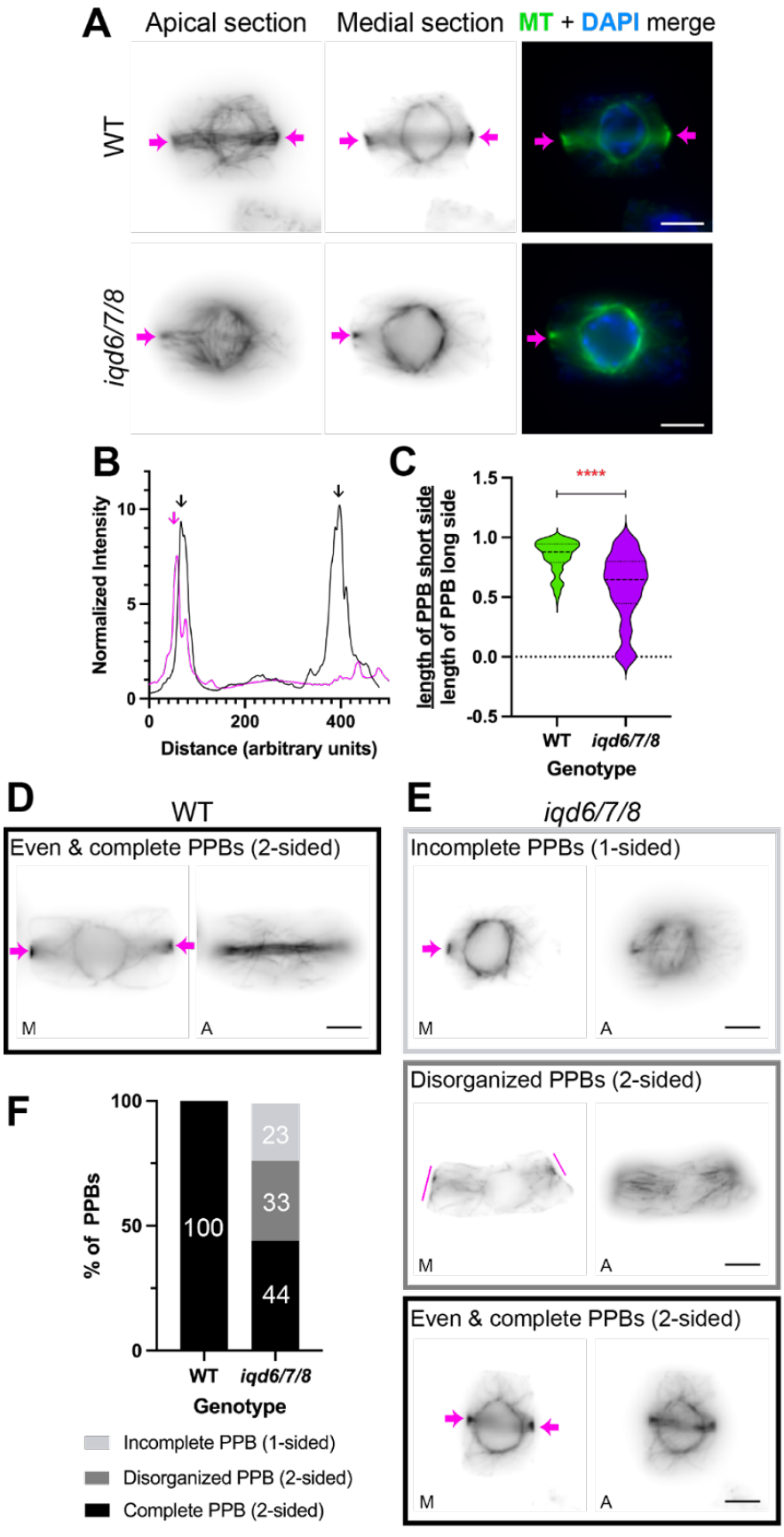
A
Apical section
Medial section
MT + DAPI merge
WT
iqd6/7/8
B
Normalized Intensity
Distance (arbitrary units)
C
length of PPB short side
length of PPB long side
****
WT
iqd6/7/8
Genotype
D
WT
Even & complete PPBs (2-sided)
M
A
E
iqd6/7/8
Incomplete PPBs (1-sided)
Disorganized PPBs (2-sided)
Even & complete PPBs (2-sided)
F
% of PPBs
100
23
33
44
Incomplete PPB (1-sided)
Disorganized PPB (2-sided)
Complete PPB (2-sided)

Figure 2.3. – IQD6/7/8 are needed to make complete and uniformly bundled PPBs
(A). Anti-tubulin immunostaining of WT and *iqd6/7/8* root cells at the PPB stage. Magenta arrows highlight PPBs.
(B). Line scan along the cell cortex of the dividing cells shown in (A) showing fluorescence intensity of MTs. The black line corresponds to WT, and the magenta to *iqd6/7/8.* The arrows indicate the position of the PPB.
(C). Quantification of PPB length ratio (ratio of the length of the short side of PPB to the length of the longer side). WT mean=0.8412 and SD=0.135 (green; n=117 cells). *iqd6/7/8* mean=0.5809 and SD=0.288 (purple; n=108 cells). ****=p<0.0001 (based on unpaired t-test).
(D-F) Quantification of PPB morphology in WT and *iqd6/7/8* **(F)**, with example cells per category shown in panels **(D-E).** PPBs were classified based on the even accumulation of MTs on either side of the cell using immunostained images of WT (n=96) and *iqd6/7/8* (n=128). Magenta arrows and lines highlight MTs). M = medial plane; A = apical plane. Scale bars = 5μm.

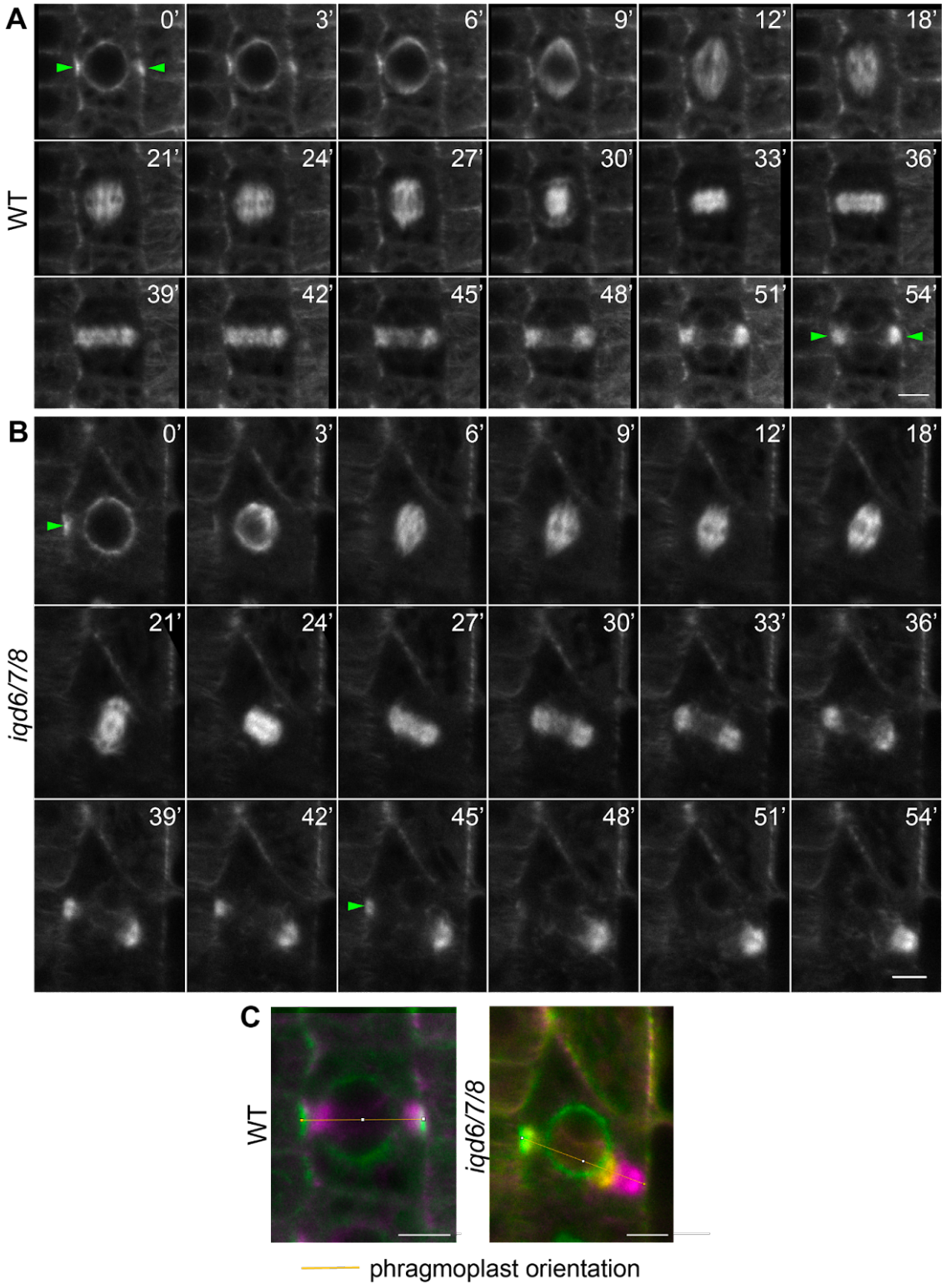

Figure 2.4. – Incomplete PPBs lead to slanted phragmoplast expansion
Timelapse confocal imaging of symmetric cell division in T2 plants of the WT **(A)** and *iqd6/7/8* **(B)** roots expressing *TUB6p:VisGreen-TUB6* to visualize MTs. Photographs

were taken at 3-minute intervals, with the time (in minutes) noted in the top right of each image. Green arrows mark the initial PPB position. The PPB marked two sides in WT (n=4) and only one in *iqd6/7/8* (n=18). The phragmoplast expanded to reach these sites. **(C).** PPB and final phragmoplast orientation for respective genotypes. Overlap of images corresponding to T=0' (green), T=54' in magenta, and T=45' in yellow (for *iqd6/7/8* only) from time-lapses shown in (A) and (B). Scale bars = 5µm.

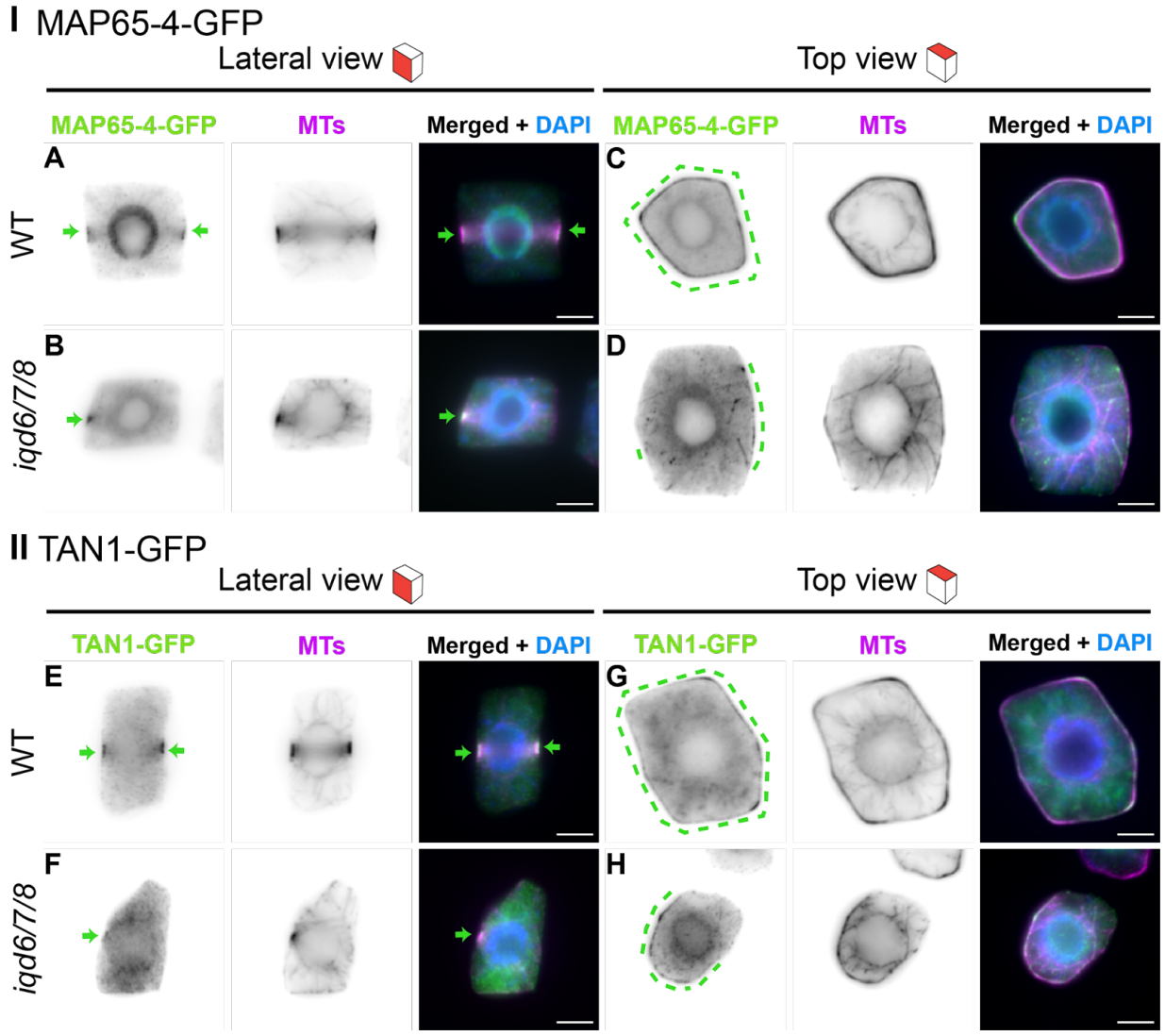

Figure 2.5. – Accumulation of PPB proteins is defective in *iqd6/7/8*
I. Immunolocalization of MAP65-4-GFP with MTs as reference at the PPB stage in T3 plants of WT **(A)** and *iqd6/7/8* **(B)** expressing *MAP65-4p:MAP65-4-GFP*. The merged image shows MTs in magenta, MAP65-4-GFP in green, and DNA in blue. *iqd6/7/8* showed uneven signal accumulation that co-localized with PPB MTs. SF10A shows

quantifications. Top views of WT (n=8) **(C)** and *iqd6/7/8* (n=12) **(D)** highlight uneven accumulation of MAP65-4 at the PPB.
II. Immunolocalization of TAN1-GFP with MTs as reference at the PPB stage in T3 WT **(E, G)** and *iqd6/7/8* **(F, H)** plants expressing *TAN1p:TAN1-GFP*. The merged image shows MTs in magenta, TAN1-GFP in green, and DNA in blue. Uneven accumulation of TAN1-GFP was observed in the *iqd6/7/8* mutant compared to WT control. SF10B shows quantifications. Incomplete accumulation of TAN1-GFP on imperfect PPBs was evident from top views in *iqd6/7/8* cells (n=12) when compared to the WT cells (n=6) **(G, H)**. Scale bars = 5µm.

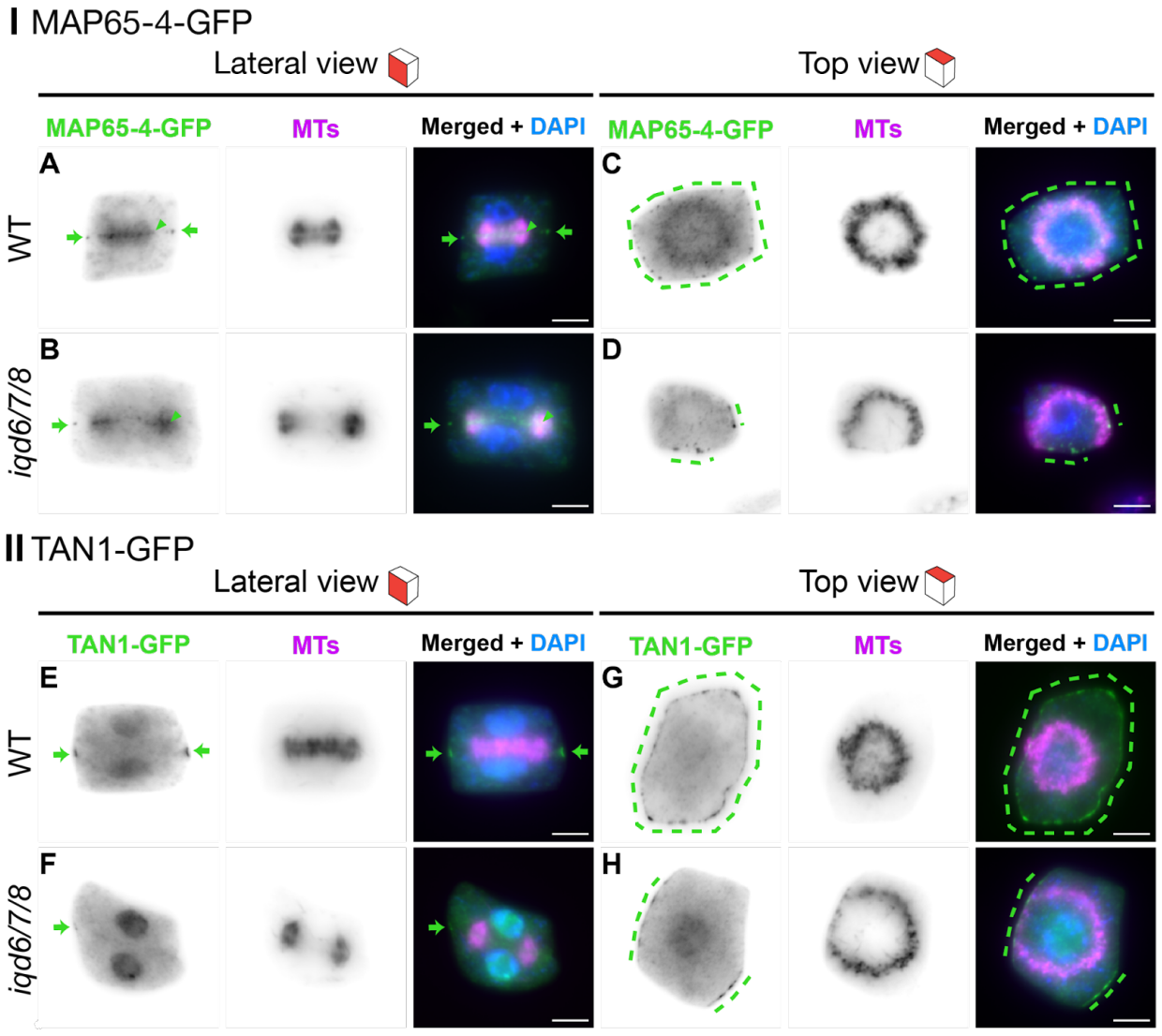

Figure 2.6. – The CDS is incomplete in *iqd6/7/8*

I. Immunolocalization of MAP65-4-GFP with MTs as reference during cytokinesis in T3 plants of WT **(A)** and *iqd6/7/8* **(B)** expressing *MAP65p:MAP65-4-GFP*. The merged image shows MTs in magenta, MAP65-4-GFP in green, and DNA in blue. Lateral views of MAP65-4-GFP in WT and *iqd6/7/8* (I) show uneven signal accumulation in *iqd6/7/8.* SF11A shows quantifications. Top views of WT (n=8) **(C)** and *iqd6/7/8* (n=19) **(D)** showed complete and incomplete deposition of MAP65-4-GFP at the CDS in WT and *iqd6/7/8*, respectively.

II. Immunolocalization of TAN1-GFP with MTs as reference during cytokinesis in T3 plants of WT **(A)** and *iqd6/7/8* **(B)** expressing *TAN1p:TAN1-GFP*. The merged image shows MTs in magenta, TAN1-GFP in green, and DNA in blue. Unlike the even TAN-1 signal in WT **(E)**, uneven accumulation of TAN1-GFP was observed in the *iqd6/7/8* **(F)**. SF11B shows quantifications. **(G)** and **(H)** correspond to top views of WT (n=13) and *iqd6/7/8* (n=41), respectively. While the WT cell showed a regular appearance of TAN1-GFP across the cell perimeter, the *iqd6/7/8* cell displayed irregular accumulation of TAN1-GFP at the CDS. Scale bars = 5μm.

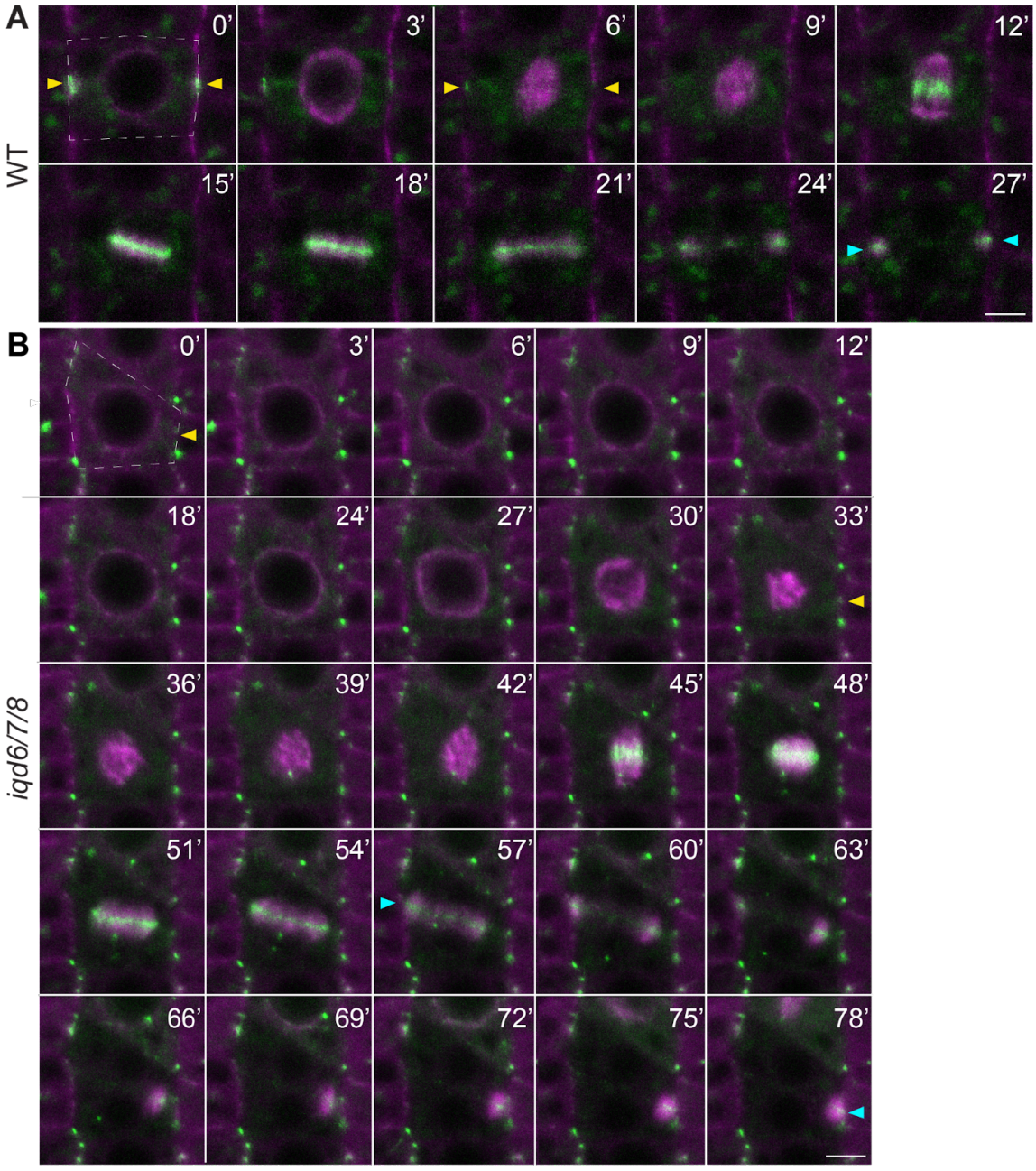

Figure 2.7 – The CDS is incomplete in *iqd6/7/8*

Timelapse confocal imaging of *MAP65-4p:MAP65-4-GFP* (green signal) and *TUB6p:mCherry-TUB6* (magenta signal) in WT **(A)** and *iqd6/7/8* **(B)** T2 plants. Photographs were taken at 3-minute intervals, with the time (in minutes) noted in the top right of each image. Yellow arrows mark MAP65-4-GFP accumulation at the PPB (0’) and CDS (6’). Cyan arrows mark the location at the parental cell wall reached by the phragmoplast. While the MAP65-4-GFP signal at the CDS was not as evident as at the PPB in this video, the WT phragmoplast reached the site marked by the PPB-localized MAP65-4-GFP (n=3). In the *iqd6/7/8* cells (n=3), only one side showed some MAP65-4-

GFP accumulation (yellow arrowhead, 0'), which was evident until the end of cytokinesis (blue arrowhead, 33'). The phragmoplast was slanted, leading to an oblique cell plate. Scale bars = 5µm.

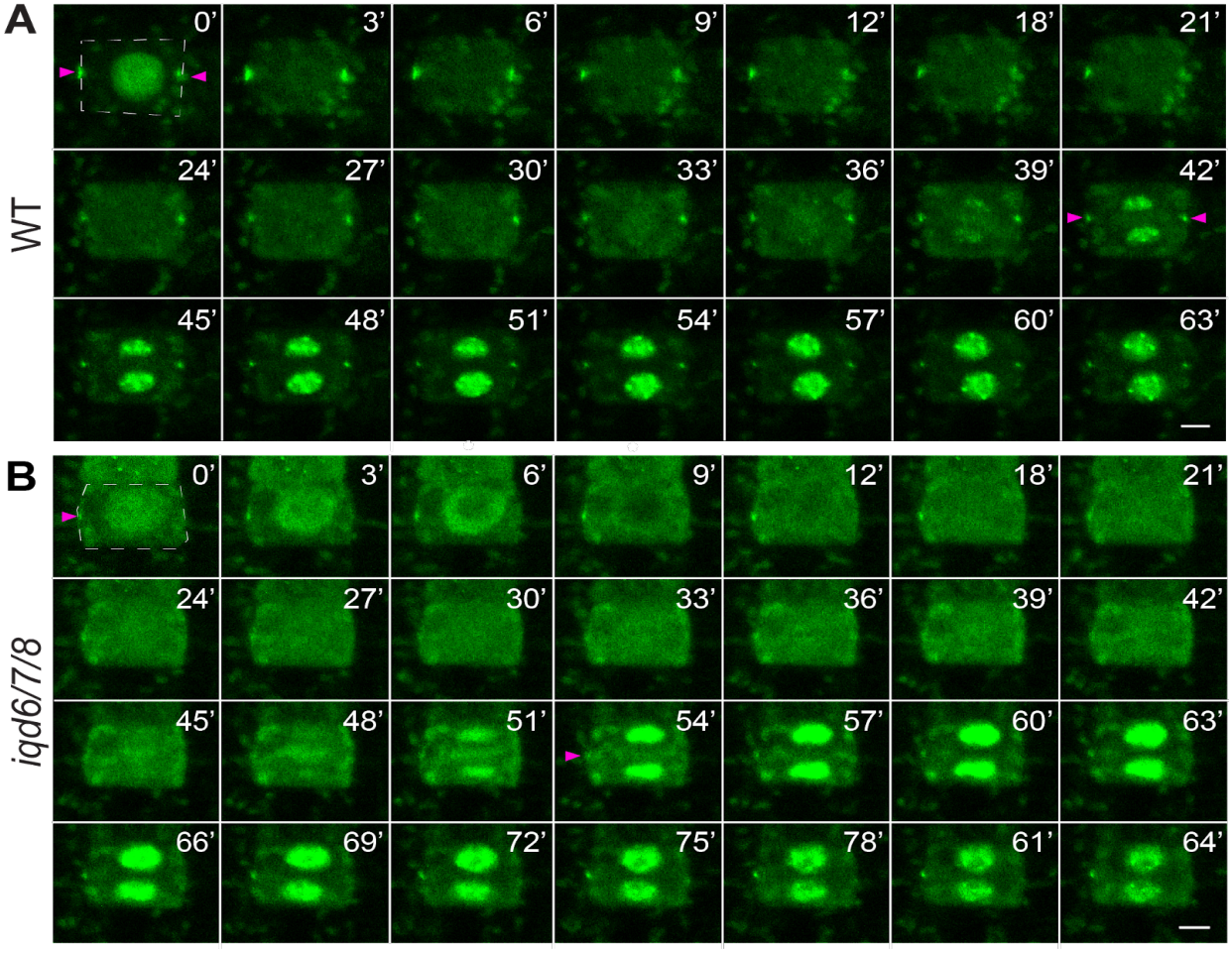

Figure 2.8. – The CDS is incomplete in *iqd6/7/8*
Timelapse confocal imaging of *TAN1p:TAN1-GFP* in WT **(A)** and *iqd6/7/8* **(B)** T2 plants. Photographs were taken at 3-minute intervals, with the time (in minutes) noted in the top right of each image. Magenta arrows mark TAN1-GFP accumulation at the PPB (0') and CDS during cytokinesis (41'). WT cells showed TAN1-GFP at the two lateral faces of the dividing cell and the nucleus right before nuclear envelope breakdown (n=3). In the *iqd6/7/8* cell, only one side showed some TAN1-GFP accumulation (0'-6'), and this signal remains at the CDS (54') on only one side of the cell (n=5). Scale bars = 5 µm.

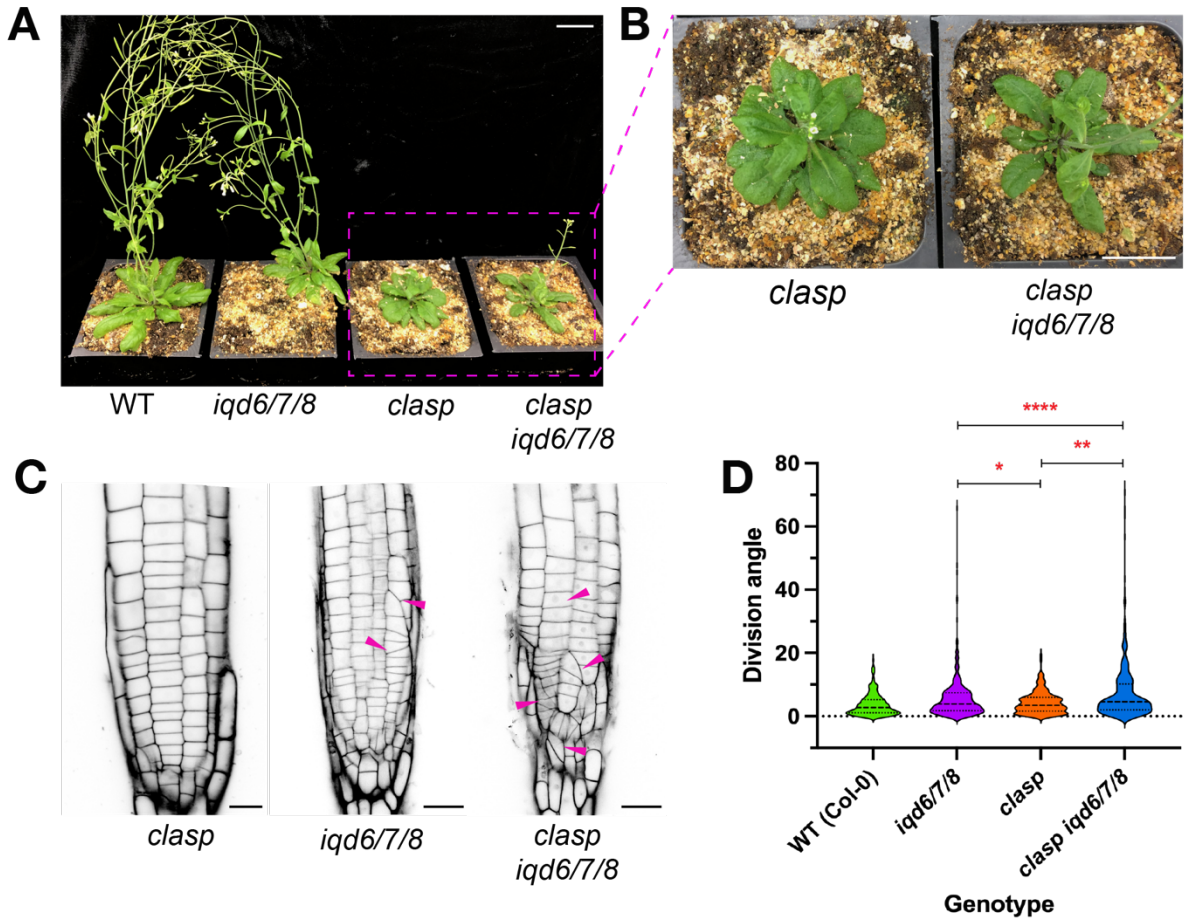
A
WT
iqd6/7/8
clasp
clasp iqd6/7/8
B
clasp
clasp iqd6/7/8
C
clasp
iqd6/7/8
clasp iqd6/7/8
D
Division angle
80
60
40
20
0
****
**
*
WT (Col-0)
iqd6/7/8
clasp
clasp iqd6/7/8
Genotype

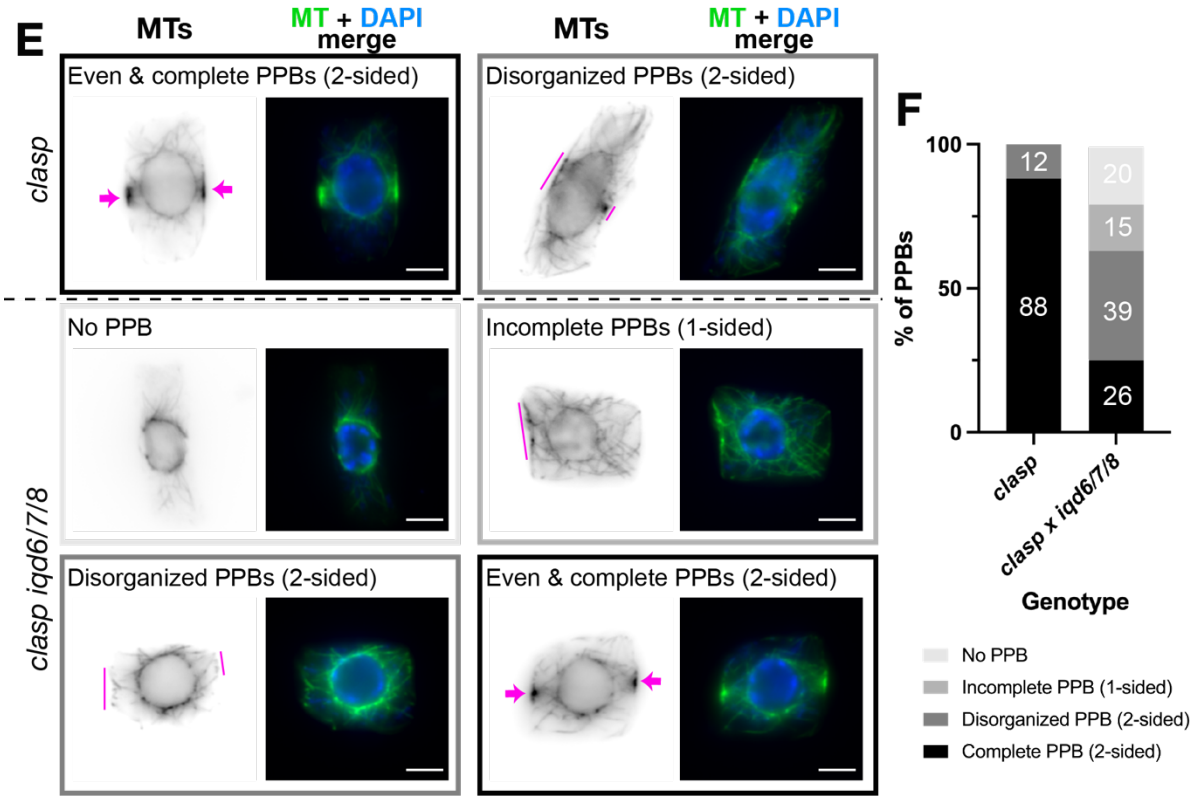
E
MTs
MT + DAPI merge
MTs
MT + DAPI merge
clasp
clasp iqd6/7/8
Even & complete PPBs (2-sided)
Disorganized PPBs (2-sided)
No PPB
Incomplete PPBs (1-sided)
Disorganized PPBs (2-sided)
Even & complete PPBs (2-sided)
F
% of PPBs
100
50
0
12
88
20
15
39
26
clasp
clasp x iqd6/7/8
Genotype
No PPB
Incomplete PPB (1-sided)
Disorganized PPB (2-sided)
Complete PPB (2-sided)

Figure 2.9. – Simultaneous loss of CLASP and IQD6/7/8 leads to absent PPBs
(A). Comparison of adult plants of WT, *iqd6/7/8, clasp,* and *clasp iqd6/7/8* mutants. Scale bars = 25mm.
(B). Closeup views of *clasp* and *clasp iqd6/7/8.* Scale bars = 25mm.
(C). PI staining of *clasp, iqd6/7/8,* and *clasp iqd6/7/8* roots at 6dpg observed in a confocal microscope. Magenta arrowheads mark oblique cell plates. Scale bars = 20μm.
(D). Quantification of division plane angles in WT, *iqd6/7/8, clasp,* and *clasp iqd6/7/8*. The values for division angle indicate angles measured from a line perpendicular to the root growth axis. WT (green) mean=3.704 (n=285 measurements from 8 plants) and *iqd6/7/8* (purple) mean=5.927 (n=343 from 7 plants) data from Figure 2.1. *clasp* (orange) mean=4.281 and SD= 3.460 (n=201 from 7 plants). *clasp iqd6/7/8* (blue) mean=7.819 and SD= 10.128 (n=279 from 6 plants). In the violin plot, the dashed line indicates the median; dotted lines represent the upper and lower quartiles. *=p<0.01, **= p<0.001; ****=p<0.0001 (based on One-way ANOVA followed by Tukey's multiple comparisons test).
(E). PPB phenotyping. Magenta arrows and lines highlight MTs. The merged image shows MTs in green and DNA in blue. A no-PPB category of cells was evident in the *clasp iqd6/7/8* quadruple mutant. Scale bars = 5μm.
(F). Quantification of PPBs morphology in *clasp iqd6/7/8*. PPBs were classified based on the even accumulation of MTs on either side of the cell using immunostained images of *claps* (n=96) and *clasp iqd6/7/8* (n=128). Example cells per category are shown in panels in E.

Supplemental figures

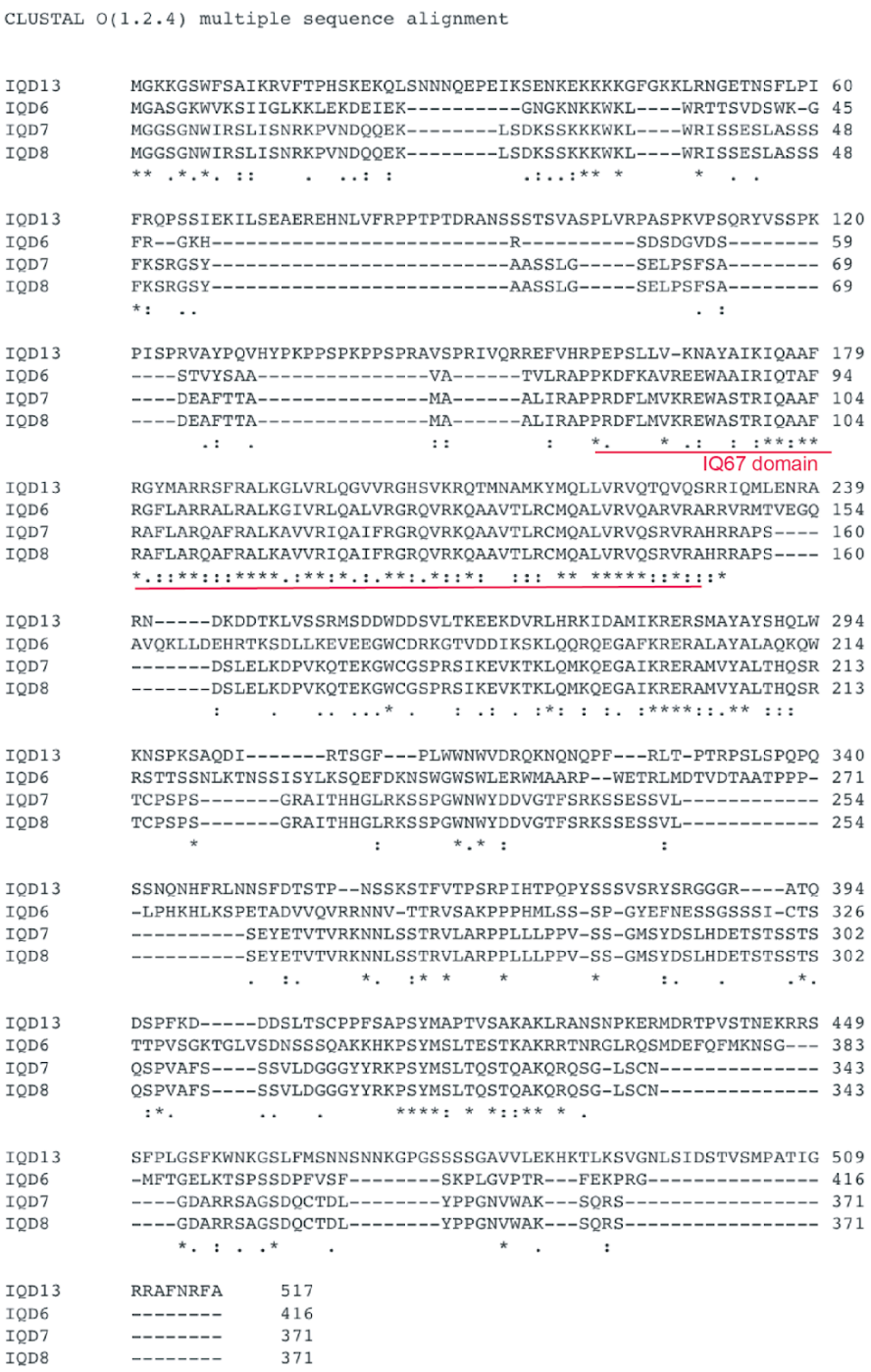

Figure S2.1. – Multiple sequence alignment of IQD6/IQD7/IQD8 and IQD13
Detailed protein alignment of IQD6/7/8 in *A. thaliana,* with IQD13 as comparison. The IQ67 domain is shown in red. Alignments were done using Clustal Omega at EMBL-EBI (Sievers et al., 2011).

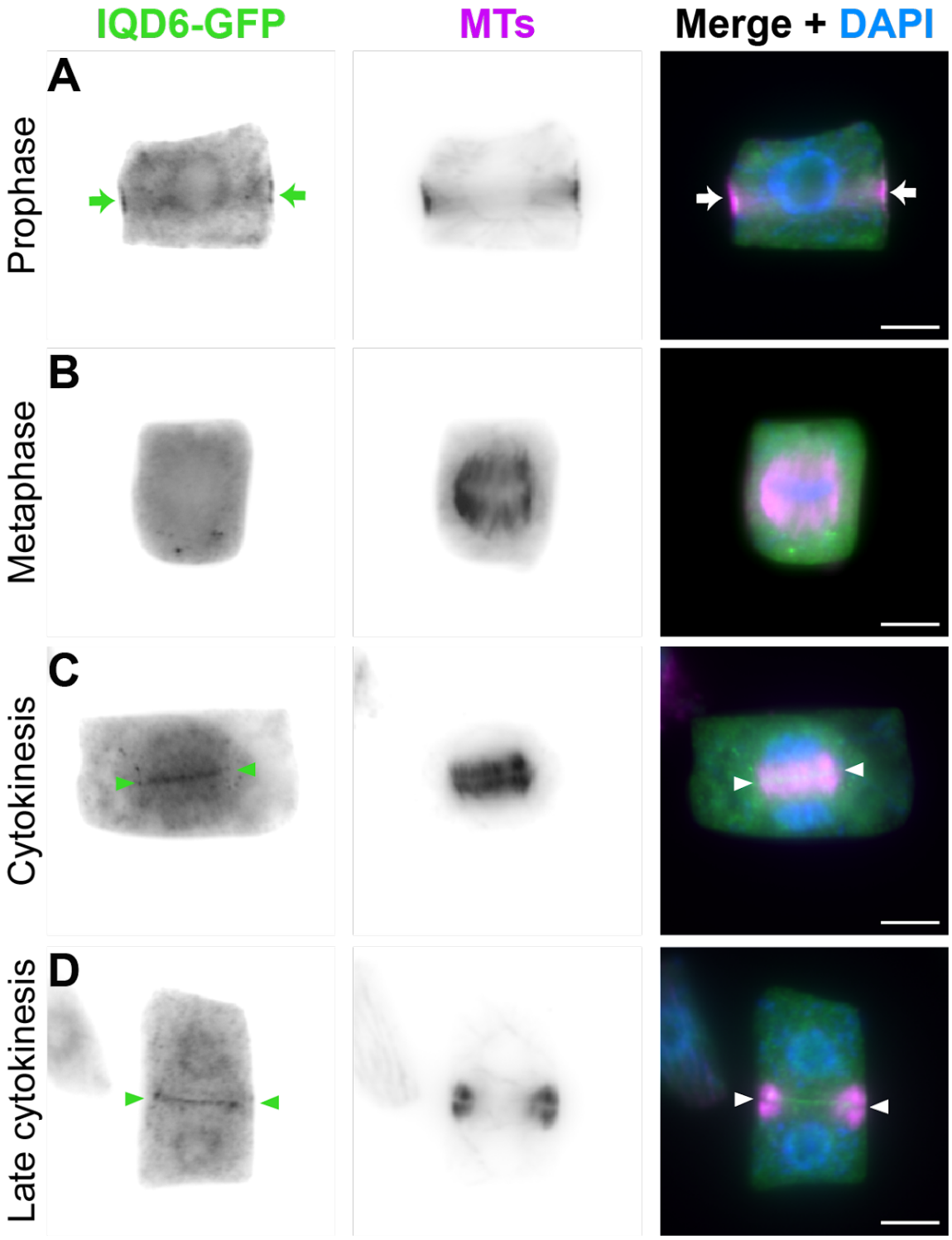

Figure S2.2. – Cell cycle-specific expression of IQD6
Immunolocalization of IQD6-GFP and MTs in T2 *iqd6/7/8* plants expressing *IQD6p:IQD6-GFP*. The merged image shows MTs in magenta, IQD6-GFP in green, and DNA in blue. IQD6-GFP accumulated at the PPB (**A**, n=8), the middle of the phragmoplast **(C)**, and the cell plate (**D**, n=7 for all cytokinesis). Scale bars = 5μm.

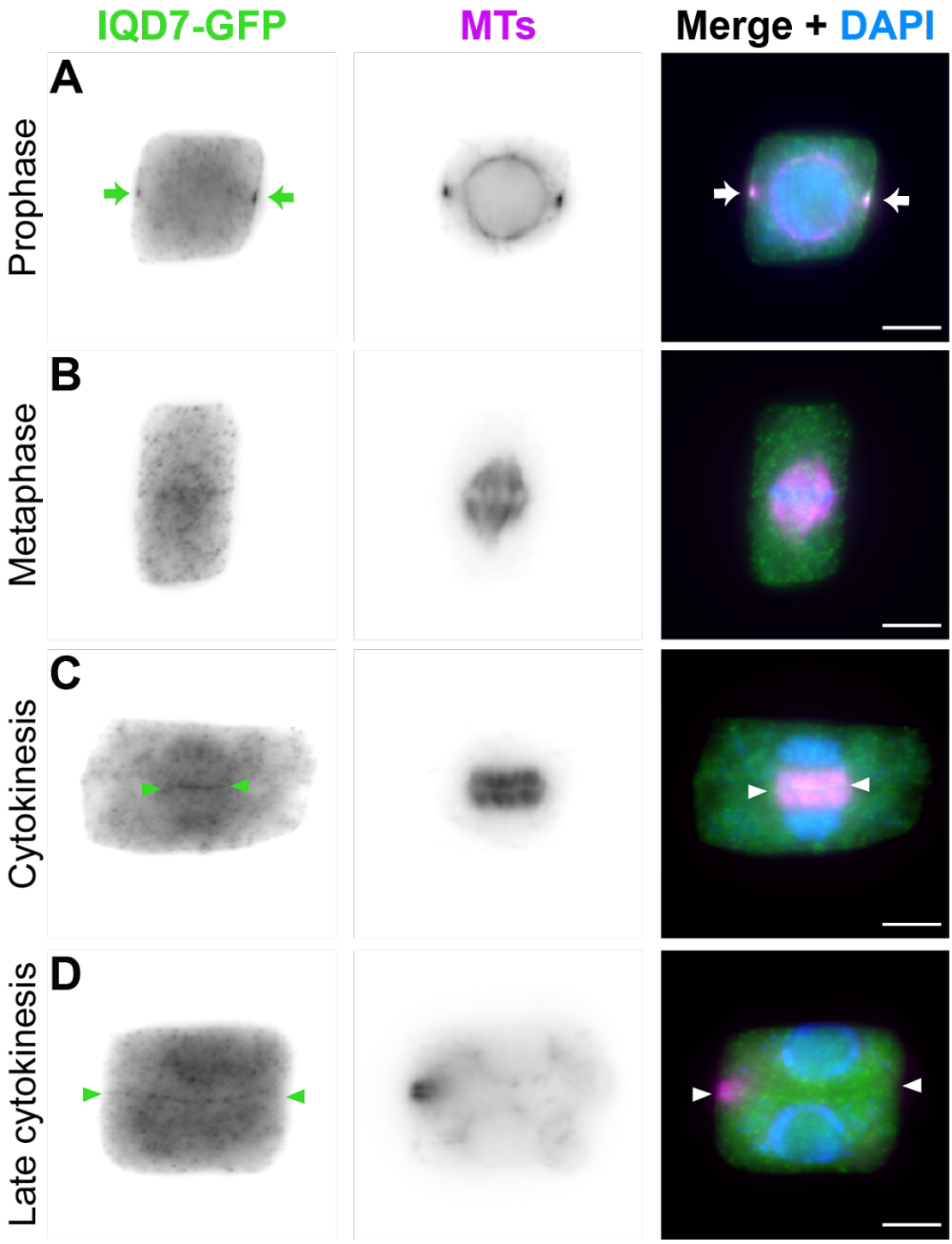

Figure S2.3. – Cell cycle-specific expression of IQD7
Immunolocalization of IQD7-GFP and MTs in T2 *iqd6/7/8* plants expressing *IQD7p:IQD7-GFP*. The merged image shows MTs in magenta, IQD7-GFP in green, and DNA in blue. IQD7 accumulated at the PPB (**A**, n=21), the middle of the phragmoplast **(C)**, and the cell plate (**D**, n=11). Scale bars = 5μm.

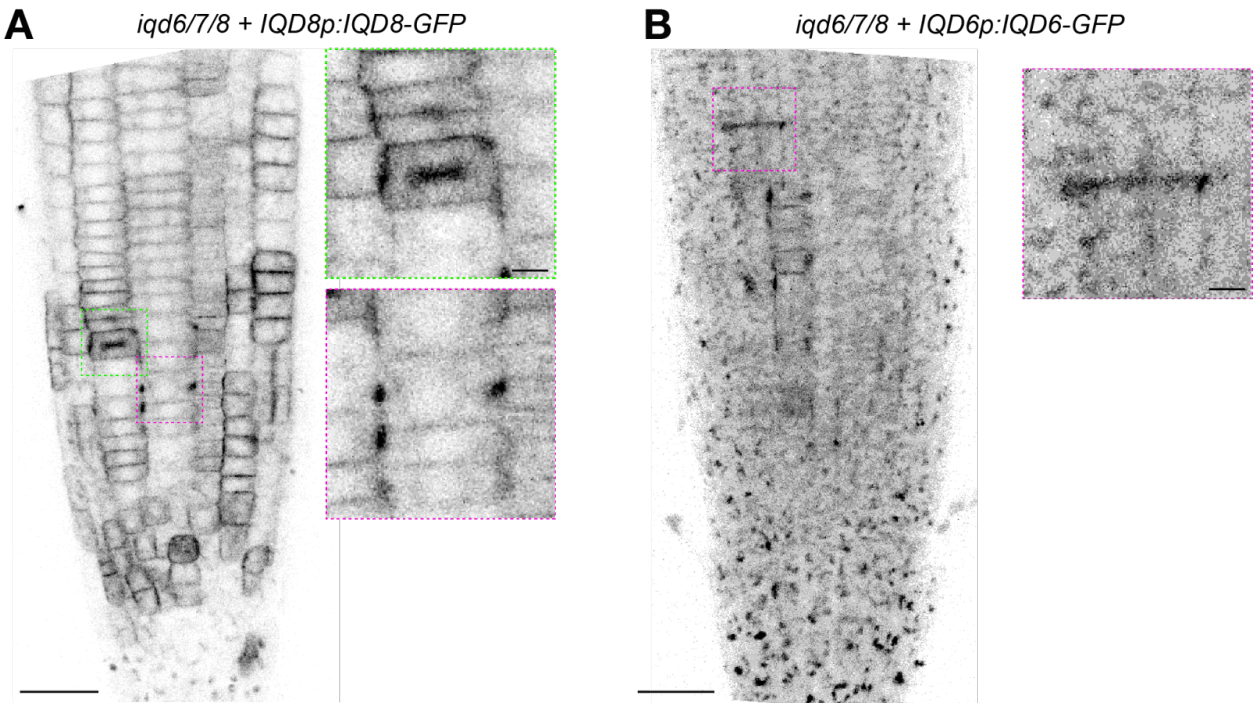

Figure S2.4. – IQD8-GFP and IQD6-GFP live imaging
Still image of roots of T2 *A. thaliana iqd6/7/8* plants expressing *IQD8p:IQD8-GFP* (n=5 plants) **(A)** and *IQD6p:IQD6-GFP* (n=4 plants) **(B).** Close-up images show a cell at the PPB stage (magenta outline) and the phragmoplast stage (green outline).
Scale bars = 25μm in whole root, 5μm in close up.

Figure S2.5. – AtIQD8 polypeptide sequence
N-terminal domain is highlighted in purple, the C-terminal domain is in blue, and the IQ67 domain is in pink.

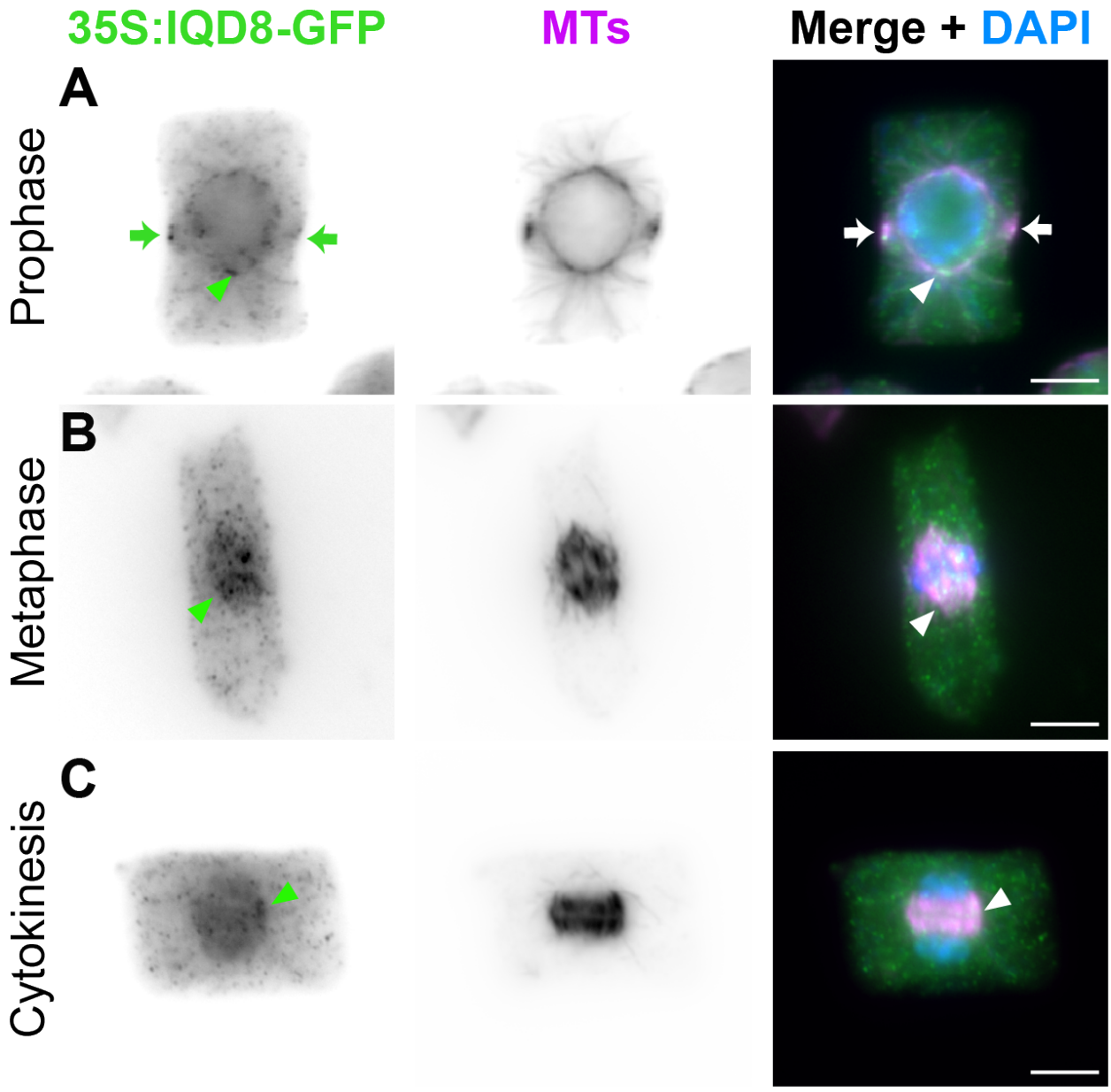

Figure S2.6. – Overexpression of IQD8 in *A. thaliana*
Immunolocalization of IQD8-GFP and MTs in T2 plants expressing *35S:IQD8-GFP*. The merged image shows MTs in magenta, IQD8-GFP in green, and DNA in blue. IQD8-GFP was detected in all mitotic cytoskeletal structures when overexpressed: **(A)** PPB and prophase spindle (n=12), **(B)** metaphase spindle (n=2), **(C)** phragmoplast (n=6). Scale bars = 5μm.

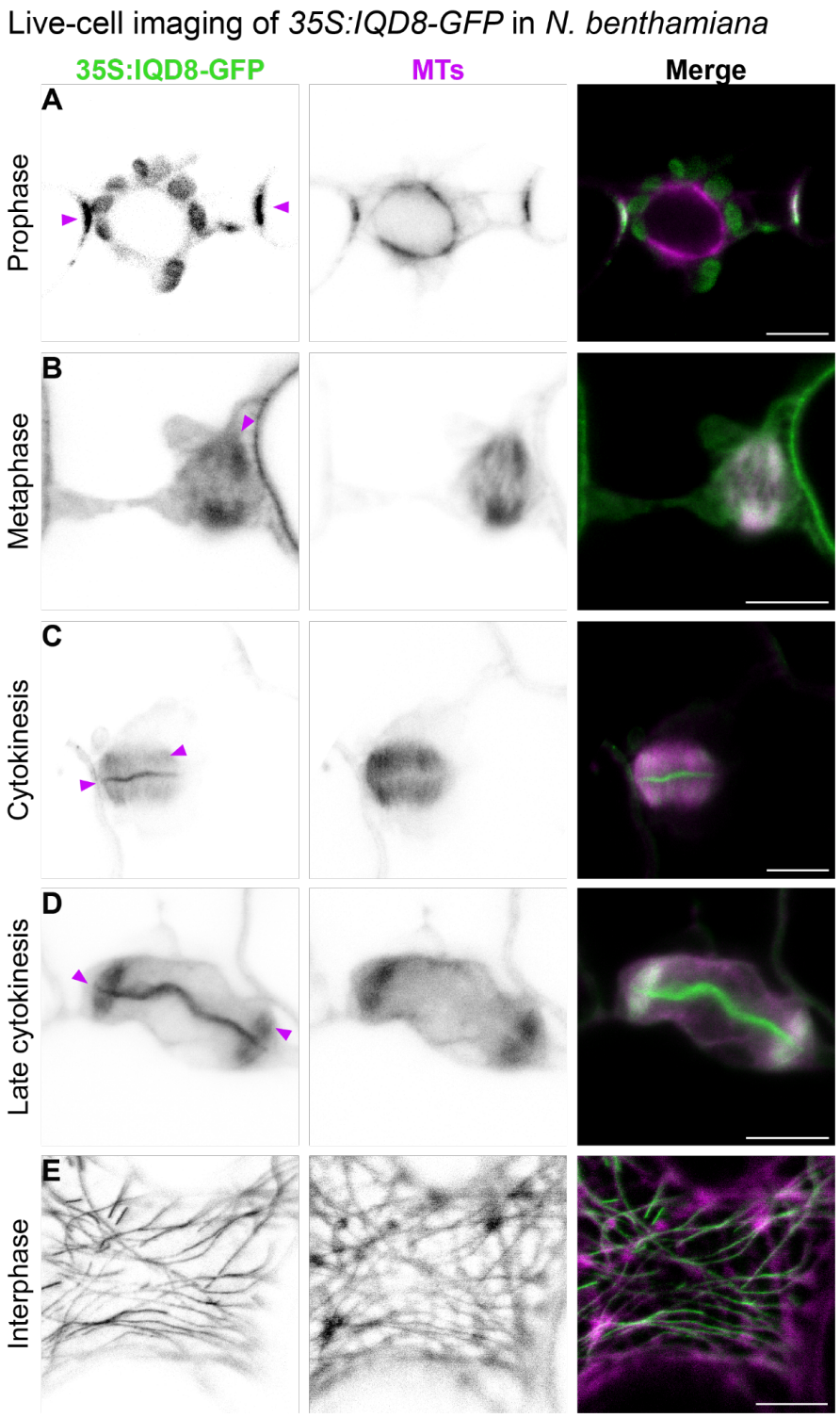

Figure S2.7. – Transient overexpression of *35S:IQD8-GFP* in *N. benthamiana*
Live-cell imaging of IQD8-GFP and MTs. The merged image shows MTs in magenta and IQD8-GFP in green. Overexpressed, IQD8-GFP associated with the PPB (**A,** n=3), spindle (**B**, n=5), phragmoplast and phragmoplast midline (**C**, n=3), and cell plate (**D**, n=3). During interphase, IQD8-GFP was observed along CMTs (**E**, n=2). Scale bars = 10μm.

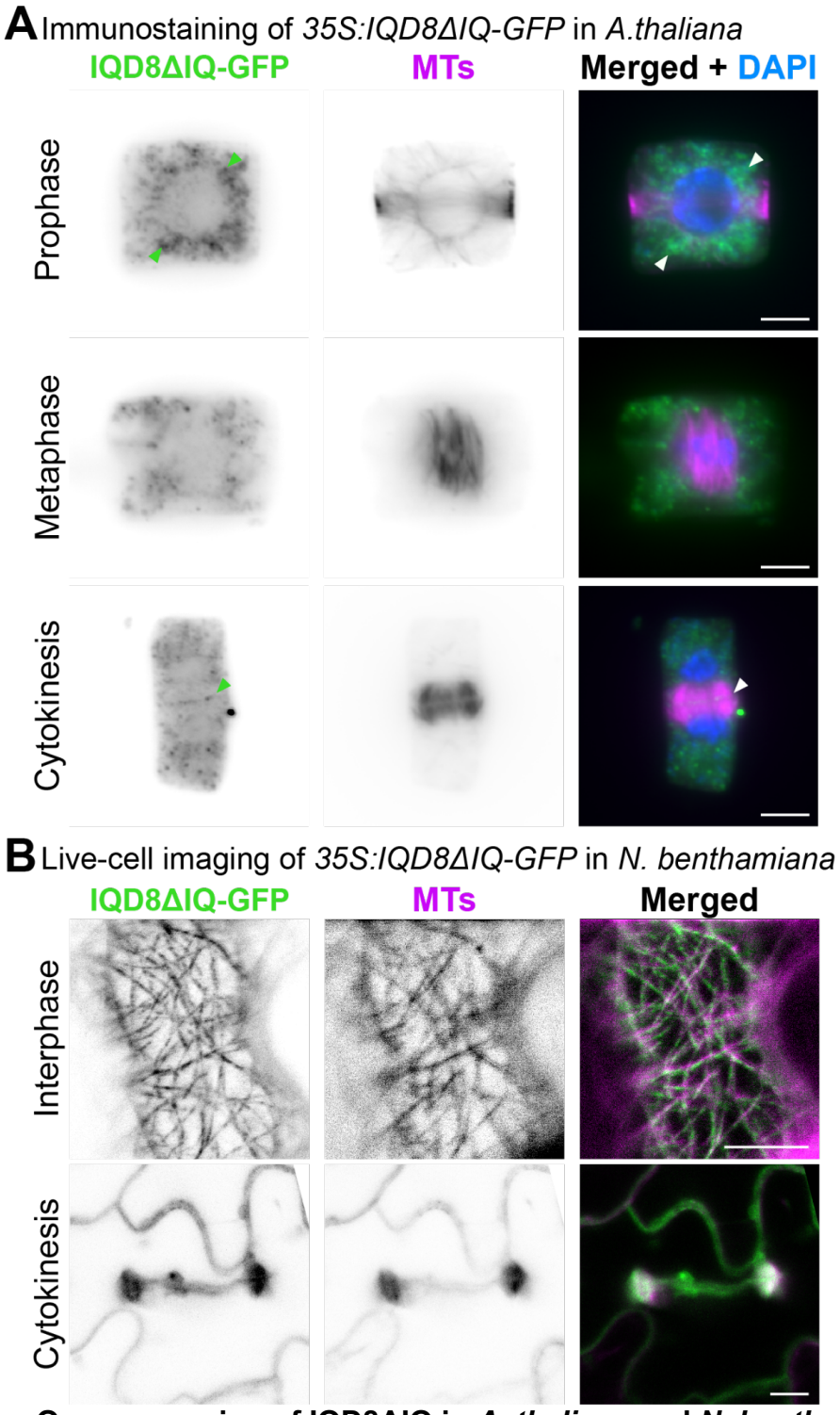

Figure S2.8. – Overexpression of IQD8ΔIQ in *A. thaliana* and *N. benthamiana* (A). Immunolocalization of IQD8ΔIQ-GFP and MTs in T2 *A. thaliana iqd6/7/8* plants expressing *35S:IQD8ΔIQ-GFP*. The merged image shows MTs in magenta, IQD8ΔIQ-GFP in green, and DNA in blue. IQD8ΔIQ-GFP was not observed at the PPB (n=13) or the CDS but was present at the phragmoplast midline and the cell plate (n=7).

Scale bar = 5μm.
(B). Live-cell imaging of *N. benthamiana* expressing *35S:IQD8ΔIQ-GFP.* IQD8ΔIQ-GFP was detected at CMTs (n=15) and less consistently at phragmoplast MTs (n=3) and the cell plate (n=2). Scale bar = 10μm.

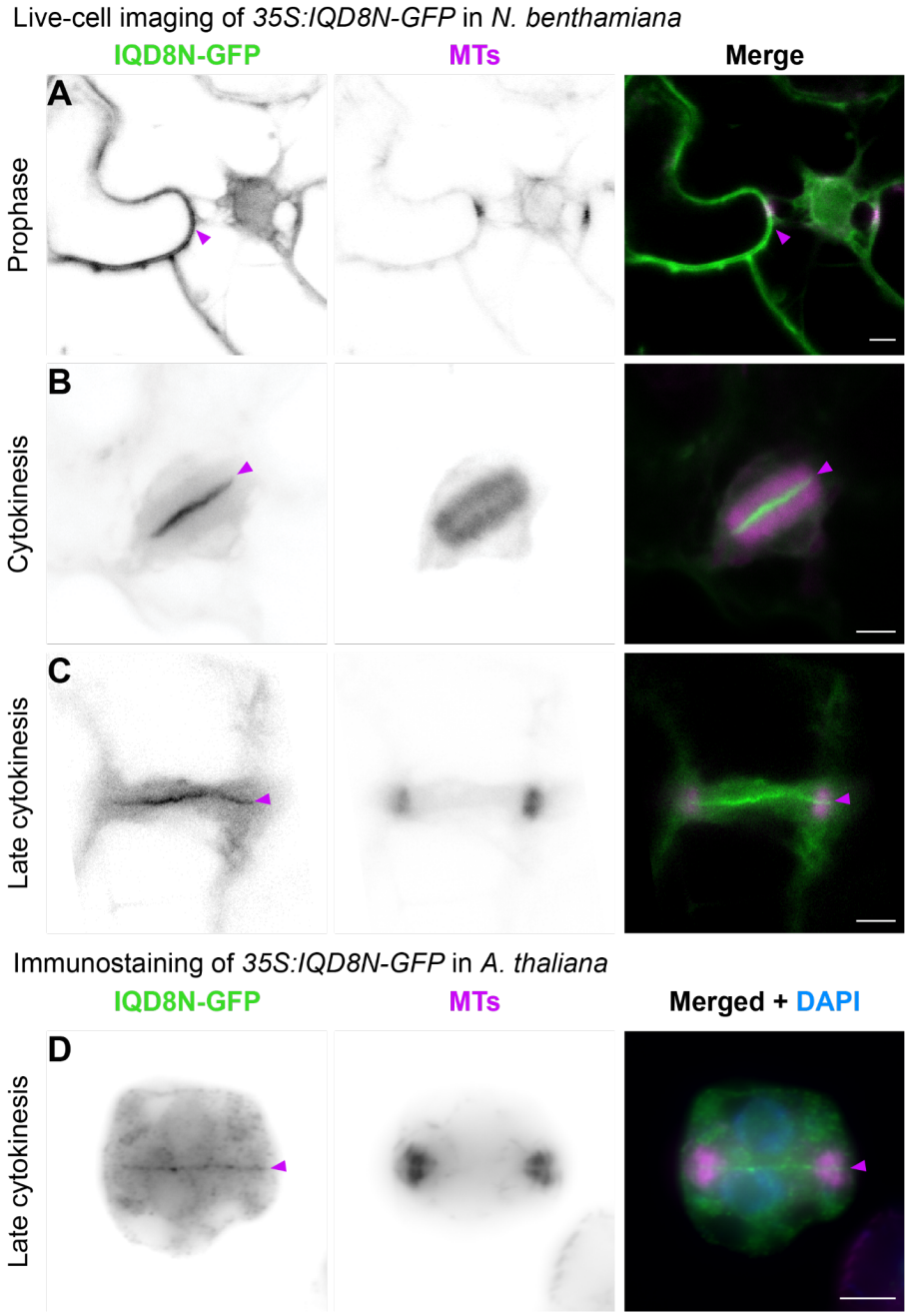

Figure S2.9. – Overexpression of IQD8N
Live-cell imaging of *N. benthamiana* dividing cells expressing *35S:IQD8N-GFP* showed IQD8N-GFP (magenta arrowheads) at the cortex during prophase (**A**, n=5), the phragmoplast midline **(B)**, and cell plate during cytokinesis (**C**, n=5 for all phragmoplasts). Scale bars = 10μm.

(D). Immunolocalization of IQD8N-GFP and MTs in T2 *A. thaliana iqd6/7/8* plants expressing *35S:IQD8N-GFP*. The merged image shows MTs in magenta, IQD8-GFP in green (magenta arrowheads), and DNA in blue. IQD8N-GFP was observed at the phragmoplast midline and cell plate (n=4). Scale bars = 5μm.

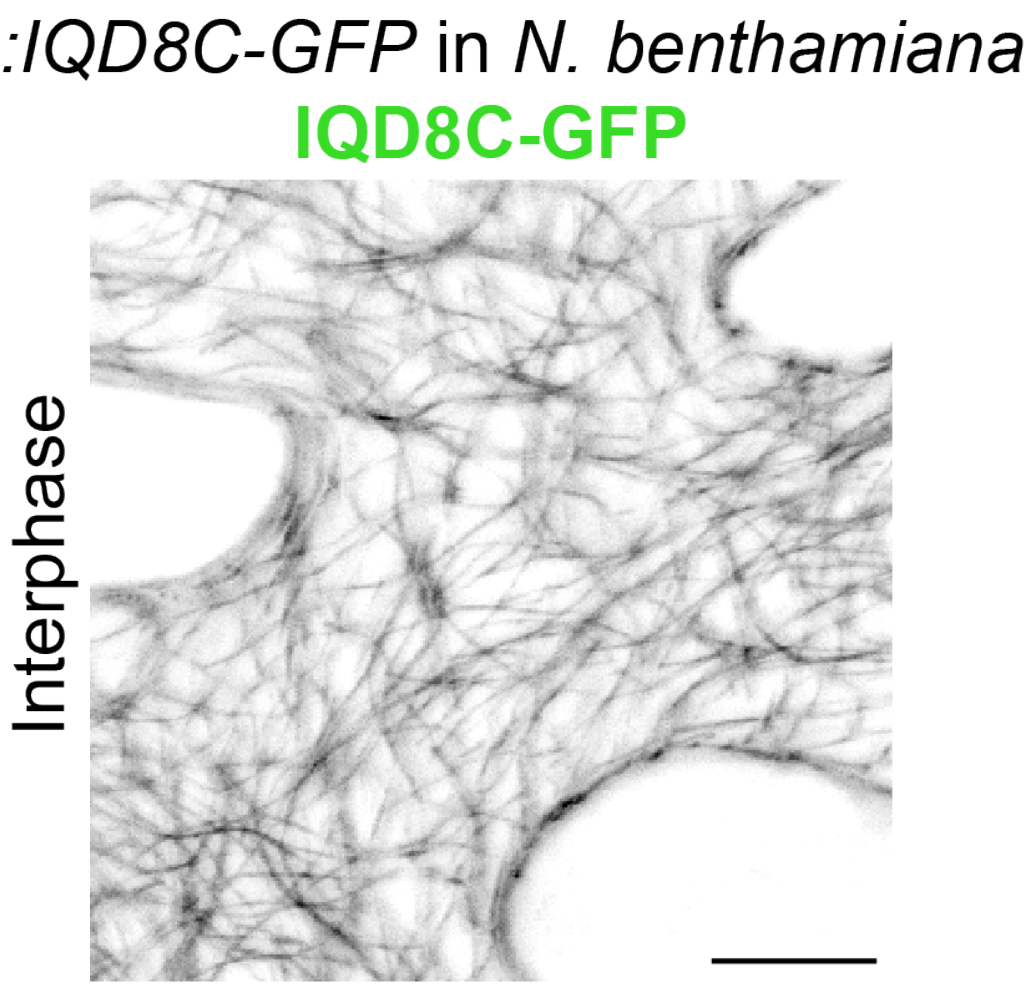

Figure S2.10. – Overexpression of IQD8C
Live-cell imaging of *N. benthamiana* dividing cells expressing *35S:IQD8C-GFP* showed IQD8C-GFP's association with CMTs in an interphase leaf epidermal cell (n=6). Scale bar = 10μm.

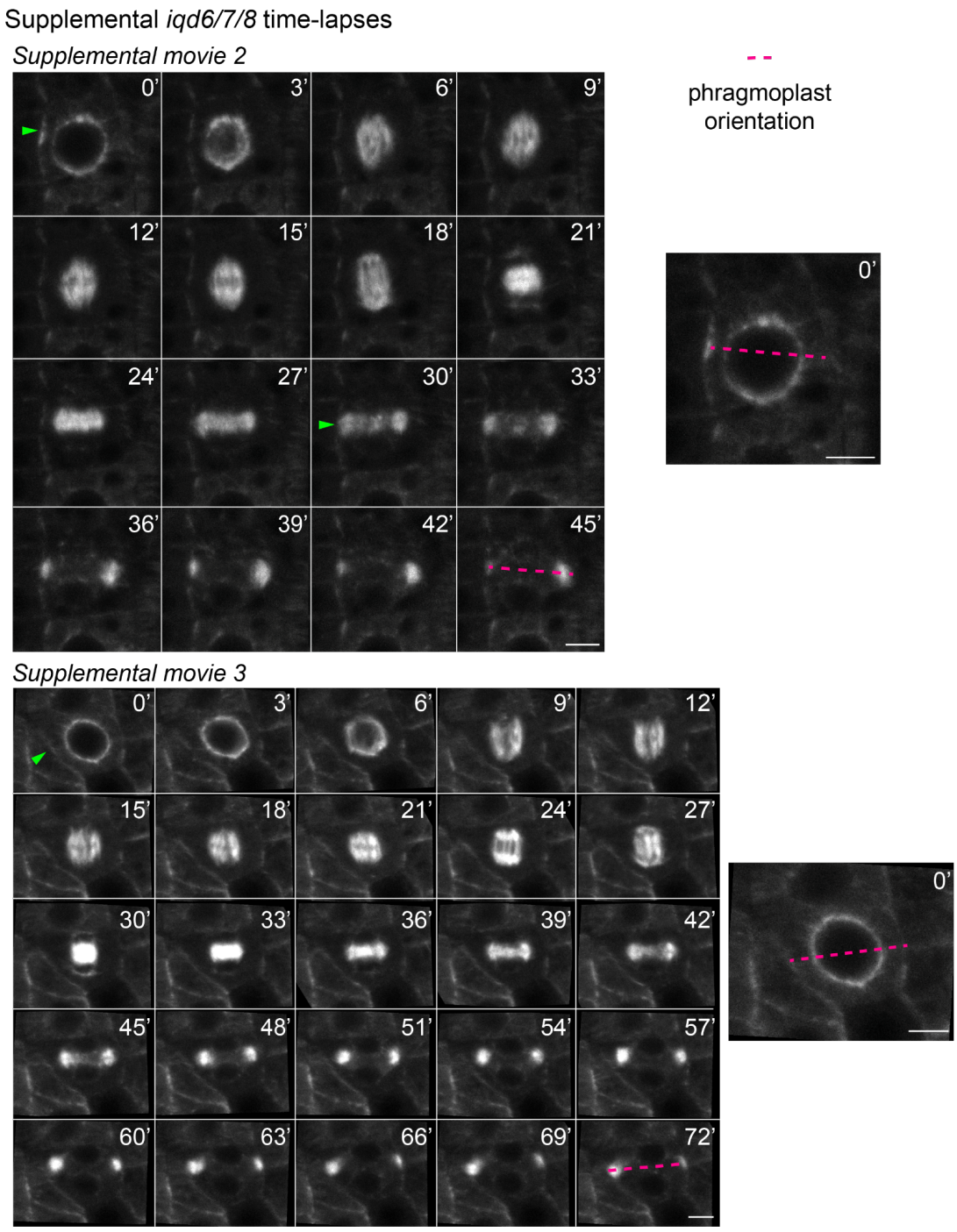

Figure S2.11. – Supplemental time-lapse images of *iqd6/7/8* cells undergoing mitotic divisions

Timelapse confocal imaging of symmetric cell division in roots of *iqd6/7/8*. MTs were visualized with *TUB6p:VisGreen-TUB6*. Photographs were taken at 3-minute intervals, with the time (in minutes) noted in the top right of each image. Green arrowheads mark the initial PPB position. The PPB was noticeable at only one side of the cell in both supplemental movies of *iqd6/7/8* mutant, although less noticeable in SM3. The phragmoplast expanded to reach these sites. Scale bars = 5μm.

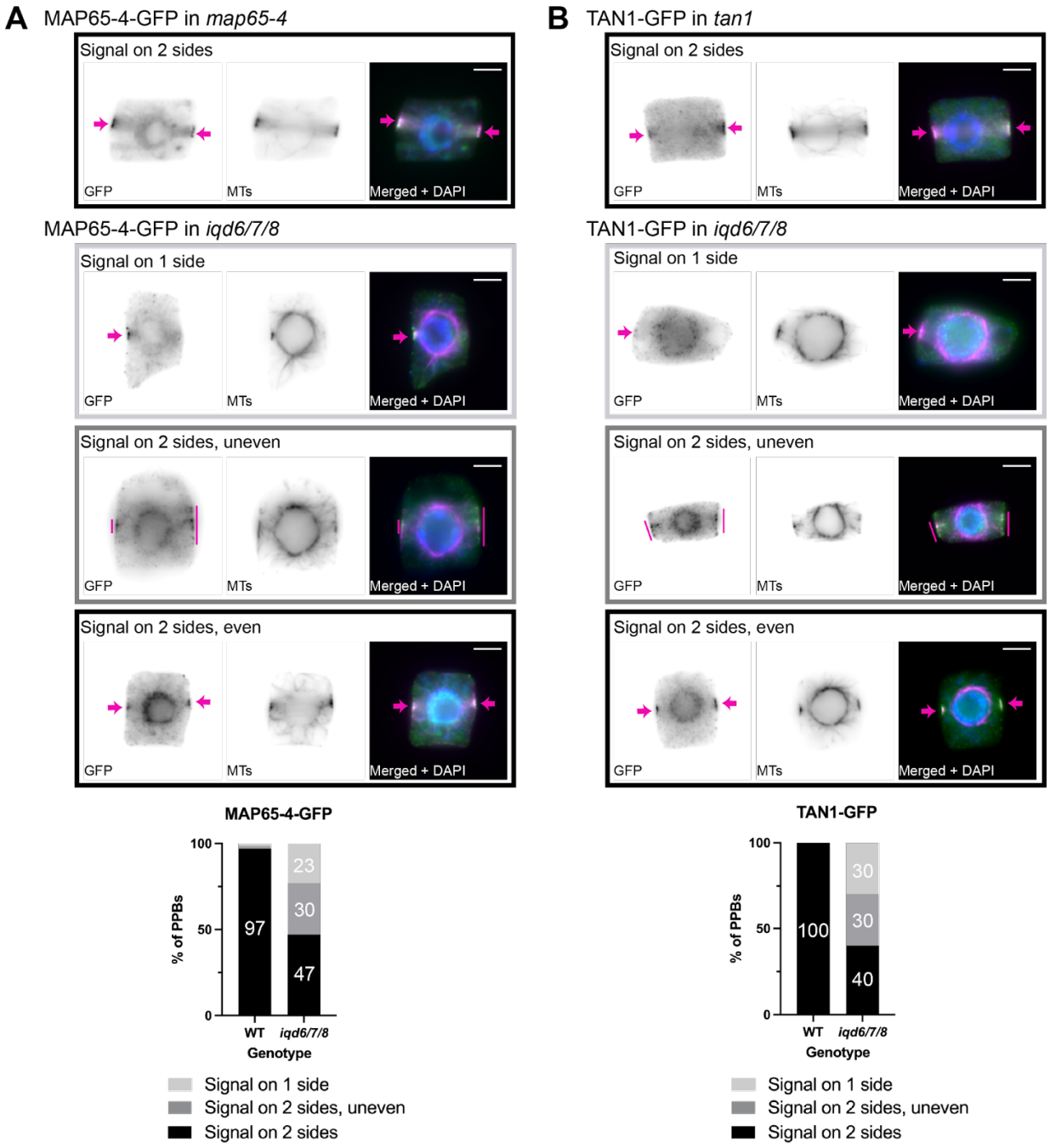

Figure S2.12. – MAP65-4 and TAN1 PPB accumulation quantification
Quantification of MAP65-4 **(A)** and TAN1 **(B)** accumulation patterns at the PPB site in WT and *iqd6/7/8* plants separately expressing *MAP65-4p:MAP65-4-GFP* and *TAN1p:TAN1-GFP.* Cells were classified using immunostained images based on the uniform or nonuniform accumulation of GFP at the PPB on either side of the cell. Example cells per category are shown in panels. For MAP65-4-GFP, n=59 (WT) and n=73 (*iqd6/7/8*). For TAN-1-GFP, n=30 (WT) and n=62 *iqd6/7/8*. Scale bars = 5μm.

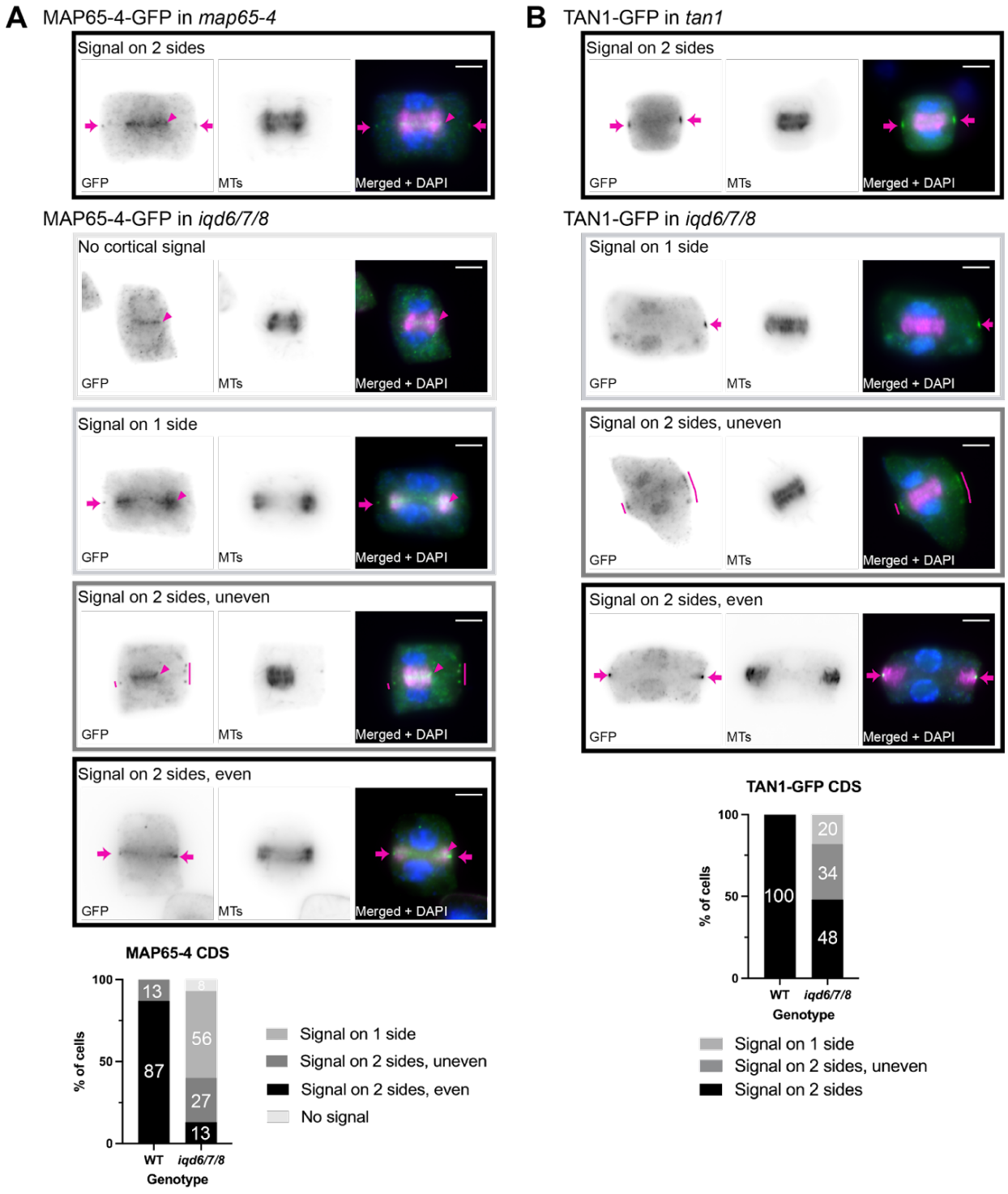

Figure S2.13. – MAP65-4 and TAN1 CDS accumulation quantification
Quantification of MAP65-4 **(A)** and TAN1 **(B)** accumulation patterns at the CDS in WT and *iqd6/7/8* plants separately expressing *MAP65-4p:MAP65-4-GFP* and *TAN1p:TAN1-GFP.* Cells were classified based on the accumulation patterns of the GFP signal at the CDS on either side of the cell. Example cells per category are shown in panels. For

MAP65-4-GFP, n=52 (WT) and n=60 (*iqd6/7/8*). For TAN-1-GFP, n=40 (WT) and n=82 *iqd6/7/8*. Scale bars = 5µm.

Supplemental MAP65-4-GFP in *iqd6/7/8* time-lapses

Supplemental Movie 2

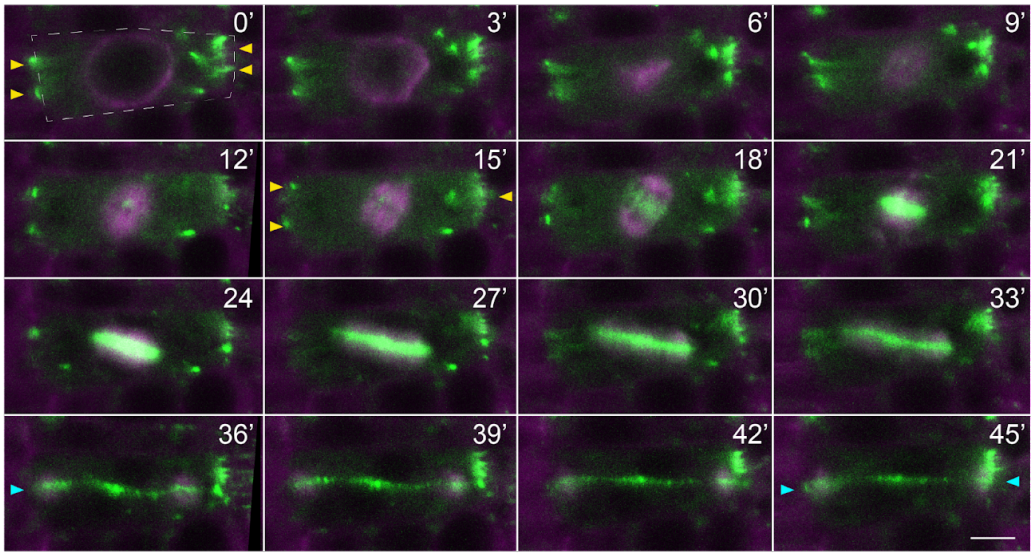

Supplemental Movie 3

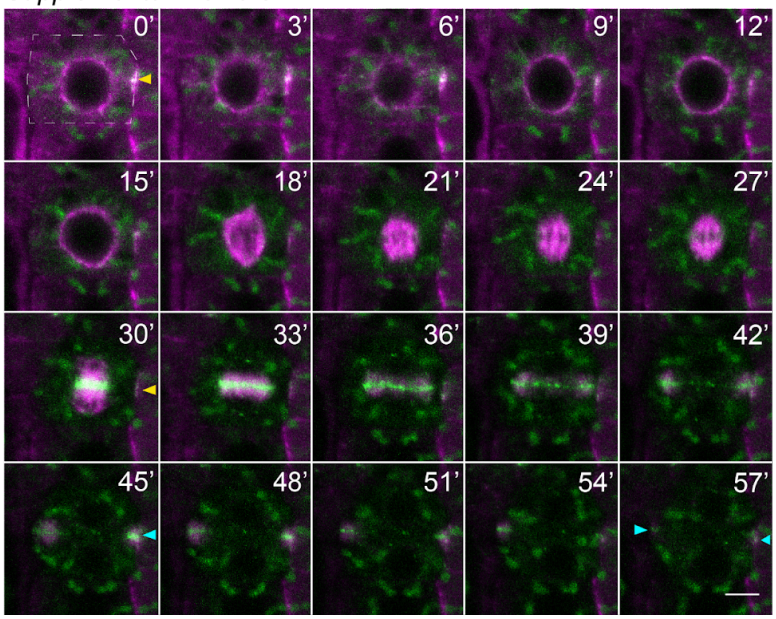

Figure S2.14. – Supplemental snapshots of MAP65-4-GFP time-lapse videos
Timelapse confocal imaging of *MAP65-4p:MAP65-4-GFP* (green signal) and *TUB6p:mCherry-TUB6* (magenta signal) in *iqd6/7/8* T2 plants. Photographs were taken at 3-minute intervals, with the time (in minutes) noted in the top right of each image. Yellow arrowheads mark MAP65-4 accumulation at the PPB (0') and CDS (15' in SM2 and 30' in SM3). Cyan arrowheads mark the location at the parental cell wall reached by

the phragmoplast. In SM2 during the PPB stage and CDS, MAP65-4 signal appeared disorganized. In SM3, MAP65-4-GFP signal at the PPB was incomplete, with only one side showing GFP accumulation (0'). This signal remained at the CDS (30') during cytokinesis. Despite the disorganization and spindle/phragmoplast rotation, the phragmoplast expanded normally in SM2. In SM3, the phragmoplast appeared slightly curved and elongated with some slant. Scale bars = 5μm.

Supplemental TAN1-GFP in *iqd6/7/8* time-lapses

Supplemental Movie 2

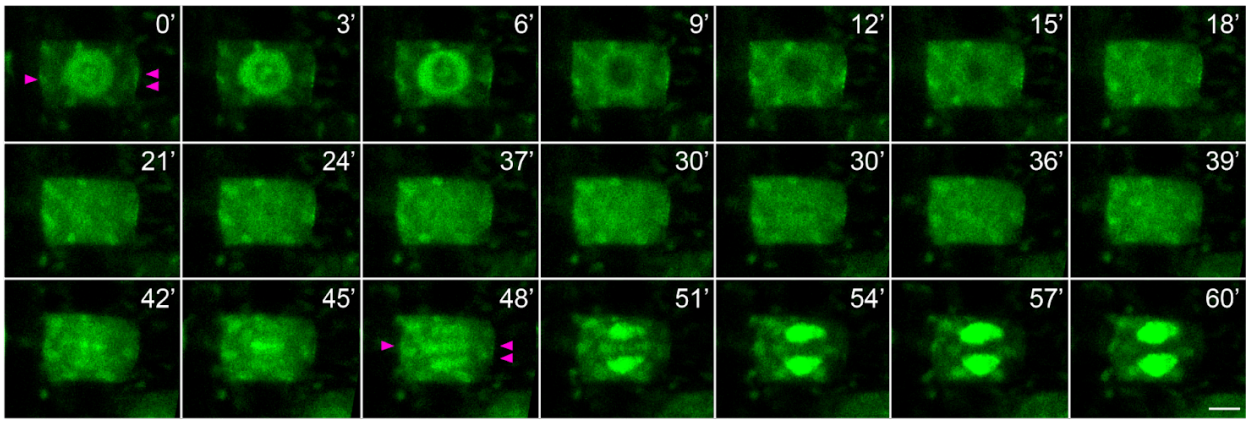

Supplemental Movie 3

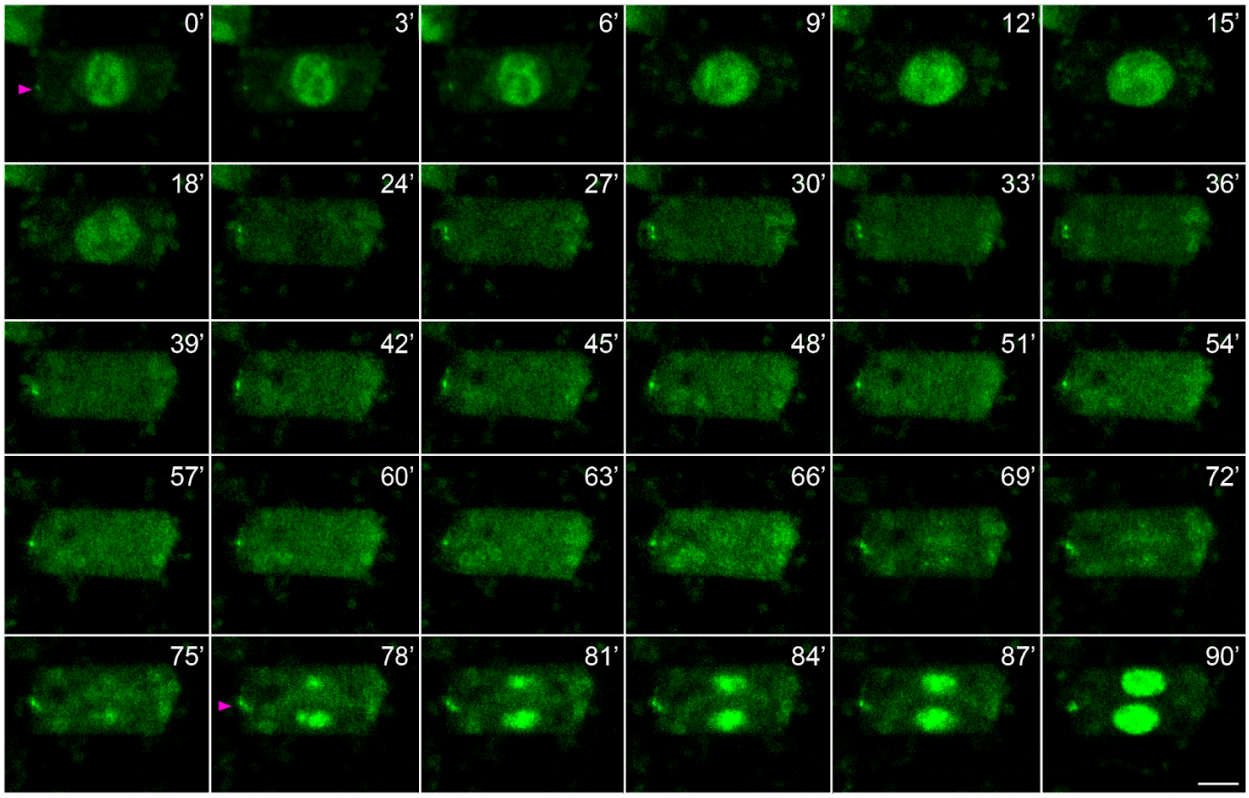

Figure S2.15. – Supplemental TAN1 videos
Timelapse confocal imaging of *TAN1p:TAN1-GFP* in *iqd6/7/8* T2 plants. Photographs were taken at 3-minute intervals, with the time (in minutes) noted in the top right of each image. Magenta arrowheads mark TAN1 accumulation at the PPB (0') and CDS during cytokinesis (48' in SM2 and 78' in SM3). In SM2 during the PPB stage and CDS, TAN1-GFP signal appeared on both sides of the cell but was of uneven width. In SM3, TAN1-GFP signal at the PPB was incomplete, with only one side showing TAN1-GFP accumulation (0'). This signal remained at the CDS (78') during cytokinesis. Scale bars = 5μm.

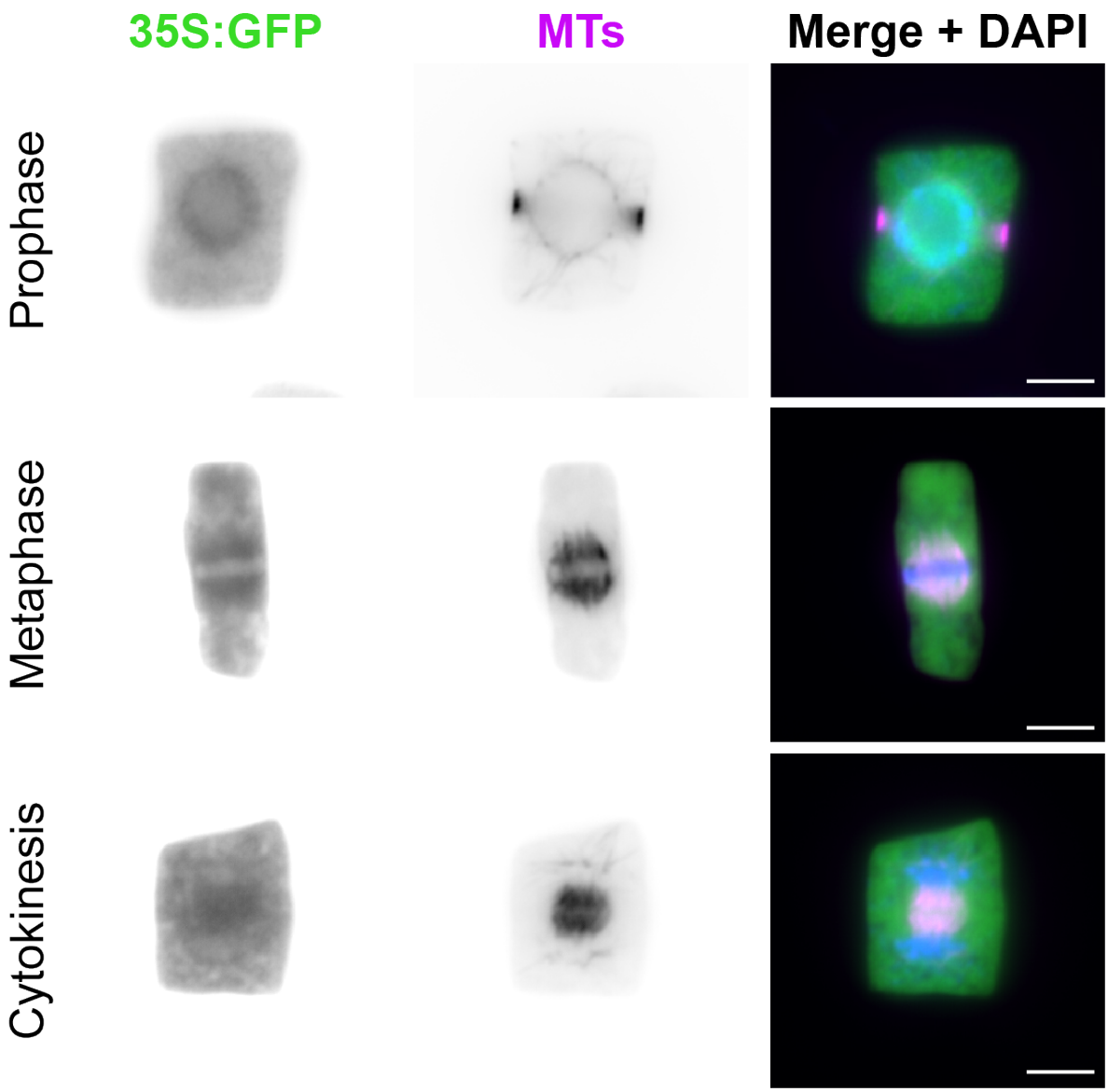

Figure S2.16. – Overexpression of GFP immunostaining control
Immunolocalization of GFP and MTs in *A. thaliana* WT plants expressing *35S:GFP*. The merged images show MTs in magenta, GFP in green, and DNA in blue. Since the PPB

MTs and their associated proteins accumulate at the cortex, we focused on the signal at cortical locations for the control. We found that the GFP signal was not emphasized at the cortex in the control cells. n=18 for PPB, 3 for spindle, and 9 for phragmoplasts. Scale bars = 5μm.

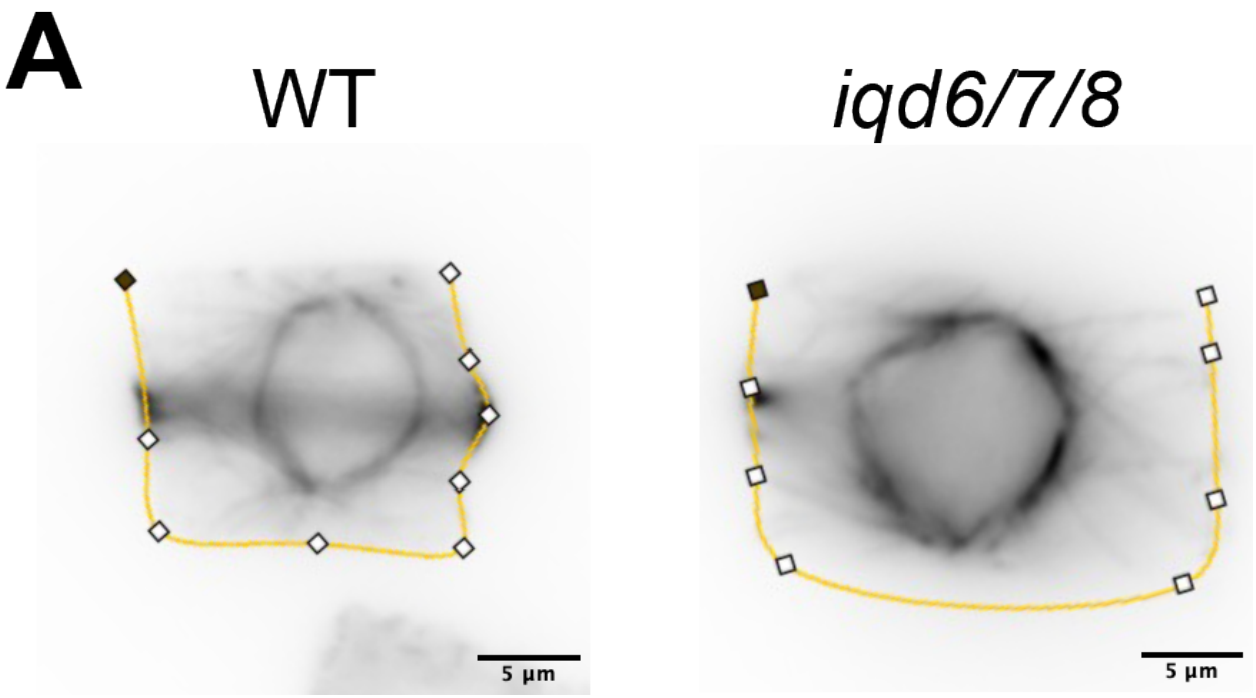

Figure S2.17. – Cell periphery trace is indicated for measuring the fluorescence intensity profiles of PPBs in the WT and *iqd6/7/8* cells.
Example screenshots show line traces used to generate fluorescence intensity profiles of PPBs, as shown in Figure 2.3B.

Supplemental tables

Table S2.1. Primers used in the construction of transgenes and the genotyping of specific alleles.

Primer Name	Sequence (5' → 3')	Purpose
SALK_107689_LP	CATATGGAAGGTTAAACAAACAAGG	Genotyping of *iqd8* FWD
SALK_107689_RP	TGAGCTAAAAGATCCTGTTAAGCAG	Genotyping of *iqd8* REV
SALK_137365_LP	AACAGGCGTAGTTGAAGTACAAATC	Genotyping of *iqd6* FWD
SALK_137365_RP	CATTATCGGTCTCAAGAAGCTAGAG	Genotyping of *iqd6* REV
SALK_25334_LP	CATATGGAAGGTTAAACAAACAAGG	Genotyping of *iqd7* FWD
SALK_25334_RP	TGAGCTAAAAGATCCTGTTAAGCAG	Genotyping of *iqd7* REV
CLASP_FWD	GTAAGCAACCTGTTAGAGATGCTG	Genotyping of *clasp* FWD
CLASP_REV	TGTTTAGGCTTCAATCATTGAGAG	Genotyping of *clasp* REV
IQD6_FWD	GGGGACAAGTTTGTACAAAAAAGCA GGCTCTTACCGCCATGCAAAAAGTTG	Amplification of AtIQD6 promoter and open reading frame FWD
IQD6_REV	GGGGACCACTTTGTACAAGAAAGCT GGGTTACCTCTCGGCTTCTCGAATCG AG	Amplification of IQD6 promoter and open reading frame REV
IQD8_FWD	GGGGACAAGTTTGTACAAAAAAGCA GGCTAGTCCTGCCAATCTCAATCTTG GT	Amplification of AtIQD8 promoter and open reading frame FWD
IQD8_REV	GGGGACCACTTTGTACAAGAAAGCT GGGTTGCCTCTCTGGCTCTTTGCCCA C	Amplification of AtIQD8 promoter and open reading frame FWD
IQD8_CDS_FWD	CACCATGGGTGGCTCTGGAAATTG	Amplification of AtIQD8 coding region FWD
IQD8_CDS_REV	GCCTCTCTGGCTCTTTGCCCAC	Amplification of AtIQD8 coding region REV
IQD8_67D_FWD	CTT TCT TGT TAA ACC TTC AGA TGG ACA GGA GTT GG	Gibson primers to delete IQ67 domain in IQD8 FWD
IQD8_67D_REV	CCA TCT GAA GGT TTA ACA AGA AAG AAA TCT TTC GGC GGA G	Gibson primers to delete IQ67 domain in IQD8 REV

IQD8N_FWD	CAT TAG AGC TGC CGA CCC AGC TTT CTT GTA	Gibson primers to amplify IQD8 N-domain FWD
IQD8N_FWD	GGT CGG CAG CTC TAA TGA CAG CAG CAA CAG	Gibson primers to amplify IQD8 N-domain REV
IQD8C_FWD	AAA AGC AGG CTC CGC AAT GGG TTG GAA TTG GCT TGA CCG	Gibson primers to amplify IQD8 C-domain FWD
D-prom-R1_REV	CATTGCGGAGCCTGCTTTTTTGTACA AAG	Gibson primers to amplify IQD8 C-domain REV
TAN1_FWD	CACC AGA TGC TCC AGA ATT TCT GGT AG	Amplification of AtTAN1 promoter and open reading frame FWD
TAN1_REV	GCCTGCGCCTGC CACTTTCCTGCTCTTCATTGGAG	Amplification of AtTAN1 promoter and open reading frame FWD
LBb1.3	ATTTTGCCGATTTCGGAAC	T-DNA primer for genotyping of SALK lines
SKTAIL-L1	TTCTCATCTAAGCCCCCATTTGG	T-DNA primer for genotyping of *clasp*

Table S2.2. Combinations of primary and secondary antibody used in this study

Figure	**Primary antibody**	**Secondary antibody**
Figure 2.3 and Figure 2.9	Monoclonal mouse DM1A anti-α-tubulin antibody (Sigma)	Fluorescein isothiocyanate (FITC)–conjugated donkey anti-mouse IgG (Rockland Antibodies & Assays)
Figures 2.2, 2.5, 2.6 and SF2.2, 2.3, 2.6, 2.8, 2.9, 2.12, 2.13, 2.16	Monoclonal mouse DM1A anti-α-tubulin antibody (Sigma) Monoclonal rabbit anti-GFP (Thermo Fisher Scientific)	Texas Red–conjugated anti-mouse IgG (Rockland Antibodies & Assays) FITC–conjugated donkey anti-rabbit IgG (Rockland Antibodies & Assays)

Table S2.3. Key resources table

Resource	**Source**
A. thaliana iqd6/7/8	This paper

A. thaliana iqd6/7/8 + pGWB4_IQD6p:IQD6-GFP	This paper
A. thaliana iqd6/7/8 + pGWB4_IQD7p:IQD7-GFP	This paper
A. thaliana iqd6/7/8 + pGWB4_IQD8p:IQD8-GFP	This paper
A. thaliana iqd6/7/8 + pGWB10_TUB6p:VisGreen-TUB6	This paper
A. thaliana map65-4	Li et al. 2017
A. thaliana map65-4 + pGWB4_MAP65-4p:MAP65-4-GFP	Li et al. 2017
A. thaliana map65-4 + pJL414_MAP65-4p:MAP65-4-GFP	This paper and (Liu et al., 2019)
A. thaliana iqd6/7/8 + pJL414_MAP65-4p:MAP65-4-GFP	This paper
A. thaliana Col-0 + *pGWB4_TAN1p:TAN1-GFP*	This paper
A. thaliana iqd6/7/8 + pGWB650_TAN1p:TAN1-GFP	This paper
A. thaliana iqd6/7/8 + pGWB605_35S:IQD8-GFP	This paper
A. thaliana iqd6/7/8 + pGWB605_35S:IQD8ΔIQ-GFP	This paper
A. thaliana clasp	This paper
A. thaliana clasp iqd6/7/8	This paper
pGWB4_IQD6p:IQD6-GFP	This paper
pGWB4_IQD7p:IQD7-GFP	This paper
pGWB4_IQD8p:IQD8-GFP	This paper
pGWB10_TUB6p:VisGreen-TUB6	*(Liu et al., 2019)*
pGWB4_MAP65-4p:MAP65-4-GFP	Li et al. 2017

pJL414_MAP65-4p:MAP65-4-GFP	*(Liu et al., 2019)*
pGWB4_TAN1p:TAN1-GFP	This paper
pGWB650_TAN1p:TAN1-GFP	This paper
pGWB605_35S:IQD8	This paper
pGWB605_35S:IQD8ΔIQ	This paper
Phusion DNA polymerase	Thermo Fisher
Cellulase	Yakult
Paraformaldehyde	Electron Microscopy Sciences Cat. 15710
SlowFade + DAPI (4’6-diamidino-2-phenylindole)	Thermo Fisher Cat. S36920

References

1. Abel, S., Savchenko, T., & Levy, M. (2005). Genome-wide comparative analysis of the IQD gene families in Arabidopsis thaliana and Oryza sativa. *BMC Evolutionary Biology*, *5*, 72. https://doi.org/10.1186/1471-2148-5-72

2. Ambrose, C., Allard, J. F., Cytrynbaum, E. N., & Wasteneys, G. O. (2011). A CLASP-modulated cell edge barrier mechanism drives cell-wide cortical microtubule organization in Arabidopsis. *Nature Communications*, *2*, 430. https://doi.org/10.1038/ncomms1444

3. Ambrose, J. C., Shoji, T., Kotzer, A. M., Pighin, J. A., & Wasteneys, G. O. (2007). The Arabidopsis CLASP gene encodes a microtubule-associated protein involved in cell expansion and division. *The Plant Cell*, *19*(9), 2763–2775. https://doi.org/10.1105/tpc.107.053777

4. Azimzadeh, J., Nacry, P., Christodoulidou, A., Drevensek, S., Camilleri, C., Amiour, N., Parcy, F., Pastuglia, M., & Bouchez, D. (2008). Arabidopsis TONNEAU1 proteins are essential for preprophase band formation and interact with centrin. *The Plant Cell*, *20*(8), 2146–2159. https://doi.org/10.1105/tpc.107.056812

5. Bürstenbinder, K., Möller, B., Plötner, R., Stamm, G., Hause, G., Mitra, D., & Abel, S. (2017). The IQD Family of Calmodulin-Binding Proteins Links Calcium Signaling to Microtubules, Membrane Subdomains, and the Nucleus. *Plant Physiology*, *173*(3), 1692–1708. https://doi.org/10.1104/pp.16.01743

6. Bürstenbinder, K., Savchenko, T., Müller, J., Adamson, A. W., Stamm, G., Kwong, R., Zipp, B. J., Dinesh, D. C., & Abel, S. (2013). Arabidopsis calmodulin-binding protein IQ67-domain 1 localizes to microtubules and interacts with kinesin light chain-related protein-1. *The Journal of Biological Chemistry*, *288*(3), 1871–1882. https://doi.org/10.1074/jbc.M112.396200

7. Camilleri, C., Azimzadeh, J., Pastuglia, M., Bellini, C., Grandjean, O., & Bouchez, D. (2002). The Arabidopsis TONNEAU2 gene encodes a putative novel protein phosphatase 2A regulatory subunit essential for the control of the cortical cytoskeleton. *The Plant Cell*, *14*(4), 833–845. https://doi.org/10.1105/tpc.010402

8. Clough, S. J., & Bent, A. F. (1998). Floral dip: a simplified method for Agrobacterium-mediated transformation of Arabidopsis thaliana. *The Plant Journal: For Cell and Molecular Biology*, *16*(6), 735–743. https://doi.org/10.1046/j.1365-313x.1998.00343.x

9. Edelstein, A. D., Tsuchida, M. A., Amodaj, N., Pinkard, H., Vale, R. D., & Stuurman, N. (2014). Advanced methods of microscope control using μManager software. *Journal of Biological Methods*, *1*(2). https://doi.org/10.14440/jbm.2014.36

10. Kirik, A., Ehrhardt, D. W., & Kirik, V. (2012). TONNEAU2/FASS regulates the geometry of microtubule nucleation and cortical array organization in interphase Arabidopsis cells. *The Plant Cell*, *24*(3), 1158–1170. https://doi.org/10.1105/tpc.111.094367

11. Kirik, V., Herrmann, U., Parupalli, C., Sedbrook, J. C., Ehrhardt, D. W., & Hülskamp, M. (2007). CLASP localizes in two discrete patterns on cortical microtubules and is required for cell morphogenesis and cell division in Arabidopsis. *Journal of Cell Science*, *120*(Pt 24), 4416–4425. https://doi.org/10.1242/jcs.024950

12. Kumari, P., Dahiya, P., Livanos, P., Zergiebel, L., Kölling, M., Poeschl, Y., Stamm, G., Hermann, A., Abel, S., Müller, S., & Bürstenbinder, K. (2021). IQ67 DOMAIN proteins facilitate preprophase band formation and division-plane orientation. *Nature Plants*, *7*(6), 739–747. https://doi.org/10.1038/s41477-021-00923-z

13. Lazzaro, M. D., Wu, S., Snouffer, A., Wang, Y., & van der Knaap, E. (2018). Plant organ shapes are regulated by protein interactions and associations with microtubules. *Frontiers in Plant Science*, *9*, 1766. https://doi.org/10.3389/fpls.2018.01766

14. Levy, M., Wang, Q., Kaspi, R., Parrella, M. P., & Abel, S. (2005). Arabidopsis IQD1, a novel calmodulin-binding nuclear protein, stimulates glucosinolate accumulation and plant defense. *The Plant Journal: For Cell and Molecular Biology*, *43*(1), 79–96. https://doi.org/10.1111/j.1365-313X.2005.02435.x

15. Li, H., Sun, B., Sasabe, M., Deng, X., Machida, Y., Lin, H., Julie Lee, Y.-R., & Liu, B. (2017). Arabidopsis MAP65-4 plays a role in phragmoplast microtubule organization and marks the cortical cell division site. *The New Phytologist*, *215*(1), 187–201. https://doi.org/10.1111/nph.14532

16. Liu, W., Wang, C., Wang, G., Ma, Y., Tian, J., Yu, Y., Dong, L., & Kong, Z. (2019). Towards a better recording of microtubule cytoskeletal spatial organization and dynamics in plant cells. *Journal of Integrative Plant Biology*, *61*(4), 388–393. https://doi.org/10.1111/jipb.12721

17. Mills, A. M., Morris, V. H., & Rasmussen, C. G. (2022). The localization of PHRAGMOPLAST ORIENTING KINESIN1 at the division site depends on the microtubule-binding proteins TANGLED1 and AUXIN-INDUCED IN ROOT CULTURES9 in Arabidopsis. *The Plant Cell*, *34*(11), 4583–4599. https://doi.org/10.1093/plcell/koac266

18. Poddar, A., Sidibe, O., Ray, A., & Chen, Q. (2021). Calcium spikes accompany cleavage furrow ingression and cell separation during fission yeast cytokinesis. *Molecular Biology of the Cell*, *32*(1), 15–27. https://doi.org/10.1091/mbc.E20-09-0609

19. Schaefer, E., Belcram, K., Uyttewaal, M., Duroc, Y., Goussot, M., Legland, D.,

Laruelle, E., de Tauzia-Moreau, M.-L., Pastuglia, M., & Bouchez, D. (2017). The preprophase band of microtubules controls the robustness of division orientation in plants. *Science*, *356*(6334), 186–189. https://doi.org/10.1126/science.aal3016

20. Sievers, F., Wilm, A., Dineen, D., Gibson, T. J., Karplus, K., Li, W., Lopez, R., McWilliam, H., Remmert, M., Söding, J., Thompson, J. D., & Higgins, D. G. (2011). Fast, scalable generation of high-quality protein multiple sequence alignments using Clustal Omega. *Molecular Systems Biology*, *7*, 539. https://doi.org/10.1038/msb.2011.75

21. Spinner, L., Gadeyne, A., Belcram, K., Goussot, M., Moison, M., Duroc, Y., Eeckhout, D., De Winne, N., Schaefer, E., Van De Slijke, E., Persiau, G., Witters, E., Gevaert, K., De Jaeger, G., Bouchez, D., Van Damme, D., & Pastuglia, M. (2013). A protein phosphatase 2A complex spatially controls plant cell division. *Nature Communications*, *4*(1), 1863. https://doi.org/10.1038/ncomms2831

22. Sugiyama, Y., Wakazaki, M., Toyooka, K., Fukuda, H., & Oda, Y. (2017). A Novel Plasma Membrane-Anchored Protein Regulates Xylem Cell-Wall Deposition through Microtubule-Dependent Lateral Inhibition of Rho GTPase Domains. *Current Biology: CB*, *27*(16), 2522–2528.e4. https://doi.org/10.1016/j.cub.2017.06.059

23. Traas, J., Bellini, C., Nacry, P., Kronenberger, J., Bouchez, D., & Caboche, M. (1995). Normal differentiation patterns in plants lacking microtubular preprophase bands. *Nature*, *375*(6533), 676–677. https://doi.org/10.1038/375676a0

24. Xu, J., Lee, Y.-R. J., & Liu, B. (2020). Establishment of a mitotic model system by transient expression of the D-type cyclin in differentiated leaf cells of tobacco (Nicotiana benthamiana). *The New Phytologist*, *226*(4), 1213–1220. https://doi.org/10.1111/nph.16309

Chapter 3
Cell cycle control of preprophase band formation during cell division in plants

Authors: M. Ximena Anleu Gil, Yuh-Ru Julie Lee, and Bo Liu*

Affiliations: Department of Plant Biology, University of California, Davis

*Corresponding author: Bo Liu (bliu@ucdavis.edu)

Author Contributions: MXAG and BL conceived the experiments. MXAG designed and carried out all experiments. YJL provided technical support. All figures were designed and prepared by MXAG. Plants were cared for by MXAG and BL. The chapter was written by MXAG and revised by BL.

Abstract

The cytoskeleton undergoes reorganization to accomplish even partition of the genetic material (mitosis) and the cytoplasm into two daughter cells (cytokinesis). Through enzymatic complexes of Cyclin-Dependent Kinases (CDKs) and Cyclins, the cell cycle machinery controls phase progression through the division cycle and associated cytoskeletal changes. Here, we investigated the roles of CYCA1;1 and CDKA;1 in preprophase band (PPB) formation and function. The PPB is a structure of bundled microtubules (MTs), actin filaments, and their associated proteins that sets up the division plane during cell division in somatic cells of land plants. First, we generated transgenic lines expressing GFP fusion proteins of CYCA1;1 and CDKA;1 in their respective T-DNA insertional mutant backgrounds. With immunostaining and live-cell imaging, we demonstrate that CYCA1;1 and CDKA;1 accumulate in the prophase nucleus and decorate the PPB and spindle. We show that the interaction between CDKA;1 and CYCA1;1 is necessary for their PPB localization. Loss-of-function *cyca1;1* mutants were isolated but showed no division plane or PPB phenotypes. Lastly, we analyzed whether MAP65-4 could be a potential target of this regulatory module but found no difference in its expression in *cyca1;1* mutant. Our results add essential details to our understanding of the activity of two important cell cycle regulators, candidate regulators of cell cycle-dependent PPB MT organization.

Introduction

The dynamic cytoskeleton carries out mitosis and cytokinesis. It reorganizes from stage to stage according to the timing set by the cell cycle to execute stage-dependent tasks required for cell division (Motta & Schnittger, 2021). In eukaryotes, the cell cycle uses a conserved mechanism involving the serine/threonine cyclin-dependent kinases (CDKs) coupled with cyclins to control cytoskeletal reorganization associated with mitotic phase transitions (Sablowski & Gutierrez, 2021). Cyclins are crucial regulators of CDKs as their interaction activates CDK's catalytic activity and specifies its substrates. Plants share the basic functional characteristics of cell cycle control with other eukaryotic organisms, with CDKA as the main CDK controlling the entry into S- and M-phase like Cdc2 in fission yeast, and plant-specific CDKBs working in G2/M-phase (Nowack et al., 2012). Plants possess a high diversity of cyclins than other organisms, with over 50 cyclin homologs of 10 different types (Jia et al., 2014; Wang et al., 2004). The emergence of these highly diversified cyclins may be related to the formation of plant-specific, cell cycle-dependent cytoskeletal cytokinetic arrays, such as the preprophase band (PPB), which determines the division plane, and the phragmoplast, which builds the new cell wall to accomplish cytokinesis. Therefore, exploring how the cell cycle controls the plant division cycle may reveal new functions and modes of regulation of this conserved cellular machinery.

In this study, we aimed to understand how the cell cycle machinery regulates PPB formation. The PPB is a transient cytoskeletal structure primarily composed of microtubules (MTs) that emerges during late G2, persists through prophase, and disassembles during nuclear envelope breakdown in mitotic somatic cells of land plants

(Rasmussen & Bellinger, 2018). It is a structure crucial for the spatial regulation of cell division because it determines where the phragmoplast will build the new cell wall during cytokinesis. Several critical cell cycle regulators have been detected at the PPB in many plant species. CDKs were the first cell cycle core proteins identified at the PPB using antibodies against a conserved epitope of Cdc2 homologs in maize (Colasanti et al., 1993). Another study surveyed the localization of cell cycle regulators during mitosis and cytokinesis in *A. thaliana* and found that a specific CDK (CDKA;1), a G2 cyclin (CYCA1;1), and other regulators accumulated at the PPB under the control of constitutively active promoters (Boruc et al., 2010). Their localization upon overexpression suggests potential roles for CDKA;1 and CYCA1;1 in PPB development.

A plausible hypothesis is that the CDKA;1-CYCA1;1 complex may regulate PPB MT stability/instability by phosphorylating MT-associated proteins necessary for PPB formation (Vavrdová et al., 2019), such as the TON-TRM-PP2A complex (TTP complex), TON1 RECRUITING MOTIF (TRM) proteins, IQ DOMAIN (IQD) proteins, and MICROTUBULE ASSOCIATED PROTEIN 65-4 (MAP65-4). These proteins are all detected at the PPB in *A*. *thaliana* and have canonical CDK phosphorylation sites in their polypeptide sequences. In addition, CDKA;1 co-purifies with TON1 protein, a regulator of PP2A activity (Van Leene et al., 2007). This evidence points to a potential function of CDK/cyclin in regulating PPB MT formation, dynamics, or disassembly.

We took the first steps in exploring the functions of CYCA1;1 and CDKA;1 during PPB formation in sporophytic mitosis of *A. thaliana*. We generated transgenic lines expressing GFP fusions of CYCA1;1 and CDKA;1 under their native promoters in their respective mutants and investigated their dynamics during mitosis. CYCA1;1- and

CDKA;1-GFP fusions consistently localized to the prophase nucleus, PPB, and the mitotic spindle. We isolated a *cyca1;1* mutant and analyzed division plane orientation and cytokinetic structures but found no difference from WT. We analyzed variants of CYCA1;1 that had different domains truncated and found that interaction with CDK was indispensable for its association with MTs, particularly the PPB. CDKA;1 required CYCA1;1 for its association with the PPB, indicating their interdependence for this location. While further studies are undoubtedly needed to determine the precise function of CDKA;1/CYCA1;1 in PPB formation, our results add to our understanding of the functional diversification of cell cycle regulators in plants.

Results

Isolation of homozygous *cyca1;1* mutant

To study the function of CYCA1;1 in cell division, we first identified a T-DNA insertional mutation in the *CYCA1;1* locus in mutant pools of *A. thaliana* generated by the community (GK-378D05) (accessible at http://signal.salk.edu/cgi-bin/tdnaexpress) (Alonso et al., 2003) and isolated homozygous mutants carrying this insertion. Because the insertion is in the first exon, this is predicted to be a loss-of-function mutation.

CYCA1;1 localizes to the PPB, prophase spindle, and metaphase spindle during mitosis

To determine the localization of CYCA1;1 during mitosis when expressed under its native promoter, we generated complementation lines by introducing into the *cyca1;1*

mutant a construct containing 1.58 kB upstream 5' sequence and 2.15 kB genomic coding sequence for *CYCA1;1* fused to a C-terminus GFP. We analyzed dividing root cells of T2 individuals of the resulting complementation lines with immunostaining and live-cell imaging (Figure 3.1). When driven with its native promoter and analyzed by immunostaining of dividing cells, the CYCA1;1-GFP fusion protein localized to the prophase nucleus, mature PPB during prophase (Figure 3.1A, n=49), and to the mitotic spindle during metaphase (Figure 3.1B, n=8). We observed the tissue-wide expression patterns of CYCA1;1-GFP with live cell imaging, and the protein accumulated in a cell cycle-dependent manner and highlighted the prophase nucleus, PPB, and prophase and metaphase spindles, recapitulating what was detected by immunolocalization (Figure 3.1C, n=13).

cyca1;1 mutant does not have division plane defects

We examined the orientation of cell divisions in wild-type Col-0 (WT) and *cyca1;1* mutant by staining six days post-germination (dpg) roots with propidium iodide and imaging them under a confocal microscope (Figure 3.2A, n=3 for WT and 6 for *cyca1;1*). Division orientation in the *cyca1;1* mutant appeared indistinguishable from that in WT, with new cell divisions positioned at around 90º of the parental cell wall.

We turned to anti-tubulin immunostaining of meristematic root cells of *A. thaliana* undergoing division to visualize cytokinetic structures of the mutant in detail but found no significant difference from WT. Like WT, PPBs in *cyca1;1* appeared complete and evenly bundled (Figure 3.2B, n=44 for WT and 51 for *cyca1;1*). With live-cell imaging, we could see that complete PPBs formed on time. The phragmoplast expanded to meet

the position previously occupied by the PPB, just like in WT (Figure 3.2C, n=3).

CDKA;1 localizes to the PPB and prophase nucleus during mitosis

It was previously reported that loss-of-function mutations in CDKA;1 result in male gametophyte lethality in *A. thaliana (Iwakawa et al., 2006)*. Another study recovered *cdka;1* mutant plant, which were reported to be able to complete embryogenesis but failed to produce roots or develop sustained shoots (Nowack et al., 2012). We obtained a heterozygous *cdka;1* line of *A. thaliana,* but could not recover *cdka;1/-* plants in its progeny. The heterozygous *cdka;1/+* mutant plants were used in the experiments.

To learn more about the native localization of CDKA;1 during mitosis, we generated complementation lines by introducing into *cdka;1/+* plants a construct containing 2.25 kB upstream 5' sequence and 2.06 kB genomic coding sequence of *CDKA;1* fused to a C-terminus GFP. We analyzed dividing root cells of T2 individuals with immunostaining and live-cell imaging. CDKA;1-GFP accumulated in interphase and prophase nuclei, the PPB (Figure 3.3A, n=28), and the mitotic spindle (Figure 3.3B, n=6).

We used time-lapse imaging to analyze CDKA;1-GFP dynamics. As with the immunostaining, we found CDKA;1-GFP in interphase and prophase nuclei and at the PPB early in division. During metaphase, CDKA;1-GFP localized around the spindle and in the reforming daughter nuclei during telophase (Figure 3.3C and SF3.1, n=4).

CYCA1;1 location at the PPB depends on interaction with CDKA;1

We then asked how the different domains of the CYCA1;1 polypeptide contributed to its subcellular localization, e.g., at the PPB. Cyclins contain two main conserved domains: a “destruction box” (Dbox) near the N terminus for ubiquitin-mediated proteolysis and a “cyclin box” (Cbox) near the C terminus for binding to CDK (SF3.2) (Wang et al., 2004). Cyclins have phase-dependent accumulation patterns throughout the cell cycle, and their protein levels are precisely controlled by degradation via ubiquitin-dependent proteolysis (Genschik et al., 1998). Destruction of cyclins inactivates CDK activity, allowing cells to progress into the next cell cycle stage. To test the contribution of the Dbox and Cbox in CYCA1;1, we made three versions of CYCA1;1 with the Dbox and Cbox deleted (ΔDbox and ΔCbox, respectively) and another with both boxes deleted (ΔDboxCbox). These CYCA1;1 truncations were expressed under the *CYCA1;1* native promoter when being transformed into the *cyca1;1* mutant. We also transformed a CYCA1;1 overexpression construct into the *cyca1;1* mutant.

We obtained T2 individuals for ΔCbox and ΔDboxCbox lines and analyzed their roots under a confocal microscope (Figure 3.4). After attempting the transformation three times, we could not recover transformants for the ΔDbox construct. Overexpression of CYCA1;1-GFP also yielded no specific expression (Figure 3.4A., n=15). Interestingly, CYCA1;1ΔCbox-GFP lost MT localization and was not visible at the PPB or spindle while detected in nuclei (Fig 3.4B, D; n=5). CYCA1;1ΔDboxCbox-GFP was also absent from MT structures but was observed later to accumulate in the nuclei

of daughter cells during telophase (Fig 3.4C, E; n=9). These results suggest that the D-box is required for its MT association while regulating CYCA1;1's protein level during mitosis. Additionally, CYCA1;1 association with CDKA;1 is necessary for localization to MTs.

CDKA;1 requires CYCA1;1 for PPB localization

The results prompted us to analyze CDKA;1's localization patterns in the absence of CYCA1;1. Therefore, we transformed the CDKA;1-GFP construct described above into the *cyca1;1* mutant and analyzed its subcellular localization via immunostaining and live-cell imaging. CDKA;1-GFP lost its association with the PPB in *cyca1;1* while retaining its nuclear (Figure 3.5A, n=35) and spindle localization (Figure 3.5B, n=7), indicating that CDKA;1 and CYCA1;1 are interdependent for their PPB localization. We used time-lapse imaging to analyze CDKA;1-GFP dynamics during mitosis and cytokinesis in the *cyca1;1* background and detected CDKA;1-GFP in interphase and prophase nuclei but not at the PPB (Figure 3.5C and SF3.3, n=3).

MAP65-4 has normal localization in *cyca1;1*

To explore possible substrates of CDKA;1/CYCA1;1, we analyzed the activities of MAP65-4 in the *cyca1;1* mutant. MAP65-4 belongs to the evolutionarily conserved MAP65/Ase1/PRC1 family of proteins of MT bundlers. It accumulates at the PPB and the cortical division site and functions redundantly with another MAP65 paralog, but its role in spatial regulation of cytokinesis is yet to be explored (Li et al., 2017). MAP65-4 has a predicted CDK phosphorylation site [S/T]PX[K/R] (SF3.4), so we hypothesized

CDKA;1/CYCA1;1 may regulate its cell cycle-dependent activities. However, we analyzed T2 plants carrying a MAP65-4-GFP reporter in *cyca1;1* with immunostaining and live imaging but found no change in its distribution compared to WT (Figure 3.6). Our results indicate that MAP65-4 localization at the PPB does not depend on CYCA1;1.

Discussion

The cell cycle machinery orchestrates the temporal dynamic reorganization of cytoskeletal networks during mitosis and cytokinesis. Plants have specialized cytokinetic cytoskeletal structures, such as the PPB and the phragmoplast, and highly diversified cell cycle regulators. This study attempted to answer how CYCA1;1 and CDKA;1 may regulate PPB formation to specify the division plane during somatic mitotic division of *A. thaliana*. We isolated and analyzed a *cyca1;1* T-DNA mutant; however, we did not detect noticeable phenotypes in PPB formation or division plane orientation in the mutant compared to the WT control. However, our localization experiments showed that CYCA1;1 and CDKA;1 consistently associate with the PPB and that their interaction is necessary for their PPB localization, suggesting that they likely have substrates associated with this cytokinetic microtubule array. We also analyzed MAP65-4 expression in *cyca1;1* as a potential target of regulation of the CDKA;1/CYCA1;1 complex but found no difference in its localization compared to WT. Site-directed mutagenesis may be informative for us to learn whether the putative phosphorylation event is necessary for the localization or activity of MAP65-4.

The lack of phenotype observed in *cyca1;1* prompts us to think that CDKA;1/CYCA1;1 mislocalization in the mutant might not be sufficient for eliminating the necessary CDK function that might be required for PPB formation. *A. thaliana* contains ten genes encoding A-type cyclins and various types of CDKs, so it is possible that other cyclins and CDKs also functionally associated with the PPB or could take over CDKA;1/CYCA1;1 function in the absence of CYCA1;1. For example, CYCB1;2 in maize (John et al., 2001), CDKB2;1 in rice (Lee et al., 2003), and a Cdc2MsF of alfalfa (Mészáros et al., 2000) have been reported to localize although less prominently at the PPB. A more recent study found that *cycb1;1 cycb1;2* and *cycb1;2 cycb1;3* double mutants have some abnormalities in their mitotic MT arrays, including a minimal increase in the incidence of double and misplaced PPBs (Romeiro Motta et al., 2022). Although it was surprising that B-type cyclins were connected to PPB MT organization since they appear after A-type cyclins and are known to control M-phase specific events (Hunt et al., 1992), the plant cyclin A proteins may have some noncanonical functions when compared to their animal and fungal counterparts.

Further experiments are needed to provide more clues about the cell cycle-dependent regulation of early MT-related events in the mitosis of plants. If the null *cdka;1* mutant is lethal, potential future experiments could be to generate *cdka;1* partial loss-of-function mutants (Yang et al., 2020). A biochemistry approach could be taken to ascertain whether CYCA1;1 and CDKA;1 interact and can form an active complex in vitro. Finally, functional analysis of other cyclins and the generation of higher-order mutants could help clarify the hypothesized functional redundancy. Our study tackles a long-standing question in plant cell division that deserves further exploration.

Materials and Methods

Plant Materials and Growth Conditions

The *Arabidopsis thaliana* plants used in this study include control WT (Col-0) plants, *cyca1;1 and cdka;1/+. cyca1;1* was isolated from seed stock GK-378D05(CS2006119), obtained from the *Arabidopsis* Biological Research Center (ABRC) at Ohio State University in Columbus, Ohio, USA. *cdka;1/+* lines (SALK_106809) were obtained from Dr. Hong Wang at the University of Saskatchewan. The primers used for genotyping are listed in Table S3.1. The LP and RP primer pairs were used for detecting the WT allele of the corresponding genes, while the LBb1.3 or o2588 and RP primer pairs were used for detecting the T-DNA insertional mutations of the SALK or GABI lines. WT Col-0 plants were used as the positive control for the WT allele and negative control for the T-DNA mutant allele. All other plant materials are described in Table S3.3.

All plants were grown in growth chambers at 21 °C with cycles of 16-h light and 8-h dark. When grown on plates, sterilized seeds were placed on solid media supplied with 1/2 Murashige & Skoog salt mixture.

Plasmid construction

The genomic fragment of *AtCYCA1;1* (AT1G44110) containing 2.15 kB of coding sequence without a stop codon and 1.58 kb of 5' non-coding region was amplified using primers CYCA1;1_FWD and CYCA1;1_REV (Table S3.1). The resulting product was then combined using Gibson reaction with pCH1 (containing a C-terminus EGFP tag)

linearized by digestion with KpnI and XhoI. This plasmid was recombined using LR with pGWB1 to make *CYCA1;1p:CYCA1;1-GFP.* The primers CYCA1;1_ATG_FWD and CYCA1;1_REV were used to amplify the *CYCA1;1* coding sequence without a stop codon. The product was combined using Gibson with pCH1 opened with KpnI and XhoI, then with pGWB605 through LR to give rise to a *35S:CYCA1;1-GFP* expression construct.

Primers CYCA1;1dbox_FWD and CYCA1;1dbox_REV with complementary sequences for Gibson reaction (Table S3.1) were used to amplify CYCA1;1ΔDbox from the pCH1_*CYCA1;1p:CYCA1;1-GFP* plasmid. The purified amplicon was re-circularized with Gibson reaction. This vector was used for recombination by LR reaction with the pGWB1 vector as the destination vector to make pGWB1_*CYCA1;1p:CYCA1;1*ΔDbox-*GFP*. Similarly, CYCA1;1cbox_FWD and CYCA1;1cbox_REV were used to amplify CYCA1;1ΔCbox from pCH1_*CYCA1;1p:CYCA1;1-GFP.* Then Gibson assembly and LR reaction were carried out to make pGWB1_*CYCA1;1p:CYCA1;1*ΔCbox-*GFP.* The Cbox primers were used to amplify CYCA1;1ΔDboxCbox from pCH1_*CYCA1;1p:CYCA1;1*ΔDbox-*GFP.* Then, the GWB1_*CYCA1;1p:CYCA1;1*ΔdboxCbox-*GFP* plasmid was produced by Gibson assembly followed by LR reaction.

2.06 kB of the genomic coding sequence of AtCDKA;1 (AT3G48750.1) without the stop codon and 2.25 kb of 5' non-coding regions were amplified using primers CDKA;1_FWD and CDKA;1_REV (Table S3.1). The purified amplicon was combined using Gibson reaction with pENTR4, previously linearized with NcoI and XhoI. The resulting plasmid was recombined with the vector pJL414 by LR reaction, which

contains a C-term GFP tag and the MT marker *TUB6p:mCherry-TUB6 (Liu et al., 2019)* combined on the same vector.

All amplifications were done with Phusion DNA polymerase. Plasmids were verified by using restriction enzyme digest. ΔDbox and ΔCbox constructs were sequenced using primers CYCA1;1_dbox_seq and CYCA1;1_cbox_seq, respectively, with vector-specific primers.

Plant transformation

Constructs for the expression of all fusion proteins were delivered into adult *A. thaliana* plants with corresponding genotypes via *Agrobacterium*-mediated transformation by standard floral dipping method (Clough & Bent, 1998). Transgenic plants were selected on antibiotic media according to antibiotic markers carried by respective vectors. Specific transformant generations were indicated in the figure legend of all confocal and immunostaining data. At least 2-3 different T2 plants were analyzed for each line.

Production of cells for immunostaining

To obtain and visualize meristematic root cells, ~10mg of *A. thaliana* seeds were plated and grown for 5-6 dpg. Seedlings were fixed on-plate for 45 minutes (first 5 minutes in a vacuum) in freshly prepared 4% paraformaldehyde in PME buffer (0.05 M PIPES buffer, pH 6.9, 1 mM $MgSO_4$, and 5 mM EGTA), rinsed several times in PME, and partially digested for 25 min in 1% cellulase solution in PME buffer. After rinsing with PME several times, root tips were cut off individually and placed on glass slides

coated with 0.2% chromium potassium sulfate and gelatin. Individual cells were released into solution by gently squashing the root tips between the coverslip and slide. After drying and rehydrating with PME, cells were treated with 0.5% Triton X-100 in PME for 15-30min and washed. Cells were treated with methanol at -20ºC for 15-30min, then washed with phosphate buffer saline (PBS). Cells were stained with the primary antibodies followed by the secondary antibodies in combinations described in Table S3.2. Antibodies were diluted 100-fold in 1XPBS and 3% BSA. Cells were mounted in SlowFade + DAPI (4'6-diamidino-2-phenylindole).

All counts presented for immunostaining images correspond to cell counts from >50 T2 plants.

Microscopy

An Axio Observer inverted microscope equipped with the LSM710 laser scanning confocal module with standard eGFP and mCherry (Carl Zeiss) settings and a 40x C-Plan (water) objective were used for live-cell imaging. For division plane counting, the roots of 5dpg (days post germination) seedlings were stained with propidium iodide (PI, 0.2 µg/mL stock) and mounted in water. For time-lapses, plants were grown in Petri dishes with coverslip bottoms and observed directly on the microscope. Images were acquired using the ZEN software (Carl Zeiss) and processed in ImageJ/Fiji (www.imagej.nih.gov/ij).

Fixed and stained root cells were observed by using an Eclipse 600 epifluorescence microscope with a Plan-Fluor 100x objective (Nikon). Images were

acquired with an OptiMOS sCMOS camera (Photometrics) controlled by μManager software package (Edelstein et al., 2014).

Figures

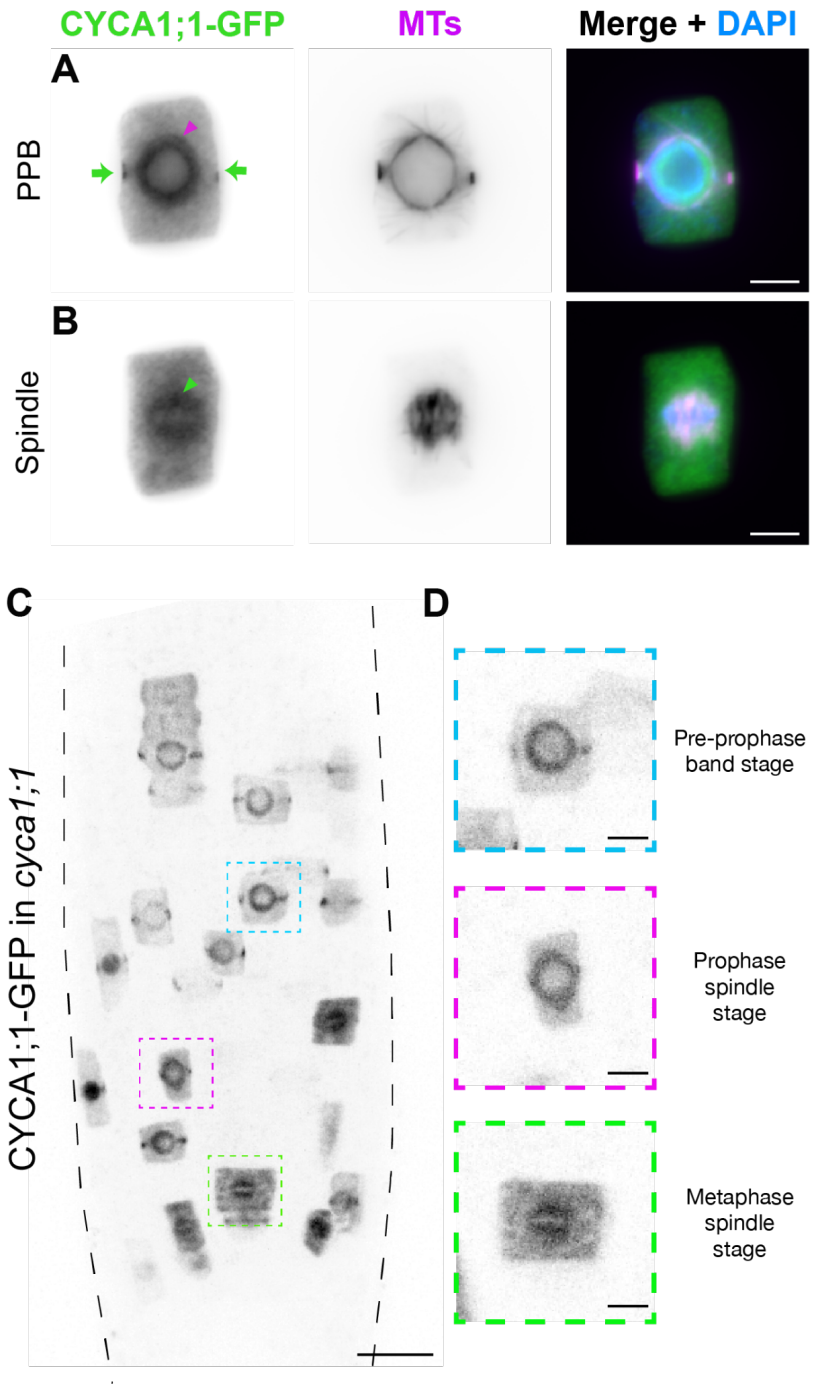

Figure 3.1. – CYCA1;1 localizes to the PPB, prophase spindle, and metaphase spindle during mitosis.
Immunolocalization of CYCA1;1-GFP with MTs as reference during mitosis and cytokinesis in T2 plants of *cyca1;1* expressing *CYCA1;1p:CYCA1;1-GFP*. The merged

images show CYCA1;1-GFP in green, MTs in magenta, and DNA (4'6-diamidino-2-phenylindole, DAPI) in blue.
(A). During prophase, CYCA1;1-GFP labeled the nucleus and the PPB (n=49).
(B). In metaphase, CYCA1;1-GFP associated with the mitotic spindle (n=8). Scale bars = 5μm.
(C). Live-cell imaging of the same line (n=13 plants). Close-up images show a cell at the PPB stage (blue outline), prophase spindle stage (magenta outline), and metaphase spindle stage (green outline). Scale bars = 20 μm in C and 5 μm in D.

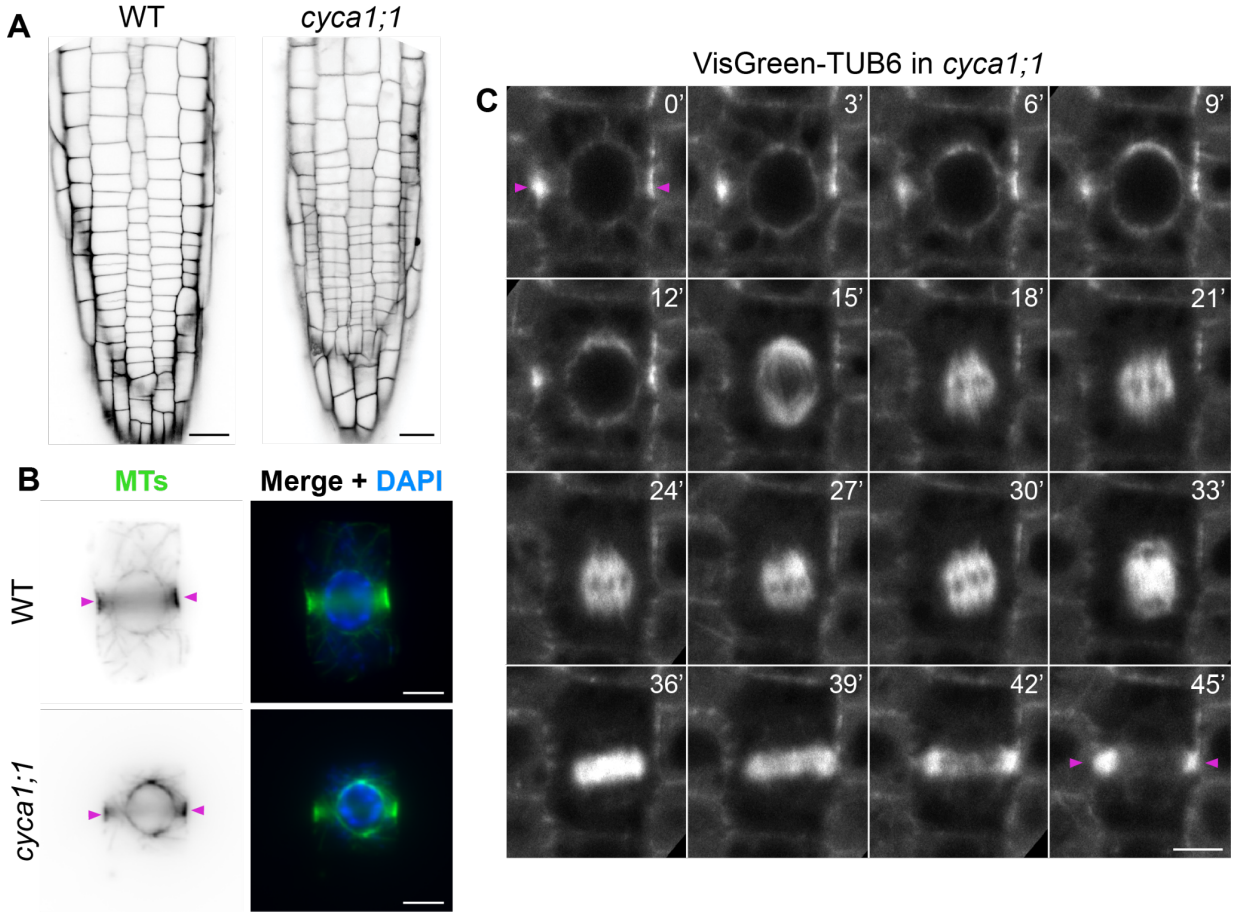

Figure 3.2. – *cyca1;1* mutant does not have division plane or PPB defects
(A). Propidium iodide staining of wild type (WT, n=3) and *cyca1;1* (n=6) roots at 6dpg observed in a confocal microscope. Scale bars = 20μm.
(B). Anti-tubulin immunostaining of WT (n=44) and *cyca1;1* (n=51) root cells at the PPB stage. Magenta arrows highlight PPBs. Scale bars = 5μm.
(C). Timelapse confocal imaging of symmetric cell division in T2 *cyca1;1* roots expressing *TUB6p:VisGreen-TUB6* marking MTs (n=3). Photographs were taken at 3-minute intervals, with the time (in minutes) noted in the top right of each image. Magenta arrows mark the initial PPB position. Scale bar = 5μm.

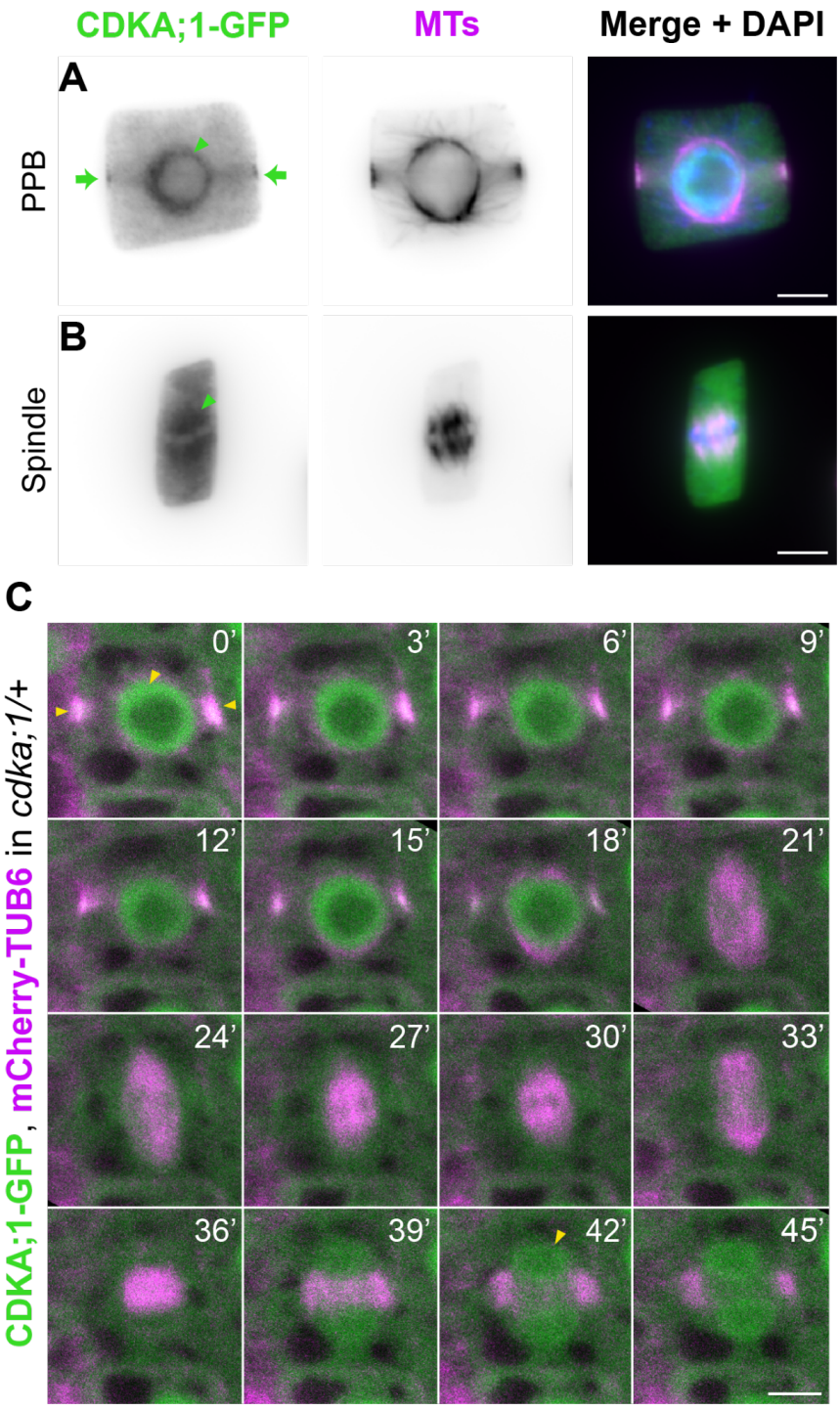

Figure 3.3. – CDKA;1 localizes to the PPB and prophase nucleus during mitosis
Immunolocalization of CDKA;1-GFP with MTs as reference during mitosis and cytokinesis in T2 plants of *cdka/+* expressing *CDKA;1p:CDKA;1-GFP*. The merged images show CDKA;1-GFP in green, MTs in magenta, and DNA (DAPI) in blue.
(A). During prophase, CDKA;1-GFP labeled the nucleus and the PPB (n=28).
(B). In metaphase, CDKA;1-GFP associated with the mitotic spindle (n=6).

(C). Timelapse confocal imaging of the same line (n=4) showing CDKA;1-GFP expression at the PPB and nucleus (yellow arrows at t=0'), spindle (see SF3.1 for single channels), and telophase nuclei (yellow arrows at 42'). Photographs were taken at 3-minute intervals, with the time (in minutes) noted in the top right of each image.
Scale bars = 5 µm.

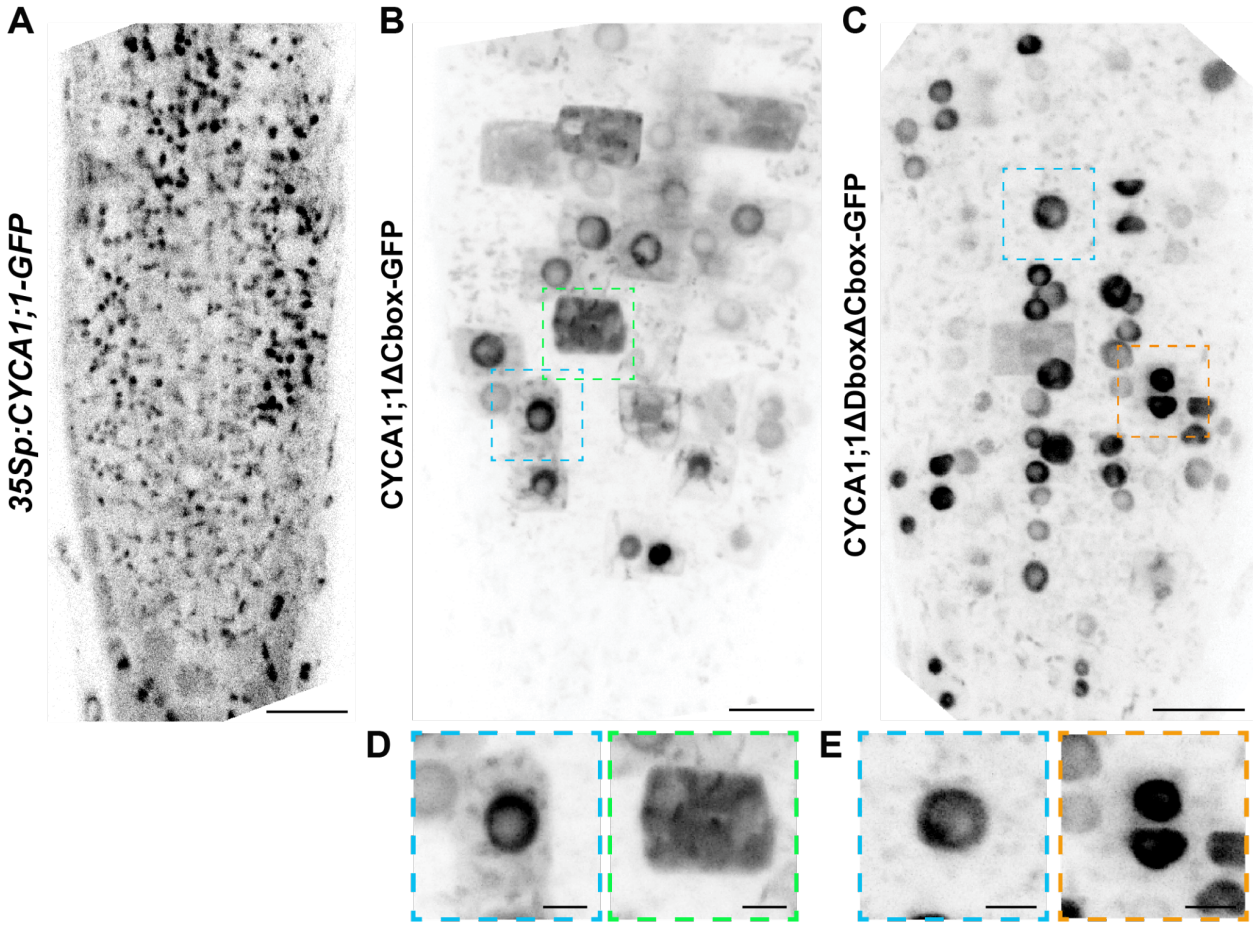

Figure 3.4. – PPB location of CYCA1;1 depends on its interaction with CDKA;1
Live-cell imaging of roots of T2 *A. thaliana cyca1;1* mutant plants expressing:
(A). *35Sp:CYCA1;1-GFP* (n=15)
(B). *CYCA1;1p:CYCA1;1Cbox-GFP* (n= 5)
(C). *CYCA1;1p:CYCA1;1DboxCbox-GFP* (n=9)
Close-up images show a cell at the PPB stage (blue outline), spindle stage (green outline), and the phragmoplast stage (orange outline). Refer to Figure 3.1C for WT localization.
Scale bars = 20µm in whole root images and 5µm in close-ups.

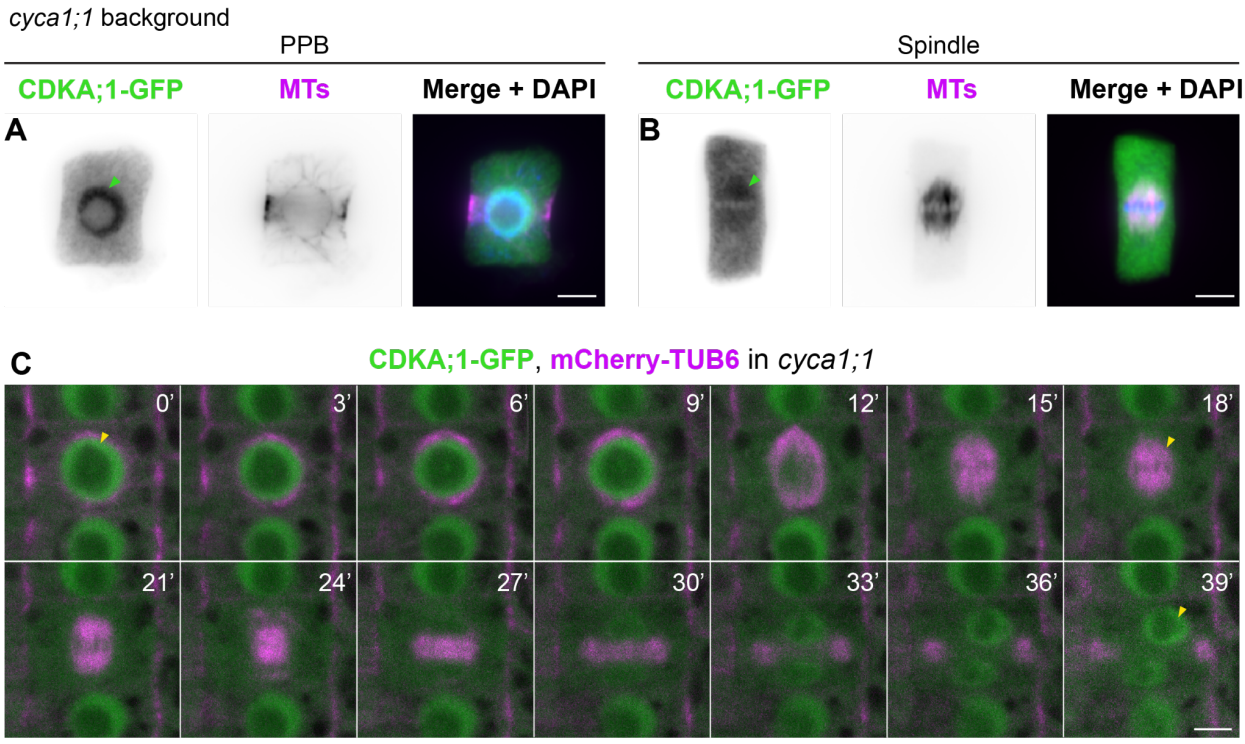

Figure 3.5. – CDKA;1 requires CYCA1;1 for PPB localization

Immunolocalization of CDKA;1-GFP with MTs as reference during mitosis and cytokinesis in T2 plants of *cyca1;1* expressing *CDKA;1p:CDKA;1-GFP*. The merged images show CDKA;1-GFP in green, MTs in magenta, and DNA in blue.
(A). During prophase, CDKA;1-GFP labeled the nucleus but not the PPB (n=35).
(B). In metaphase, CDKA;1-GFP associated with the mitotic spindle (n=7).
(C). Timelapse confocal imaging of the same line (n=3) showing CDKA;1-GFP was not associated with the PPB but was present in the nucleus (yellow arrows at t=0'), spindle (yellow arrows at t=18'), and telophase nuclei (yellow arrows at t=39') in *cyca1;1*. Photographs were taken at 3-minute intervals, with the time (in minutes) noted in the top right of each image. Single channels are shown in SF3.3. Scale bars = 5μm.

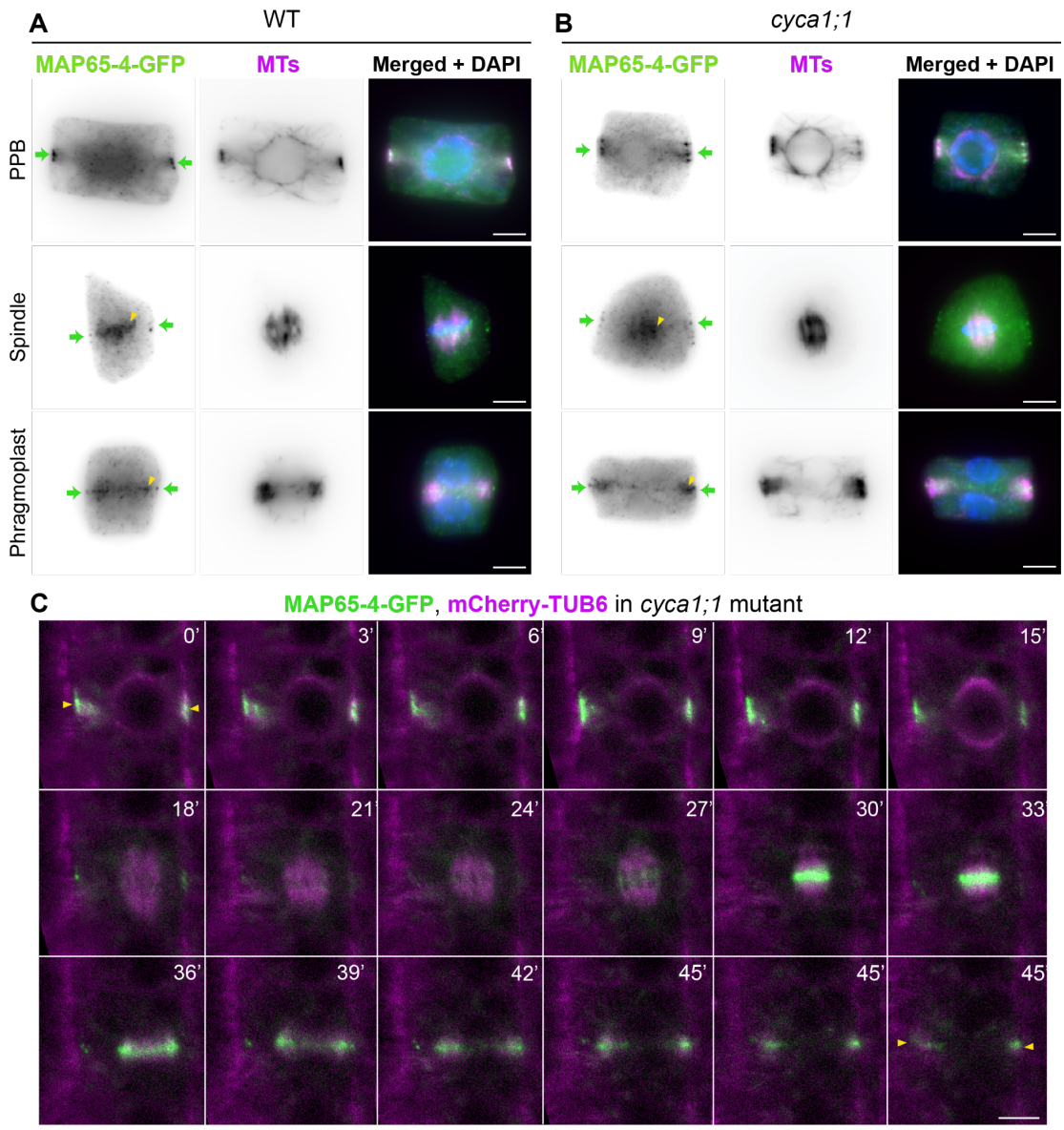

Figure 3.6. – MAP65-4 has normal localization in *cyca1;1*

Immunolocalization of MAP65-4-GFP with MTs as reference during mitosis and cytokinesis in T2 plants of WT (**A**, n=59 PPBs, 15 spindles, and 31 phragmoplasts) and *cyca1;1* (**B**, n=10 PPBs, 2 spindles, and 7 phragmoplasts) expressing *MAP65-4p:MAP65-4-GFP, TUB6p:mCherry-TUB6*. The merged images show MAP65-4-GFP in green, MTs in magenta, and DNA in blue.

(C). Timelapse confocal imaging of the same line (n=2). No difference in MAP65-4-GFP expression was observed in *cyca1;1* mutant, compared to the WT control. Photographs were taken at 3-minute intervals, with the time (in minutes) noted in the top right of each image. Scale bars = 5μm.

Supplemental figures

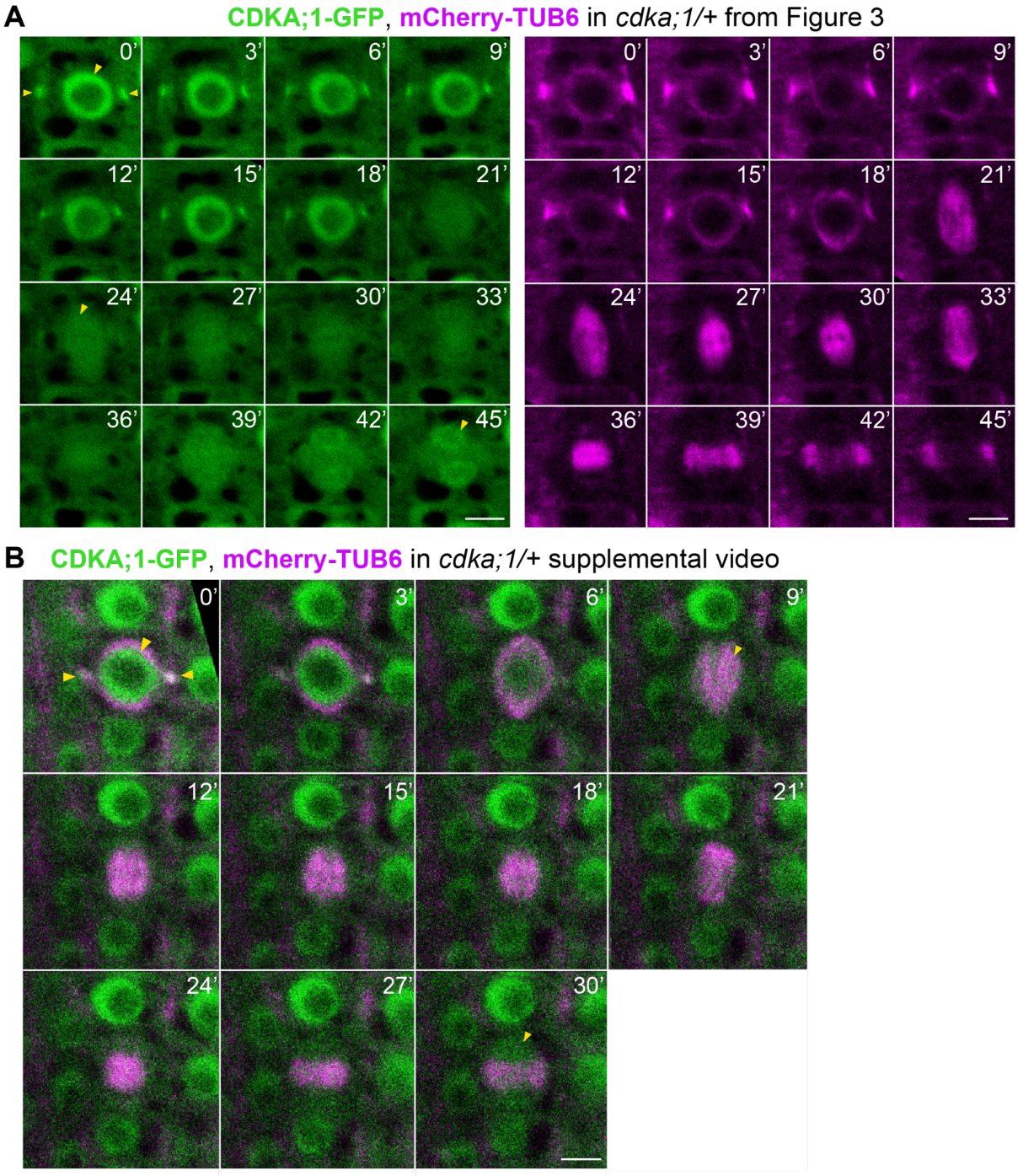

Figure S3.1. – CDKA;1-GFP live-cell imaging
(A). Single channel of timelapse in Figure 3.3B.
(B). Supplemental movie of CDKA;1-GFP in *cdka;1/+.* CDKA;1-GFP accumulated at the PPB and nucleus (yellow arrows at t=0’), spindle (yellow arrows at t=9’), and telophase nuclei (yellow arrows at t=30’). Scale bars = 5 μm.

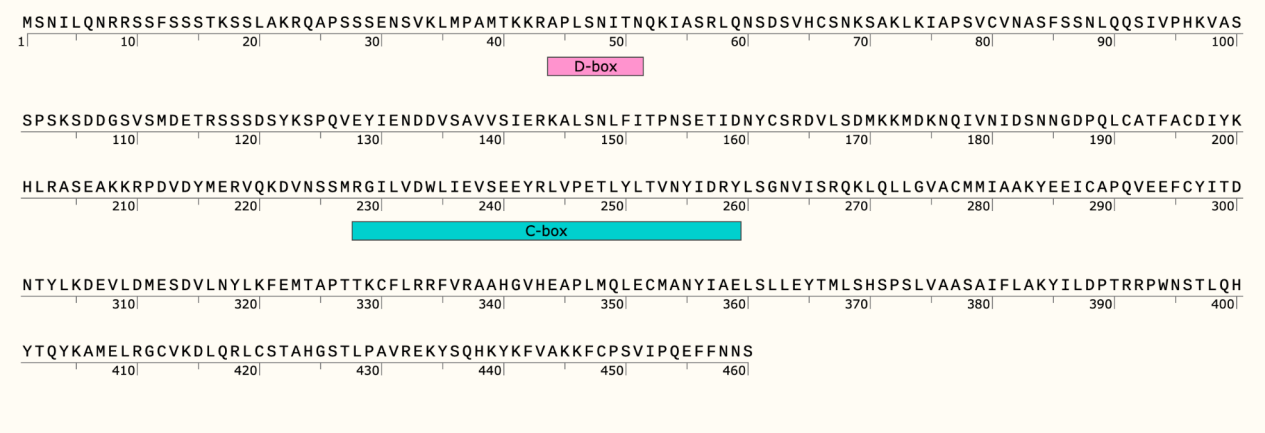

Figure S3.2. – AtCYCA1;1 polypeptide sequence
The position of the Destruction box is marked with a pink box and of the Cyclin box with a turquoise box.

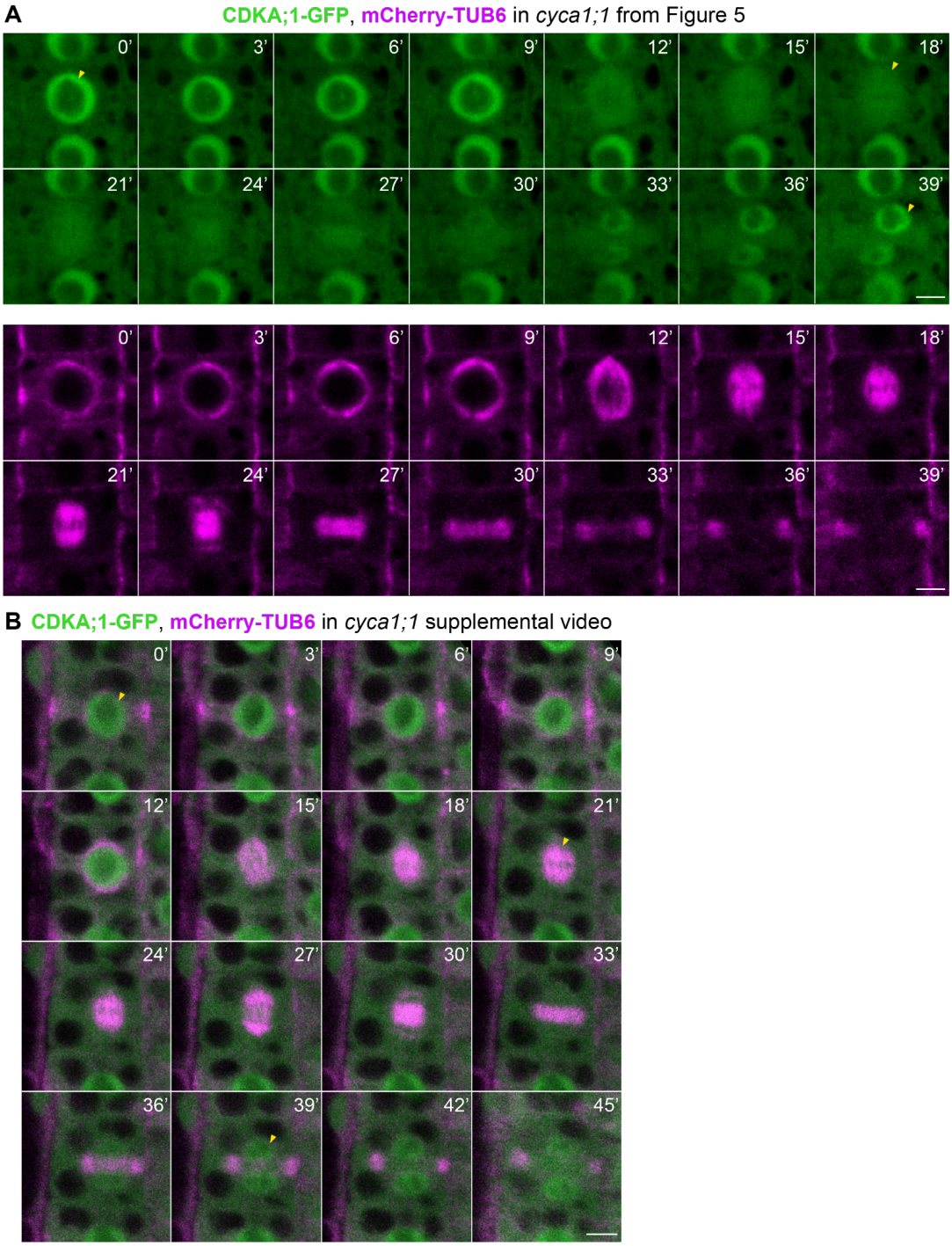

Figure S3.3. – CDKA;1-GFP in *cyca1;1* live-cell imaging
(A). Single channel of timelapse in Figure 3.5B.
(B). Supplemental movie of CDKA;1-GFP in *cyca1;1.* No noticeable signal was detected at the PPB. CDKA;1-GFP was visible in the nucleus (yellow arrows at t=0’), spindle (yellow arrows at t=21’), and telophase nuclei (yellow arrows at t=38’). Scale bars = 5μm.

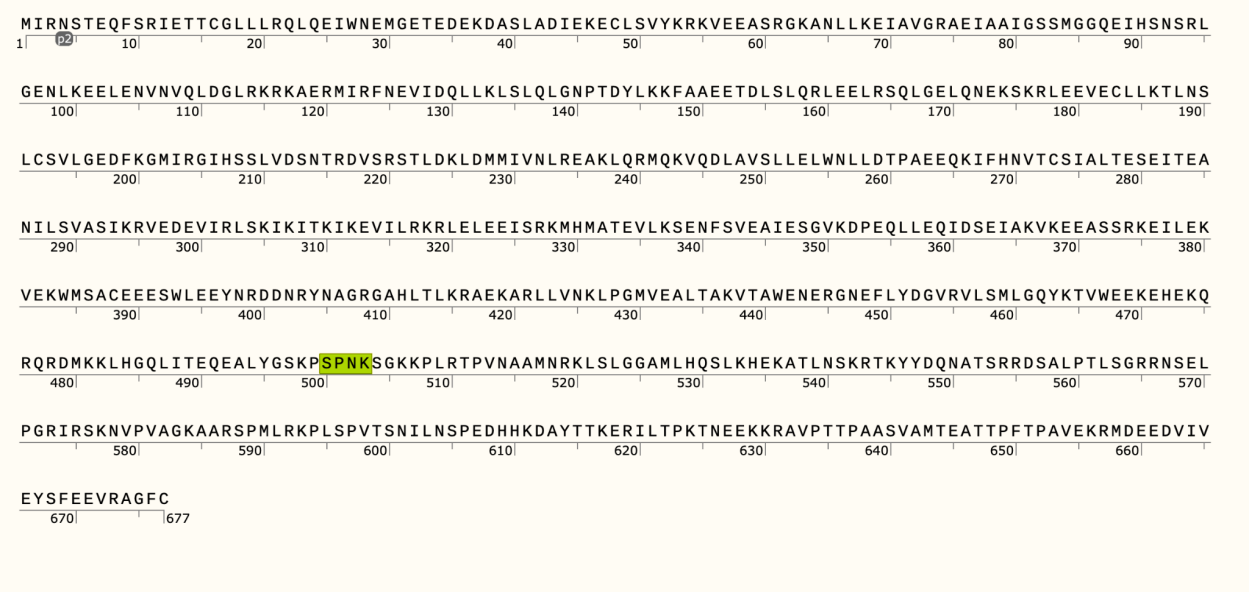

Figure S3.4. – AtMAP65-4 peptide sequence and potential CDK phosphorylation site (green)

Supplemental tables

Table S3.1. Primers used in the construction of transgenes and the genotyping of specific alleles.

Primer Name	Sequence (5' → 3')	Purpose
CYCA1;1_LP	ACT TAG CCA CGA CTA GTA TCG GTG	Genotyping of *cyca1;1* FWD
CYCA1;1_RP	GCT GAC TTG TTT GAA CAA TGT ACC	Genotyping of *cyca1;1* REV
CDKA;1_RP	TAC GAG AAA GTT GAG AAG ATT	Genotyping of *cdka;1* FWD
o2588	CGCCAGGGTTTTCCCAGTCACG ACG	T-DNA primer for genotyping of GABI-Kat lines
LBb1.3	ATTTTGCCGATTTCGGAAC	T-DNA primer for genotyping of SALK lines
CYCA1;1_FWD	caattcagtcgactggatccggtacGCCGTT CCATTGTACATCTTAAG	Gibson primers to amplify CYCA1;1 from promoter FWD
CYCA1;1_ATG_FWD	caattcagtcgactggatccggtacATGTCG AACATTCTTCAGAATCGG	Gibson primers to amplify CYCA1;1 from cDNA
CYCA1;1_REV	agaggatccagatgaaccagaagaaccGC TGTTGTTGAAGAACTCTTGTGG	Gibson primers to amplify CYCA1;1 no stop
CDKA1_FWD	GTA CAA AAA AGC AGG CTC CAC CAA GAC ACC AAG CGC A	Gibson primers to amplify CDKA;1 from promoter FWD
CDKA1_REV	GTA CAA GAA AGC TGG GTC TAG ATA TCC AGG CAT GCC TCC AAG ATC C	Gibson primers to amplify CDKA;1 from promoter FWD
CYCA1;1dbox_FWD	CAA AAA ATC GCT AGC CGA TTA CAA AAT TCT GAT TCG GTG AGG	Gibson primers to amplify CYCA1;1 without Dbox from pENTR FWD
CYCA1;1dbox_REV	GTA ATC GGC TAG CGA TTT TTT GTT TCT TCG TCA TCG CCG GCA TAA G	Gibson primers to amplify CYCA1;1 without Dbox from pENTR REV
CYCA1;1cbox_FWD	GTG AAT TCG AGT ATG TTA TCT GGG AAT GTG ATT AGT AGA CAG	Gibson primers to amplify CYCA1;1 without Cbox from

		pENTR FWD
CYCA1;1cbox_REV	CCC AGA TAA CAT ACT CGA ATT CAC ATC TTT CTG AAC	Gibson primers to amplify CYCA1;1 without Cbox from pENTR FWD
CYCA1;1 dbox seq	ATG TCG AAC ATT CTT CAG AAT CGG	Primer to sequence Dbox constructs
CYCA1;1 cbox seq	GTA ATC TGT TCA TAA CGC CGA ATT C	Primer to sequence Cbox constructs

Table S3.2. Combinations of primary and secondary antibody used in this study

Figure	Primary antibody	Secondary antibody
Figure 3.2	Monoclonal mouse DM1A anti-α-tubulin antibody (Sigma)	Fluorescein isothiocyanate (FITC)–conjugated donkey anti-mouse IgG (Rockland Antibodies & Assays)
Figures 3.1, 3.3, 3.5 and 3.6	Monoclonal mouse DM1A anti-α-tubulin antibody (Sigma) Monoclonal rabbit anti-GFP (Thermo Fisher Scientific)	Texas Red–conjugated anti-mouse IgG (Rockland Antibodies & Assays) FITC–conjugated donkey anti-rabbit IgG (Rockland Antibodies & Assays)

Table S3.3. Key resources table

Resource	Source
A. thaliana cyca1;1	This chapter
A. thaliana cdka;1	Dr. Hong Wang, University of Saskatchewan
A. thaliana cyca1;1 + pGWB1_CYCA1;1p:CYCA1;1-GFP	This chapter
A. thaliana cdka;1 + pJL414_CDKA;1p:CDKA;1-GFP	This chapter
A. thaliana cyca1;1 + pGWB10_TUB6p:VisGreen-TUB6	This chapter
A. thaliana cyca1;1 + pGWB605o_35Sp:CYCA1;1-GFP	This chapter

A. thaliana cyca1;1 + pGWB1_CYCA1;1p:CYCA1;1ΔDbox-GFP	This chapter
A. thaliana cyca1;1 + pGWB1_CYCA1;1p:CYCA1;1ΔDboxΔCbox-GFP	This chapter
A. thaliana map65-4 + pJL414_MAP65-4p:MAP65-4-GFP	Chapter 2 of this thesis and (Liu et al., 2019)
A. thaliana cyca1;1 + pJL414_MAP65-4p:MAP65-4-GFP	This chapter
A. thaliana cyca1;1 + pJL414_CDKA;1p:CDKA;1-GFP	This chapter
pGWB1_CYCA1;1p:CYCA1;1-GFP	This chapter
pJL414_CDKA;1p:CDKA;1-GFP	This chapter
pGWB10_TUB6p:VisGreen-TUB6	*(Liu et al., 2019)*
pGWB605o_35Sp:CYCA1;1-GFP	This chapter
pGWB1_CYCA1;1p:CYCA1;1ΔDbox-GFP	This chapter
pGWB1_CYCA1;1p:CYCA1;1ΔDboxΔCbox-GFP	This chapter
pJL414_MAP65-4p:MAP65-4-GFP	Chapter 2 of this thesis and (Liu et al., 2019)
pJL414_CDKA;1p:CDKA;1-GFP	This chapter
Phusion DNA polymerase	Thermo Fisher
Cellulase	Yakult
Antibodies (see Table S3.2)	
Paraformaldehyde	Electron Microscopy Sciences Cat. 15710
SlowFade + DAPI (4'6-diamidino-2-phenylindole)	Thermo Fisher Cat. S36920

References

1. Alonso, J. M., Stepanova, A. N., Leisse, T. J., Kim, C. J., Chen, H., Shinn, P., Stevenson, D. K., Zimmerman, J., Barajas, P., Cheuk, R., Gadrinab, C., Heller, C., Jeske, A., Koesema, E., Meyers, C. C., Parker, H., Prednis, L., Ansari, Y., Choy, N., … Ecker, J. R. (2003). Genome-wide insertional mutagenesis of Arabidopsis thaliana. *Science*, *301*(5633), 653–657. https://doi.org/10.1126/science.1086391

2. Boruc, J., Mylle, E., Duda, M., De Clercq, R., Rombauts, S., Geelen, D., Hilson, P., Inzé, D., Van Damme, D., & Russinova, E. (2010). Systematic localization of the Arabidopsis core cell cycle proteins reveals novel cell division complexes. *Plant Physiology*, *152*(2), 553–565. https://doi.org/10.1104/pp.109.148643

3. Clough, S. J., & Bent, A. F. (1998). Floral dip: a simplified method for Agrobacterium-mediated transformation of Arabidopsis thaliana. *The Plant Journal: For Cell and Molecular Biology*, *16*(6), 735–743. https://doi.org/10.1046/j.1365-313x.1998.00343.x

4. Colasanti, J., Cho, S. O., Wick, S., & Sundaresan, V. (1993). Localization of the Functional p34cdc2 Homolog of Maize in Root Tip and Stomatal Complex Cells: Association with Predicted Division Sites. *The Plant Cell*, *5*(9), 1101–1111. https://doi.org/10.1105/tpc.5.9.1101

5. Genschik, P., Criqui, M. C., Parmentier, Y., Derevier, A., & Fleck, J. (1998). Cell cycle -dependent proteolysis in plants. Identification Of the destruction box pathway and metaphase arrest produced by the proteasome inhibitor mg132. *The Plant Cell*, *10*(12), 2063–2076. https://doi.org/10.1105/tpc.10.12.2063

6. Hunt, T., Luca, F. C., & Ruderman, J. V. (1992). The Requirements for Protein Synthesis and Degradation, and the Control of Destruction of Cyclins A and B in the Meiotic and Mitotic Cell Cycles of the Clam Embryo. *The Journal of Cell Biology*, *116*(3). https://rupress.org/jcb/article-pdf/116/3/707/1468575/707.pdf

7. Iwakawa, H., Shinmyo, A., & Sekine, M. (2006). Arabidopsis CDKA;1, a cdc2 homologue, controls proliferation of generative cells in male gametogenesis. *The Plant Journal: For Cell and Molecular Biology*, *45*(5), 819–831. https://doi.org/10.1111/j.1365-313X.2005.02643.x

8. Jia, R.-D., Guo, C.-C., Xu, G.-X., Shan, H.-Y., & Kong, H.-Z. (2014). Evolution of the cyclin gene family in plants. *Journal of Systematics and Evolution*, *52*(5), 651–659. https://doi.org/10.1111/jse.12112

9. John, P. C., Mews, M., & Moore, R. (2001). Cyclin/Cdk complexes: their involvement in cell cycle progression and mitotic division. *Protoplasma*, *216*(3-4), 119–142. https://doi.org/10.1007/BF02673865

10. Lee, J., Das, A., Yamaguchi, M., Hashimoto, J., Tsutsumi, N., Uchimiya, H., &

Umeda, M. (2003). Cell cycle function of a rice B2-type cyclin interacting with a B-type cyclin-dependent kinase. *The Plant Journal: For Cell and Molecular Biology*, *34*(4), 417–425. https://doi.org/10.1046/j.1365-313x.2003.01736.x

11. Li, H., Sun, B., Sasabe, M., Deng, X., Machida, Y., Lin, H., Julie Lee, Y.-R., & Liu, B. (2017). Arabidopsis MAP65-4 plays a role in phragmoplast microtubule organization and marks the cortical cell division site. *The New Phytologist*, *215*(1), 187–201. https://doi.org/10.1111/nph.14532

12. Liu, W., Wang, C., Wang, G., Ma, Y., Tian, J., Yu, Y., Dong, L., & Kong, Z. (2019). Towards a better recording of microtubule cytoskeletal spatial organization and dynamics in plant cells. *Journal of Integrative Plant Biology*, *61*(4), 388–393. https://doi.org/10.1111/jipb.12721

13. Mészáros, T., Miskolczi, P., Ayaydin, F., Pettkó-Szandtner, A., Peres, A., Magyar, Z., Horváth, G. V., Bakó, L., Fehér, A., & Dudits, D. (2000). Multiple cyclin-dependent kinase complexes and phosphatases control G2/M progression in alfalfa cells. *Plant Molecular Biology*, *43*(5-6), 595–605. https://doi.org/10.1023/a:1006412413671

14. Motta, M. R., & Schnittger, A. (2021). A microtubule perspective on plant cell division. *Current Biology: CB*, *31*(10), R547–R552. https://doi.org/10.1016/j.cub.2021.03.087

15. Nowack, M. K., Harashima, H., Dissmeyer, N., Zhao, X. ’ai, Bouyer, D., Weimer, A. K., De Winter, F., Yang, F., & Schnittger, A. (2012). Genetic framework of cyclin-dependent kinase function in Arabidopsis. *Developmental Cell*, *22*(5), 1030–1040. https://doi.org/10.1016/j.devcel.2012.02.015

16. Rasmussen, C. G., & Bellinger, M. (2018). An overview of plant division-plane orientation. *The New Phytologist*, *219*(2), 505–512. https://doi.org/10.1111/nph.15183

17. Romeiro Motta, M., Zhao, X. ’ai, Pastuglia, M., Belcram, K., Roodbarkelari, F., Komaki, M., Harashima, H., Komaki, S., Kumar, M., Bulankova, P., Heese, M., Riha, K., Bouchez, D., & Schnittger, A. (2022). B1-type cyclins control microtubule organization during cell division in Arabidopsis. *EMBO Reports*, *23*(1), e53995. https://doi.org/10.15252/embr.202153995

18. Sablowski, R., & Gutierrez, C. (2021). Cycling in a crowd: coordination of plant cell division, growth and cell fate. *The Plant Cell*. https://doi.org/10.1093/plcell/koab222

19. Van Leene, J., Stals, H., Eeckhout, D., Persiau, G., Van De Slijke, E., Van Isterdael, G., De Clercq, A., Bonnet, E., Laukens, K., Remmerie, N., Henderickx, K., De Vijlder, T., Abdelkrim, A., Pharazyn, A., Van Onckelen, H., Inzé, D., Witters, E., & De Jaeger, G. (2007). A Tandem Affinity Purification-based Technology Platform to Study the Cell Cycle Interactome in Arabidopsis thaliana*. *Molecular & Cellular Proteomics: MCP*, *6*(7), 1226–1238.

https://doi.org/10.1074/mcp.M700078-MCP200

20. Vavrdová, T., ˇSamaj, J., & Komis, G. (2019). Phosphorylation of Plant Microtubule-Associated Proteins During Cell Division. *Frontiers in Plant Science*, *10*, 238. https://doi.org/10.3389/fpls.2019.00238

21. Wang, G., Kong, H., Sun, Y., Zhang, X., Zhang, W., Altman, N., DePamphilis, C. W., & Ma, H. (2004). Genome-wide analysis of the cyclin family in Arabidopsis and comparative phylogenetic analysis of plant cyclin-like proteins. *Plant Physiology*, *135*(2), 1084–1099. https://doi.org/10.1104/pp.104.040436

22. Yang, C., Sofroni, K., Wijnker, E., Hamamura, Y., Carstens, L., Harashima, H., Stolze, S. C., Vezon, D., Chelysheva, L., Orban-Nemeth, Z., Pochon, G., Nakagami, H., Schlögelhofer, P., Grelon, M., & Schnittger, A. (2020). The Arabidopsis Cdk1/Cdk2 homolog CDKA;1 controls chromosome axis assembly during plant meiosis. *The EMBO Journal*, *39*(3), e101625. https://doi.org/10.15252/embj.2019101625

Chapter 4
Conclusions

The research findings presented in this thesis shed light on the molecular processes that regulate plant cell division, focusing on the formation and organization of the preprophase band (PPB). Precise spatial control of the division plane is essential for shaping tissues and organs, and the PPB is an evolutionary landmark that coordinates this control. The PPB is a transient structure consisting of bundled cortical microtubules (MTs), actin filaments, and associated proteins that establishes the division plane early in the mitotic cells in somatic tissues by leaving a molecular memory of its location that guides subsequent insertion of the cell plate during cytokinesis.

Identifying IQD6/7/8 as microtubule-binding proteins exclusively associated with PPB MTs offers insights into the PPB formation and maintenance process. IQD6/7/8 are mitotic members of the IQ67 DOMAIN (IQD) family of plant-specific calcium/calmodulin-binding proteins. We show they are crucial for establishing a solid PPB MT array that specifies the cell division plane. The *iqd6/7/8* triple mutants exhibit frequent defects of oblique cell division planes, indicating the significance of a robust and uniform PPB for organizing divisions in three-dimensional space. IQD proteins are characterized by a conserved IQ67 domain that binds calmodulin (CaM) in the presence of calcium (Ca^{2+}). We found that the IQ domain of IQD8 was necessary for the protein's PPB localization, but the significance of Ca^{2+}/CaM in division plane regulation remains to be explored. We also established that CLASP cooperates with IQD6/7/8 in maintaining PPB MT organization and stability. Future biochemical, genetic, and cell biology experiments may help determine whether these proteins interact directly.

Analyzing CLASP localization in the *iqd6/7/8* mutant and vice versa could answer if these proteins depend on each other for association with the PPB.

The presence of CYCA1;1 and CDKA;1 at the PPB introduces a connection between cell cycle regulators and the generation of spatial cues by the PPB. While we reveal an interesting interdependence between CDKA;1 and CYCA1;1 for their localization at the PPB, their function at this cytoskeletal structure remains unclear. Since the cyclin subfamilies have significantly expanded in plants, analyzing other cyclin proteins and their corresponding mutants can help answer whether other cyclins play redundant roles at the PPB. Additionally, given the potential lethality of the *cdka;1* mutation, we could use sensitized CDKA;1 variant rescue lines (Su et al., 2017) to inactivate the kinase by using ATP-competitive molecules and study the consequences of this inactivation in PPB formation and division plane establishment without having to generate null mutants.

It remains unclear when the PPB arose during the evolution of plants. Tracing the emergence of PPB-like structures in the Streptophyte algae and their collaboration with the phragmoplast would add a unique dimension to our understanding of plant cytokinesis. Unraveling the ancestral functions of homologs of PPB-localized proteins in the Streptophyte algae would be an interesting avenue for further exploration in the evolution of plant cell division.

Many questions remain in our understanding of the spatial regulation of cell division in plants. To further elucidate the underlying mechanism, the roles of PPB-associated proteins with unknown functions, the complexities of communication between the expanding phragmoplast and the cortical division site (CDS), and the

functions of cell cycle regulators at the PPB need further investigation. Advanced cell biology techniques, developing tools for non-model systems, and comparative mutant analysis could help provide deeper insights into the molecular mechanisms directing plant cell division.

References

1. Su, J., Zhang, M., Zhang, L., Sun, T., Liu, Y., Lukowitz, W., Xu, J., & Zhang, S. (2017). Regulation of Stomatal Immunity by Interdependent Functions of a Pathogen-Responsive MPK3/MPK6 Cascade and Abscisic Acid. *The Plant Cell*, *29*(3), 526–542. https://doi.org/10.1105/tpc.16.00577